Spring 2019

Modeling of Magnetic Resonance Wireless Electric Vehicle Charging

Erhuvwu Ayisire

MODELING OF MAGNETIC RESONANCE WIRELESS ELECTRIC VEHICLE CHARGING

by

ERHUVWU AYISIRE

(Under the Direction of Adel El Shahat)

ABSTRACT

Due to the fast-growing market for an electric vehicle, it is necessary that the drawbacks involved in electric vehicle technology should be overcome, therefore introducing a wireless charging technique which is more convenient as battery cost, recharge time and weight has been removed. Different wireless charging techniques for electric vehicles are discussed. This research work investigates the feasibility of wireless power transfer for electric vehicles by electromagnetic resonance coupling. Wireless power transfer (WPT) for electric vehicles by magnetic resonance coupling is of high priority due to its efficiency, high power transmission, and more considerable charging distance. Simulation results show the energy transfer efficiency between two magnetically coupled resonating coils. However, results show the effects of parameters such as an inductor, capacitor, load and coupling coefficient on efficiency. Additionally, implementation of a closed loop circuit using a three-level cascaded PI controller for the dynamic wireless electric vehicle charging to eliminate the variation of voltage because of varied spacing existing between both coils as the vehicle is in motion and thereby delivering a constant voltage and constant current to the load is carried out. Simulation results and comparison with a single level PI controller indicate the effectiveness of the control method. A fuzzy logic and neuro-fuzzy controller are implemented for the wireless electric vehicle transfer which is seen to be more robust than the PI controller as there is no undershoot in the output voltage. Furthermore, wireless power transfer with three - level cascaded PI controller with MPPT is designed. The proposed system consists of a solar PV array, boost DC/DC converter, inverter, transmitter coil, a receiver coil, rectifier, buck converter, and batteries. The design of

the MPPT controller tracks the highest voltage and current from the PV array required to charge a battery in which the highest power point voltage is 61.5 V. The stability analysis for the closed-loop system has been done and the system is asymptotically stable.

INDEX WORDS: Wireless Power Transfer (WPT), Electric Vehicle (EV), Dynamic Wireless Power Transfer (DWPT), Online Electric Vehicle (OLEV), Maximum Power Point Tracking (MPPT), Fuzzy Logic Control (FLC), Fuzzy Inference System (FIS), Adaptive Neuro Fuzzy Inference System (ANFIS), Membership Function (MF), Proportional Integral (PI), PV array.

MAGNETIC RESONANCE COUPLING MODELLING OF ELECTRIC VEHICLE WIRELESS CHARGING

by

ERHUVWU AYISIRE

B.S., University of Ilorin, Nigeria, 2012

M.S., Georgia Southern University, 2019

A Thesis Submitted to the Graduate Faculty of Georgia Southern University

in Partial Fulfillment of the Requirements for the Degree

MASTER OF SCIENCE

STATESBORO, GEORGIA

MAGNETIC RESONANCE COUPLING MODELLING OF ELECTRIC VEHICLE WIRELESS CHARGING

by

ERHUVWU AYISIRE

Major Professor:	Adel El Shahat
Committee:	Mohammad Ahad
	Seungmo Kim

Electronic Version Approved:
May 2019

DEDICATION

I dedicate this work to God and my wonderful parent.

ACKNOWLEDGMENTS

I express my devoted gratitude to my supervisor Dr. Adel El Shahat for his unceasing supervision, wonderful encouragement, and support in the progress of this research work. My appreciation is to my committee members Dr. Mohammad Ahad and Dr. Seungmo Kim for their contribution to the success of this work. I would also express my gratitude to my colleague Sharaf Sumaiya for her advice and help in this thesis. Finally, my heartfelt gratitude is to my family and my best friend Damilare Olukotun for their moral, financial, and spiritual support throughout my program.

TABLE OF CONTENTS

LIST OF TABLES

LIST OF FIGURES

LIST OF SYMBOLS

I= Current

R= Resistance

C= Capacitance

L= Inductor

V= Voltage

Z= Impedance

Q= Quality factor

M= Mutual Inductance

N= No of turns

l= Length of air core

r= Radius

d= Diameter

w= Thickness of coil

D= Duty cycle

Di= Inner diameter

F_{sw}= Switching frequency

P_{loss}= Power loss

Z_{in}= Source impedance

ω= angular frequency

K= Coupling coefficient

S_{11}= Reflection coefficient

S_{21}= Transmission coefficient

η_{11}= Efficiency of power reflection

η_{21}= Efficiency of power transmission

CHAPTER ONE

INTRODUCTION

1.1 Overview of Wireless Power Transfer (WPT)

Transfer of wireless power has been an innovation of great interest since the invention of the mode of wireless power transfer by Nikola Tesla (Tesla, 1982). Magnetic resonance wireless transfer is preferred due to its efficiency and considerable charging distance. It is widely used in day-to-day and modern applications like charging cell phones, electric vehicles wirelessly (Hui, 2013), and biomedical implants (Ahn, 2014), etc.

Among the records of early endeavors to utilize wireless power innovation for a lot of power is a report conducted in 1980 in which wireless power transfer supplies energy to electric trains running in a mine in the Soviet Union (IHI, 2013). Probably, the usage of the wireless power transfer system was due to the danger of flame in the mine. Results show then that the frequency of power transmission was at 5 kHz, so the productivity was most likely not very high. The power transfer was over a separation of just a couple of centimeters. In the 1990s, it was feasible to control huge amounts of currents at moderately high frequencies of 20 kHz or more, which quickly improved wireless power transfer innovation (IHI, 2013). Its application is evident in, for example, unmanned carriages running in semiconductor generation plants where there is a prohibition of dust. This resulted in 90% power transfer efficiency, and WPT system of this sort is presently the standard. Nonetheless, not much work is done on the enhancement of the transmission distance; however, it relies upon the size of the coil (IHI, 2013).

1.2 Joint Improvement of Wireless Charging Systems

The current joint improvement of profoundly coupled magnetic resonance charging innovation by IHI and WiTricity Corporation (U.S.) has empowered transmission of power over several

centimeters with high effectiveness (IHI, 2013). In 2007, this innovation emerged from research conducted by MIT's group of researchers who were able to light a bulb of 60W at 2m (Lu, 2015). This result negated the then current information of WPT innovation with reference to the transmitting distance, which increased its popularity in 2007 (Kurs, 2007; Habib, 2012). The company, which had assumed control over the innovation from MIT, started joint improvement of remote charging frameworks. This change was almost total at the research facility level, so development was concentrated on the useful utilization of this innovation. With our emphasis on charging EVs and PHEVs, we strive continuously to build up a framework that can be user-friendly. In this advancement, convenience and comfort of users are of utmost priority (IHI, 2013).

1.3 Wireless Power Transmission System for Electric Vehicle Charging

The three most important things to consider in WPT systems when lowering the reluctance effect concerning the efficiency of the power transferred for great air gaps are shape, dimensions of coils, choosing coil and core materials (Jeong, 2016; Haque, 2017). The charging operation for wireless electric vehicles is as depicted in Figure 1. Here, the inverter converts the AC power from the grid to a DC power needed by the converter and again rectified to AC suitable for the transmitting coil placed on the ground. The transmission of this AC power took place wirelessly by magnetic resonance method to the receiving coil placed under the vehicle's chassis and converted back to DC power used to charge the battery (Choi, 2014).

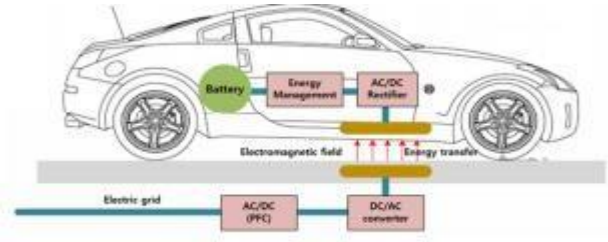

Figure 1-1 Wireless Power Transfer System for Electric (Choi, 2014)

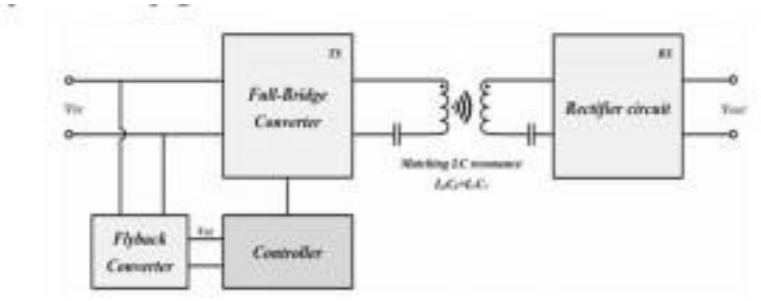

Figure 1-2 Wireless Power Transfer System Block Diagram (Choi, 2014)

1.4 Features of WPT Structure for Charging Electric Vehicles

There are three essential requirements an effective and suitable electric vehicle charging structure has to meet: large air gap, high power and high efficiency (Beh, 2010). Electromagnetic waves serve as a means of propagating energy in an RF & Microwave system (Sample, 2011). This transfer of power takes place over air gaps within some km; however, it results in some drawbacks such as line of sight transmission, low power (less than 1 kW) transmission, a great loss in the air, low efficiency and an extensive effect on its environment (Wang, 2011). Inductive Power Transfer (IPT) (Xui, 2013) also referred to as non-resonant inductive method (Karalis, 2008) or electromagnetic induction or inductive coupling method (Sample, 2011) has low charging distance (about few centimeters) (Xui, 2013) because of its loose coupling between the receiving and transmitting coils respectively (Hasanzadeh, 2012). The MIT research team proposed the magnetic coupling resonant technique (Kurs, 2007), also referred to as resonant inductive power transfer (Musavi, 2012) in 2007 which has been demonstrated alluring for EV and PHEV charging applications due to its mid-range charging distance efficiency (100-300mm), low loss in its surrounding, low interference and its omnidirectional characteristics (Cheon, 2011).

1.4.1 Different Techniques for Wireless Electric Vehicle Charging

There are different techniques developed for charging electric vehicle battery, these include:

Magnetic induction

Microwave

Capacitive coupling

Magnetic resonance coupling

1.4.2 Magnetic Induction Coupling

The magnetic induction coupling makes use of the principle of electromagnetic induction in which an electric vehicle is wirelessly charged. Its arrangement is composed of two coils. Current flows through the transmitting coil, which produces a varying magnetic field, thus inducing a current in the receiving coil, which in turn charges the electric vehicle.

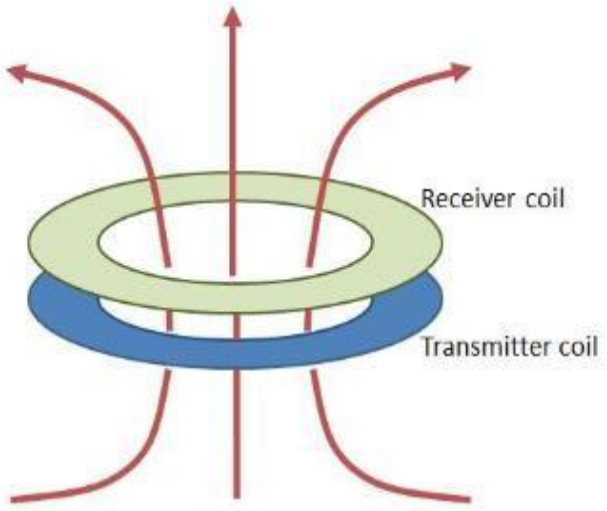

Figure 1-3 Operation of magnetic induction method

For inductive coupling to be efficient, the transmitting and the receiving coil must be near each other and well aligned. This method forms the foundation for the creation of the Wireless Power Consortium (WiTricity, 2014) (world's first international wireless charging standard-QI.) The standard started with low power (about 5W) at a 4 cm distance, published in 2009. The rule stretched to medium-power (about 120W) in 2011. IPT systems are resilient to environmental conditions and

thereby very convenient for all situations and need little or no maintenance (Shital, 2016). The IPT technique needs ferrites for flux guidance, which makes it operate at low frequencies; hence, the size reduces due to core losses (Covic, 2013; Haque, 2018).

Furthermore, in the magnetic induction method, there is a wireless power transfer through magnetic coupling from a fixed transmitter to the various moving secondary receiver (Wu, 2011). The transmitter and receiver coils have a large air gap, which causes the magnetic coupling effect between the coils to change. The change decreases the stability of the system due to the different charging cycles of the electrical properties (Siqi and Chunting, 2015). Based on the power specifications, it can only be a one-phase or three phase supply. A WPT system is usually composed of the battery, transmitting coil, receiving coil, electrical grid, microcontrollers, sensors, matching circuit (Vilathgamuwa, 2015). The topologies of the inductive power transfer are either distributed or lumped based on the coil's magnetic configuration (Mahbub, 2019). The magnetic field created from the primary coil can be controlled and strong for wirelessly transferring power due to its constant frequency current. From the electrical grid, there is a generation of low-frequency alternating current created in the transmitting coil. The coupling of the transmitting coil and the series of receiving coils is via magnetic fields.

Advancement in power electronics technology has led to the discovery of a new application based on the IPT system like wireless EV charging over large air gaps, power wirelessly generated used by professional devices. These are examples of high-power applications (Swain, 2012). Lighting, medical implants, and mobile phones are examples of low power applications (Wang, 2005). In general, the mutual coupling in the IPT system is weak (Shital, 2016). Some of the advantages of IPT systems are as follows (Shital, 2016):

The system is safe.

The cost of maintenance is minimal

It is durable.

Conservation of energy.

The system is reliable

No magnetic field radiation.

Disadvantages include:

Misalignment of transmitter and receiver coils

Charging is only efficient on short distances (less than the coil diameter)

1.4.3 Microwave Power Transfer (MPT)

Radiative (far field) technique is another name for MPT. This type of wireless power transfer involves the use of radio waves to transmit power and the wavelength of the radio wave is lowered to that produced by microwave (Kawasaki, 2013). The components of MPT include a receiver, transmitter antenna, and generator (Kawasaki, 2013). It is important to note that there is no magnetic coupling between the transmitter and receiver antennas (Kawasaki, 2013). In this type of WPT system, transmitting and receiving antennas are magnetically separable therefore variation in the impedance of the transmitting and receiving antennas are not considered whereas, in the magnetic inductive and magnetic resonance coupling, there are considerations for variation in impedance (Shinohara, 2013). Microwave power transfer for the electric vehicle is a relatively new concept that works more efficiently than others. The transmitter of the microwave phased array generates a beam at frequencies of about 2.44 GHz and 5.79 GHz by direct current supply and discharges to rectenna of the EV underneath the vehicle.

The drawbacks of this system include: high power transmission in MPT (therefore detrimental to human health), minimal efficiency and its limitation to only straight-line propagation (Hossain, 2012).

1.4.4 Capacitive Wireless Power Transfer

The capacitive coupling method for transferring power wirelessly is newly applied in the EV battery charging. Its interface is composed of metallic sheets with an insulating coating at the secondary and primary side (Rozario, 2016). An inverter with a high frequency triggers the coupling interface, which in turn generates an electric field in between the primary and secondary side thereby allowing the flow of current; hence, power is transferred (Rozario, 2016; Haque, 2018). Figure below is the capacitive coupling system represented with a simple diagram by Young Soo. Here, a direct current voltage transformed to an alternating current voltage is with a high frequency, which in turn delivered to two primary metallic sheets by the inverter with high frequency (You, 2016). The flow of displacement current generated by the electric field is because of the closeness between the primary and secondary metallic sheets. A rectifier then converts the AC to DC voltage (You, 2016).

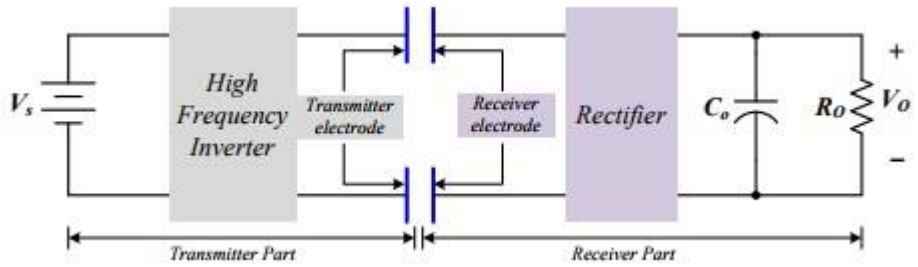

Figure 1-4 Operation of capacitive coupling method

One of the major advantages of the capacitive wireless power transfer is that the electric field passes through metal constraints with minimal power loss generated which makes it good for EV charging (Vincent, 2017). The metallic sheet can be Al, and this is cheap in comparison with litz

inductive coupling (Vincent, 2017). By coating the surfaces of coupling plates with dielectric materials, the coupling capacitance can improve in providing electrical isolation. When an inductor is connected in series with the coupling plates and the equivalent coupling capacitor is tuned, enough power is achieved (Liu, 2011; Haque, 2018). There is no need for ferrites for flux guidance which makes it suitable to work at high frequencies and hence have higher efficiency and power transfer densities than an inductive coupling technique (Lu, 2016). The system of capacitive coupling has a simple structure in comparison with other WPT techniques making it overcome misalignment problems greatly (Vincent, 2017). Advantages by

Murata include:

The devices on the charging pad are positioned freely.

Flat metal plates.

There is a minimal rise in the electrode's temperature.

Reduced power and frequency utilization because of the great potential difference across the metal plate

Disadvantages include:

Efficiency is very low.

Coupling capacitance is small.

The table below summarizes the comparison between the different WPT charging of Electric Vehicle charging.

Table 1: Comparing various WPT techniques for EV Charging (Qui, 2014)

Energy-carrying medium	Technology		Power	Range	Efficiency	Comments
Electromagnetic field	Near field	Traditional IPT	High	Low	High	Range is too small for EV charging.
		Coupled Magnetic Resonance	High	Medium	High	Capable for EV charging
	Far field	Laser, Microwave,	High	High	High	Need direct line-of-sight transmission path, large antennas, and complex tracking mechanisms.
		Radio wave	High	High	Low	Efficiency is too low for EV charging.
Electric field	Capacitive power transfer		Low	Low	High	Both power and range are too small for EV charging.
Mechanical force	Magnetic gear		High	Medium	High	Capable for EV charging

CHAPTER TWO

LITERATURE REVIEW

Wireless electric vehicle charging techniques have been popular for some time now due to their safety, convenience and efficiency. There are several ways to increase the WPT efficiency of a system. First is by the proposed Series–Series (SS) resonant compensation topology alongside the design of radio frequency feedback (Tan, 2017). This proposed model was experimented and tested with a 500W laboratory prototype and it was found that the efficiency was above 90%, an air gap was 15 cm, distance was 10 cm and over an operating input voltage of 120VAC (Tan, 2017). The second method used to enhance WPT efficiency is by varying the operating frequency ranging from 81.38-90 kHz, the duty ratio and input voltage respectively (Ravikiran, 2017). The other technique employed was by finding a reference voltage in the secondary side using the simultaneous estimation of the secondary side's mutual inductance and a voltage at the primary side (Hata, 2016). In addition, the compensation topologies play a key role in the power transfer efficiency, therefore, this paper gives a detailed comparison between the SS and PS compensation topologies (Ravikiran, 2017). Simulation results show that the PS topology is good for power applications of medium range. This paper uses secondary side LCC impedance matching circuit under a rectifier load to enhance the maximum efficiency transferred (Liao, 2017).

To keep up with the pace of battery capacities, it is essential to increase the rate at which an electric vehicle battery is wirelessly charged. One of the ways of increasing battery performance is by designing the coupling factor of the coil system appropriately and ensuring that the rate of displacement is large (Klaus, 2017). Another way to increase the power transfer system of an electric vehicle is to use two extra coils in between the transmitter and the receiver coils with experimental verification with a 6.6KW circuit (Tran, 2018). This results in an efficiency of 97.08% for 3.4KW. For different challenges associated with WPT to be addressed, this paper proposed employing an

improved floor surface for shielding the transmitting coil area, high-frequency switches with large bandgap switches and polygon iron core (Mahmud, 2017). These components help to improve the system's efficiency.

Subsequently, a wireless power charging system requires a constant current flow and output voltage alongside a maximum efficiency. This leads to the design of a control based maximum efficiency tracking system that controls the transmitter current based on the information the receiver receives via Bluetooth (Yeo, 2017). This gives a constant output voltage and constant current flow with increased efficiency in the WPT system. A fixed voltage source and fixed current load are modeled, analyzed and verified experimentally to increase the wireless power charging system's efficiency (Zhang, 2017). The voltage transmitted in a wireless power transfer depends on the distance between two coils. This paper implements a proportional integral controller at the receiver side of the wireless power transfer to eliminate the variation of voltage for a varied distance between the two coils (Yeo, 2017).

Furthermore, the high electromagnetic field generated between the transmitter coil and the receiver coil is detrimental to human life, hence the need to alleviate the magnetic field leakage between the coils. This high electromagnetic field leakage between the two coils is because of the large air gaps that occur between the transmitter coil and the receiver coil (Kim, 2016; Haque, 2018). One of the ways to lower the magnetic field leakage between the two coils is by designing a system that generates low magnetic leakage of about 19.8mG and high WPT efficiency of 96% over a 156mm air gap (Zhang, 2016). To lessen system loss, the transmitting coil was designed in a way to turn on or off while the EV is in motion (Cho, 2016) with an optimal receiving coil design ratio of radius 4, height 5 and distance 13 resulting to a 50% higher power transfer efficiency. The work of Cho investigated the relation between the coupling coefficient and the efficiency of Grouped Periodic Series Spiral Coupler (GPSSC) (Cho, 2016). Another way to reduce the electromagnetic field leakage between the transmitter and the receiver and at the same time increase the power transfer

efficiency is to use metamaterials, which help to concentrate the magnetic field (Dolara, 2017). A metamaterial was designed in this paper which showed that efficiency was increased to about 44.2% and magnetic leakage decreased to about 3.49dBm over 20 cm distance.

Also, for the risk associated with exposure to an electromagnetic field of the power pad of an electric vehicle to be decreased, a magnetic shielding technique was introduced using conductive panels (Campi, 2017), and an aluminum plate and aluminum ring (Campi, 2017). Here in this work, there were considerations for the conducted emission in charging the electric vehicle wirelessly using the SS and LCC compensation topologies (Cho, 2016). Results show that SS topology reduces the conducted emissions of WPT (Cui, 2018).

Due to the high power transferred between the coils, there is a need to consider meeting the requirements of the electromagnetic safety (Hui, 2013). Results show that a person sitting in the car or behind the vehicle is minimally exposed to an electromagnetic field, therefore, meeting the electromagnetic safety requirements. Humans lying in the back of the car have a larger exposure to an electromagnetic field (Mandip, 2011). The work in Wang (2016) also considers the numerical study of the electromagnetic field generated by an EV wirelessly transferring power. There were considerations for the electromagnetic field generated in and out of the EV, various charging modes and alignment/misalignment of the coils and results compared with the ICNIRP safety level (Wang, 2016).

CHAPTER THREE

MAGNETIC RESONANCE WIRELESS POWER EV CHARGING

3.1 Methodology

Magnetic induction operates on the principle of a transmitting coil that generates a magnetic field and a receiving coil inside the magnetic field, which induces the current in the coils (Hui, 2013). Generally, this leads to a short range because of the measure of energy needed to deliver a magnetic field. Therefore, the non-resonant method is incompetent for longer distances making it waste more energy when transmitting over longer distances. The resonance here improves efficiency drastically by channeling the electromagnetic field to the receiving coil resonating at a matching frequency (Hui, 2013), thereby increasing the charging distance as compared to other methods, which make it have the highest potential in the future. It is important to note that due to resonance characteristics, power transfer affects objects operating at a matching frequency and has no effect on objects with nearly matching frequencies. (Hadley, 2007.)

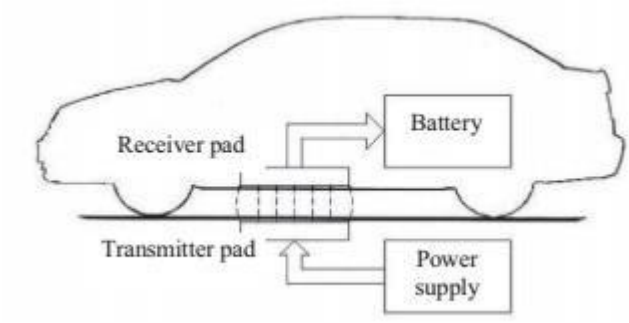

Figure 3-1 Wireless stationary vehicle charging (Hui, 2013)

The above figure shows a simple structure of the magnetic resonance coupling. The primary coils are used as a transmitting pad beneath the ground and the secondary coils are the receiver pad. There is an electric power transfer from the pad underneath the ground to the one mounted on the chassis of the vehicle without there being any contact with the two pads when the electric vehicle is parked

at a fixed place (Bahareh, 2018). The resonant compensation helps to remove the great inductance leakage, and the small coupling to transfer power productively (Ching, 2017). The main compensation structures for magnetic resonant WPT method are PP, SS, PS-SP networks (Zhang, 2016).

Furthermore, the method is explained with the principle of a vibrating tuning fork, which is an application of the sound resonance. When a coil vibrates, the surrounding coil, having the same natural frequency, is excited thereby producing energy for charging the electric vehicle.

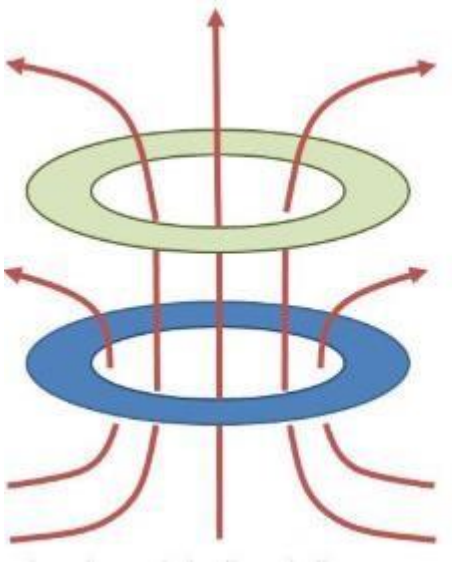

Figure 3-2 Magnetic Resonance Operation technique

Advantages

High frequency

High power

Longer charging distance

Disadvantages

Its big size

3.2 Magnetic Resonance System Model

Investigation of the model is done by defining the different types of resonant circuits and the corresponding equivalent circuit.

3.2.1 Resonant Circuits

There are two types of resonance circuits namely:

Series Resonance

Parallel Resonance

3.2.2 Series Resonance

In this circuit, the inductor (L), Capacitor (C) and Resistor (R) are all connected in a series, which is referred to as a series LCR circuit. The illustration of the LCR circuit is in the figure below.

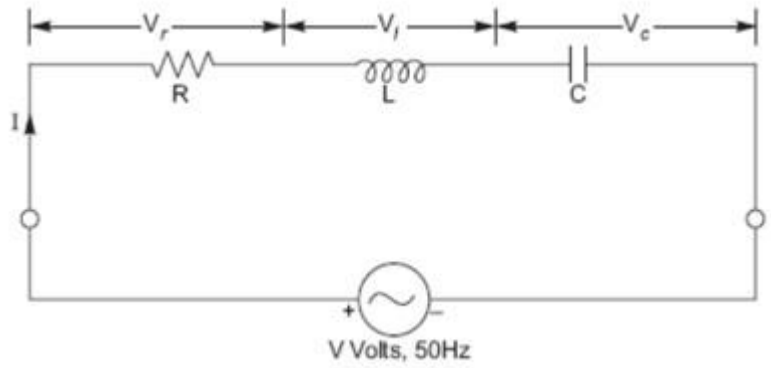

Figure 3-3 Series RLC circuit connected to a voltage source

The impedance Z measured in ohms of the circuit is as follows:

$$Z = R + j\,\omega L + \frac{1}{j\omega C} \text{.....3.1}$$

Where R is resistance measured in ohms; L is inductor measured in Henry; C is capacitance measured in Farad; ω is an angular frequency of the applied voltage measured in rad/sec.

Resonance takes place when the average electromagnetic energy stored in the Inductor (Wm) is equal to the average electric energy stored in Capacitance (We) (Gao, 2016).

$$W_m = \frac{1}{4}|I|^2 L \text{.....3.2}$$

$$W_e = \frac{1}{4}|I|^2 \frac{1}{\omega^2 C} \text{.....3.3}$$

At Resonance, $W_e = W_m$, and Z_{in}=R

$$\omega_o = \frac{1}{\sqrt{LC}} \text{.....3.4}$$

The quality factor (Q)

The measurement of the losses occurs in a resonant circuit. Calculation of Q is as follows:

$$Q = \omega_o \frac{stored\ energy\ in\ L\ and\ C}{average\ power\ dissipated} \text{.....3.5}$$

$$= \omega_o \frac{W_m + W_e}{P_{loss}} \text{.....3.6}$$

Where $Power_{loss}$ is the power the resistor R dissipates

$$Power_{loss} = \frac{1}{2}|I|^2 R \text{.....3.7}$$

At Resonance,

$$Q = \omega_o \frac{2W_e}{P_{loss}} \text{.....3.8}$$

$$= \omega_o \frac{2.\frac{1}{4}|I|^2 L}{\frac{1}{2}|I|^2 R} \text{.....3.9}$$

$$Q = \frac{\omega_o L}{R} \text{……..3.10}$$

$$Q = \omega_o \frac{2W_m}{P_{loss}} \text{……...3.11}$$

$$Q = \omega_o \frac{2.\frac{1}{4}|I|^2 \frac{1}{\omega_o{}^2 C}}{\frac{1}{2}|I|^2 R} \text{…….....3.12}$$

$$Q = \frac{1}{\omega_o RC} \text{……..3.13}$$

3.2.3 Parallel Resonance

Here, energy is stored in the inductor and capacitor, in which a transfer of this energy is like that of the series resonance circuit.

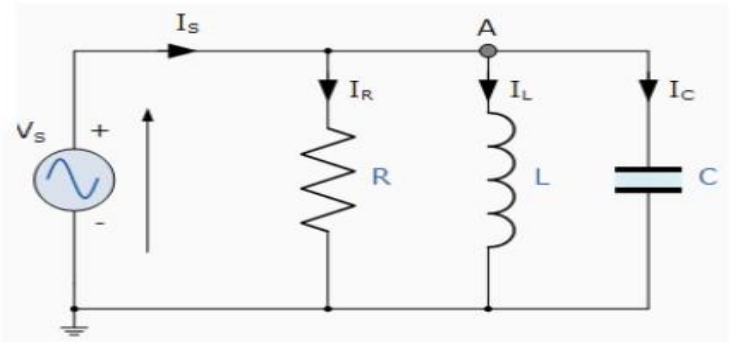

Figure 3-4 Parallel RLC circuit connected to a voltage source

Ideally, in a half cycle of the power curves, the rate at which the capacitor absorbs energy is equal to the rate the inductor releases energy. In the other half cycle, it is reversed i.e. the rate at which the inductor absorbs energy is equal to the rate the capacitor releases energy. Therefore, at resonance, the total reactive power is equal to zero.

$$Z_{in} = \left(\frac{1}{R} + j\omega c + \frac{1}{j\omega L}\right)^{-1} \text{…….3.14}$$

$$P_{loss} = \frac{1}{2}\frac{|V|^2}{R} \text{…….3.15}$$

$$W_m = \frac{|V|^2}{4\omega^2 L} \text{……...3.16}$$

$$W_e = \frac{1}{4}|V|^2 C \text{.....3.17}$$

At resonance, $W_e = W_{m,}$ and Z_{in}=R

$$\omega_o = \frac{1}{\sqrt{LC}} \text{.....3.18}$$

$$Q = \omega_o \frac{2W_m}{P_{loss}} \text{.....3.19}$$

$$Q = \omega_o \frac{2.\frac{1}{4}|V|^2 \frac{1}{\omega_o{}^2 L}}{\frac{1|V|^2}{2\ R}} \text{.....3.20}$$

$$Q = \frac{R}{\omega_o L} \text{.....3.21}$$

$$Q = \omega_o \frac{2W_e}{P_{loss}} \text{.....3.22}$$

$$Q = \omega_o \frac{2.\frac{1}{4}|V|^2 C}{\frac{1|V|^2}{2\ R}} \text{.....3.23}$$

$$Q = \omega_o RC \text{.....3.24}$$

3.3 Equivalent Circuit

Magnetic resonance wireless power transfer occurs at the point where the transmitter and the receiver coil are in resonance (Sample, 2011). This resonance is of two types; the first is self-resonance controlled by the self-inductance and self-capacitance of the coils and the second is external and excited resonance, which is controlled by the self-inductance and the installed capacitance of the coil (Etacheri, 2011).

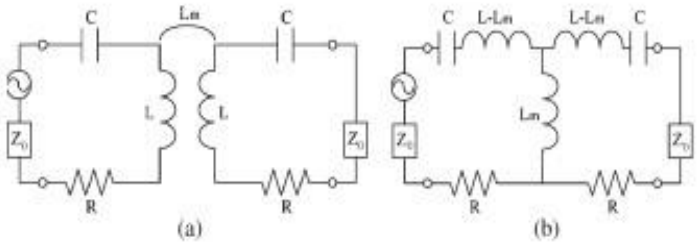

Figure 3-5 Magnetic Resonance Equivalent Circuit

From the circuit above, at resonance, the reactance is equal to zero as in the equation below:

$$\frac{1}{\omega L_m} + \frac{2}{\omega(L-L_m)-\frac{1}{\omega C}} = 0 \text{……3.25}$$

$$W_m = \frac{\omega_o}{\sqrt{1+k}} = \frac{1}{(\sqrt{L+L_m})+C} \text{…….3.26}$$

$$W_e = \frac{\omega_o}{\sqrt{1-k}} = \frac{1}{(\sqrt{L-L_m})+C} \text{……3.27}$$

$$K = \frac{L_m}{L} = \frac{w_e^2 - w_m^2}{w_e^2 + w_m^2} \text{……..3.28}$$

3.4 Efficiency

The efficiency calculation is done by using the reflection and transmission coefficient respectively:

$$\eta_{11} = S_{11}^2 \times 100\% \text{.....3.29}$$

$$\eta_{21} = S_{21}^2 \times 100\% \text{.....3.30}$$

$$S_{21}^2 = \frac{2jL_m Z_o \omega}{L_m^2\omega^2 - \left(\omega L - \frac{1}{\omega C}\right)^2 + 2jZ_o\left(\omega L - \frac{1}{\omega C}\right) + Z_o^2} \text{....3.31}$$

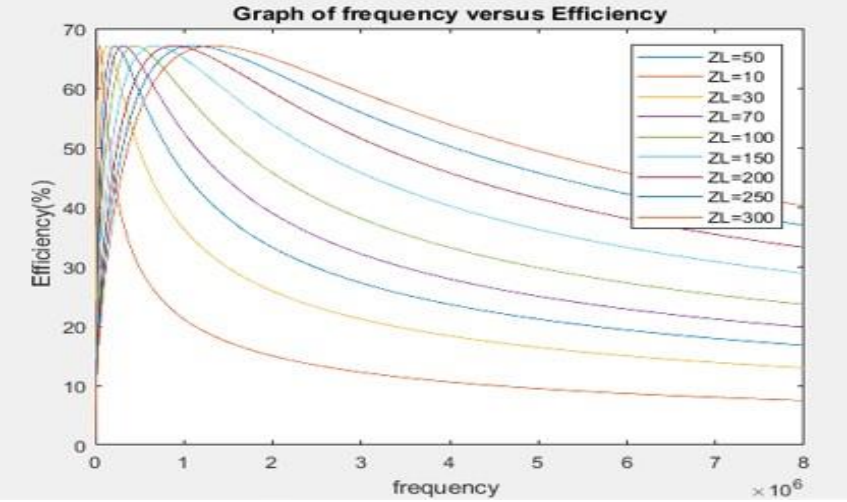

Figure 3-6 Graph of a Varying Load keeping other Parameters Constant

From figure 3-6, when the load (ZL) is varied, the efficiency value remains constant but the frequency increases as the load increases.

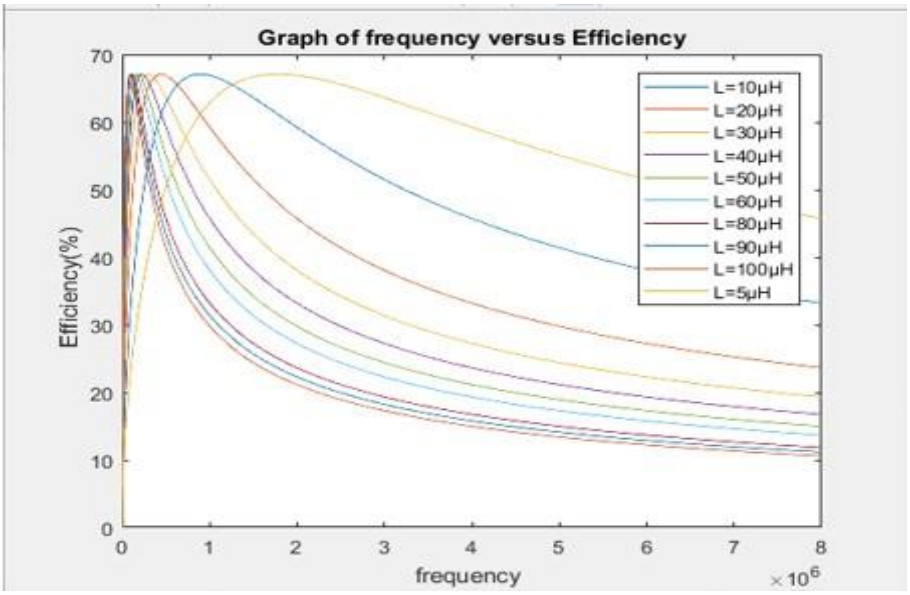

Figure 3-7 Graph of a Varying Inductor keeping other Parameters Constant

Figure 3-7 indicates that when the inductor value (L) is varied, the efficiency value remains constant but the frequency increases as the inductor decreases.

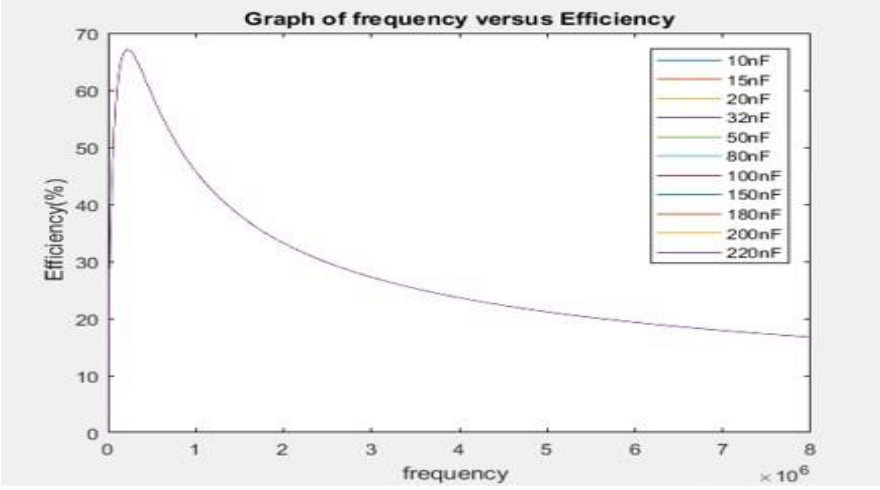

Figure 3-8 Graph of a Varying Capacitor keeping other Parameters Constant

From figure 3-8, the change in the capacitor value does not have any effect on efficiency and frequency.

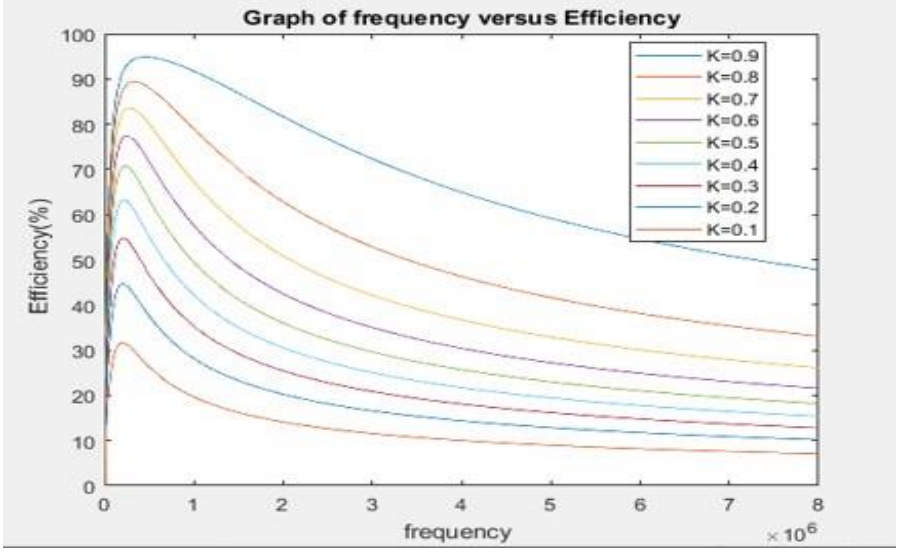

Figure 3-9 Graph of a Varying Coupling Coefficient keeping other Parameters Constant

From figure 3-9 above, the frequency remains the same as the coupling coefficient (K) varies while the efficiency increases with an increase in the coupling coefficient (K).

CHAPTER FOUR

INTRODUCTION

4.1 3D Modeling of a Transmitter and Receiver Coil

The 3D modeling of a transmitter and receiver coil is designed by using ANSYS Maxwell software. Both coils consisted of copper for high electrical conductivity and placed 100 mm apart. Between the transmitting and the receiving coils is a transparent rectangular plate placed to capture the magnetic field that exists between both coils. Two lids connect to each of the transmitting and receiving coils respectively for current excitation. The lid consists of copper of 500 mm length and 1mm thickness. A region of 1000mm^3 composed of air where simulations will take place. The solving of ANSYS Maxwell is done by creating a boundary to place the two coils. The figure below shows the transmitting coil and the receiving coil in ANSYS Maxwell. The two coils consist of equal dimensions to give a better coupling coefficient.

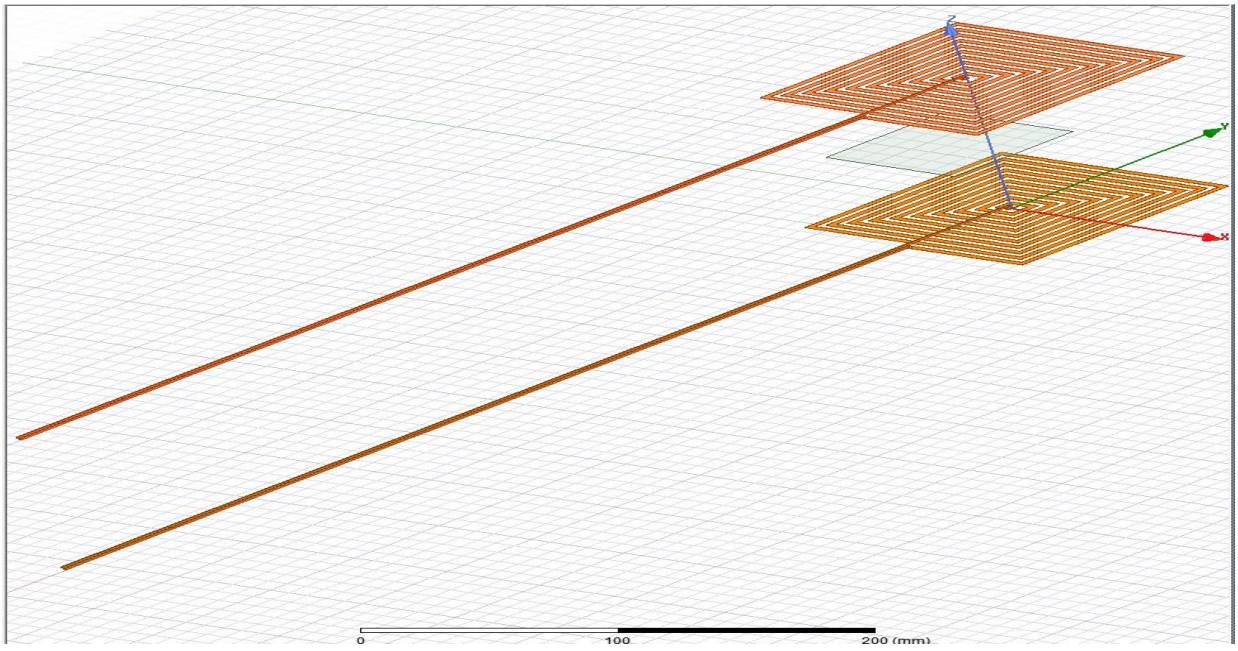

Figure 4-1 Design of a transmitter coil and receiver coil

Table 2: Property of the Coil

Name	Value	Unit	Evaluated Value	Description
Version	2.0			
Xpos	0	Mm	0mm	X Position of a start point
Ypos	0	Mm	0mm	Y Position of a start point
Distance	6	Mm	6mm	Distance between turns
Turns	10			Number of turns
Width	3	Mm	3mm	The width of the spiral coil
Thickness	3	Mil	3mil	Thickness of the spiral coil

Table 3 Property of the rectangular plate

Name	Value	Unit	Evaluated Value
Command	CreateRectangle		
Coordinate System	Global		
Position	50, 0, 70	Mm	50mm, 0mm, 70mm
Axis	Z		
XSize	-70	Mm	-70mm
YSize	-70	Mm	-70mm

4.2 Simulations and Results

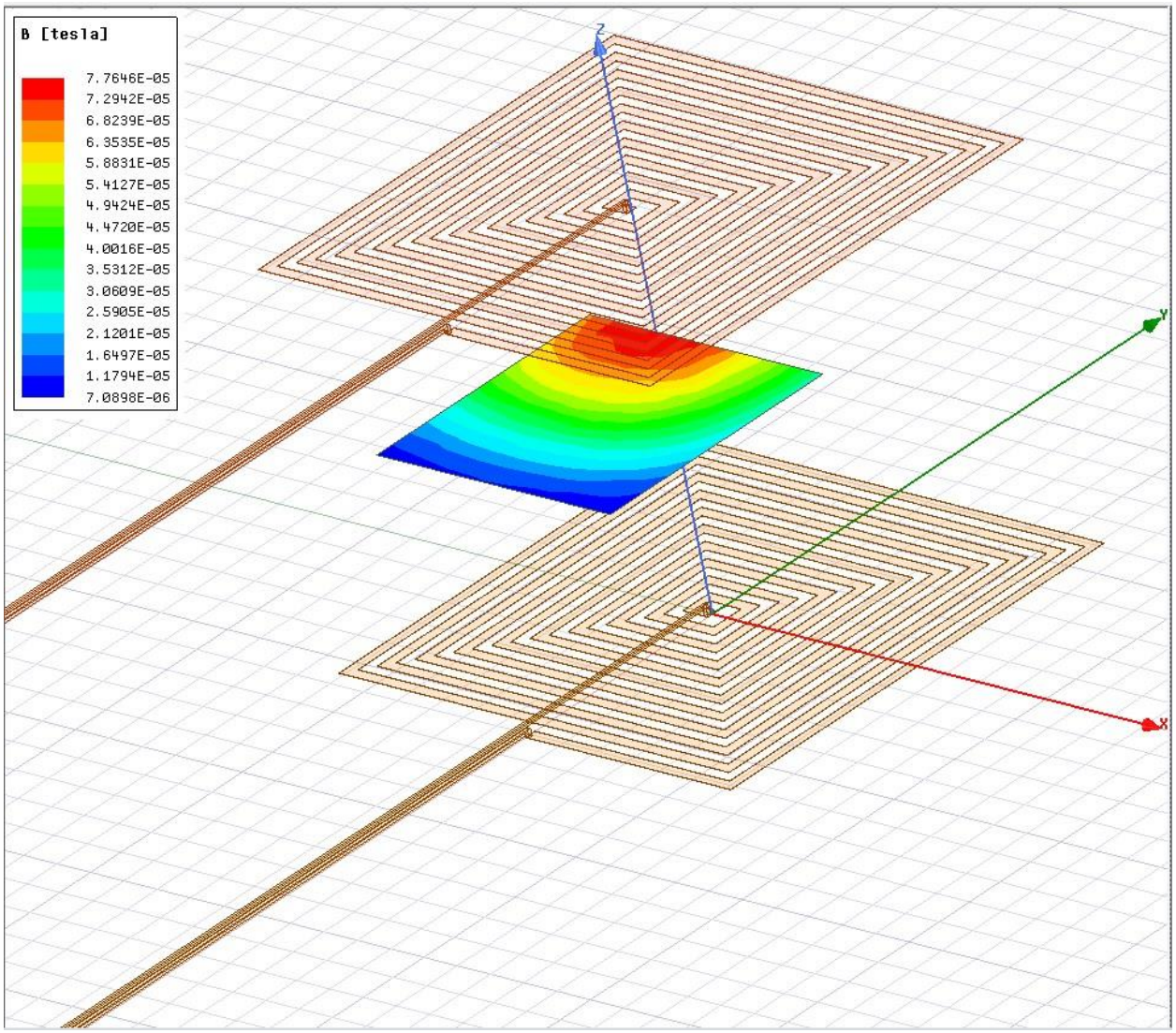

Figure 4-2 Magnetic field between the transmitter and receiver coil

From Figure 4-2, the magnetic field between both coils decreases as the distance between them increases.

Table 4 Magnetic field between the transmitter and receiver coil

	Z_Space [mm]	CpCoef [Receiver_in, Receiver_in] Setup1: Last Adaptive	CpCoef [Receiver_in, Transmitter_in] Setup1: Last Adaptive	CpCoef [Transmitter_in, Receiver_in] Setup1: Last Adaptive	CpCoef [Transmitter _in, Transmitter _in] Setup1: Last Adaptive
1	30.000000	1.000000	0.284473	0.284473	1.000000
2	50.000000	1.000000	0.155227	0.155227	1.000000
3	60.000000	1.000000	0.117961	0.117961	1.000000
4	90.00000	1.000000	0.056590	0.056590	1.000000
5	100.00000	1.000000	0.045229	0.045229	1.000000
6	120.00000	1.000000	0.029556	0.029556	1.000000
7	150.00000	1.000000	0.016671	0.016671	1.000000
8	180.00000	1.000000	0.009991	0.009991	1.000000
9	191.00000	1.000000	0.008307	0.008307	1.000000
10	200.00000	1.000000	0.007300	0.007300	1.000000
11	210.00000	1.000000	0.006267	0.006267	1.000000
12	240.00000	1.000000	0.004076	0.004076	1.000000
13	250.00000	1.000000	0.003568	0.003568	1.000000
14	270.00000	1.000000	0.002730	0.002730	1.000000
15	300.00000	1.000000	0.001882	0.001882	1.000000

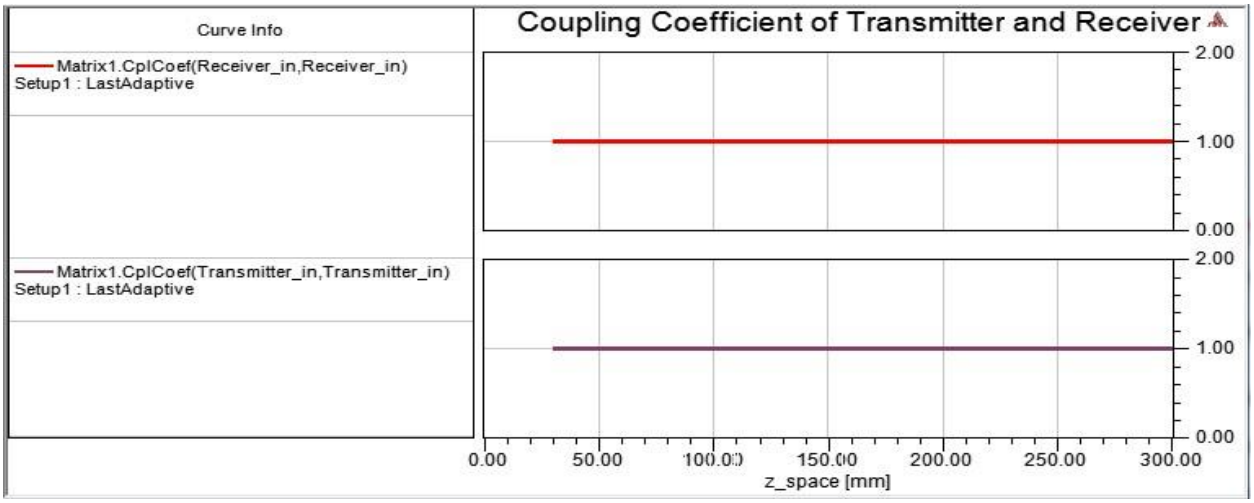

Figure 4-3 Coupling Coefficient of transmitter and receiver coil

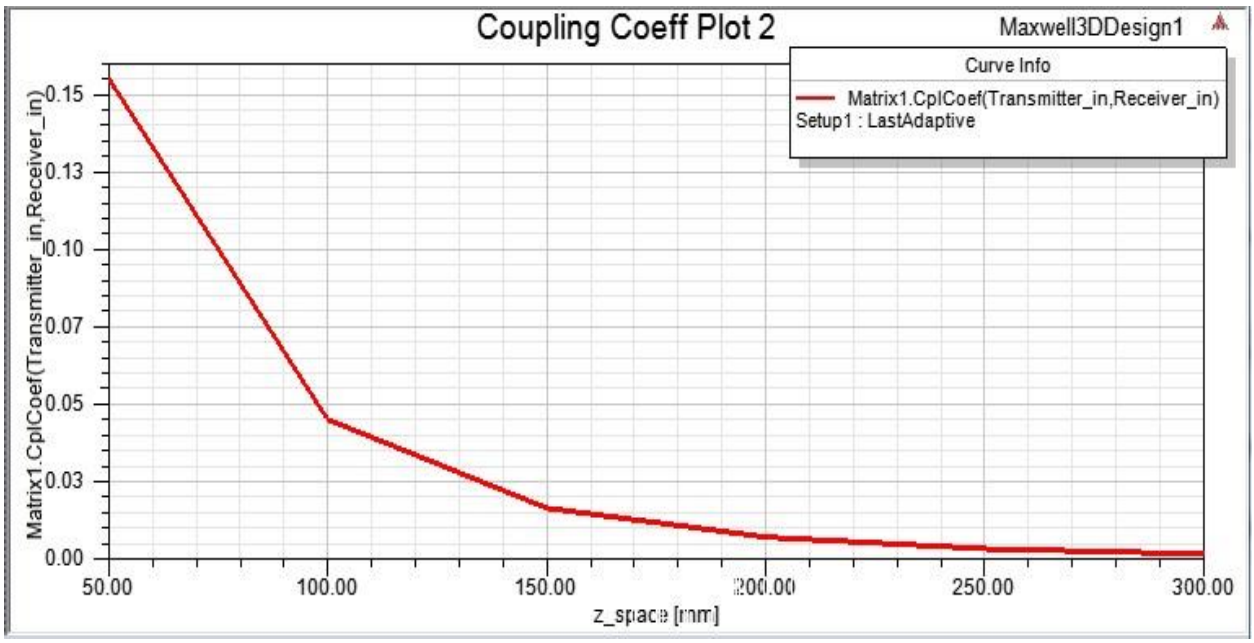

Figure 4-4 Coupling Coefficient versus Coil Spacing

From figure 4-3 and table 4, the coupling coefficient of the transmitting and the receiving coil respectively is 1 because it is self-coupling. Whereas, in figure 4-4, the coupling coefficient between the transmitting and the receiving coil increases as the spacing between them decreases.

Table 5 Mutual Inductance between the transmitting coil and receiving coil

	Z_Space [mm]	L [Receiver_in, Receiver_in] (µH) Setup1: Last Adaptive	L [Receiver_in, Transmitter_in] (µH) Setup1: Last Adaptive	L [Transmitter_in, Receiver_in] (µH) Setup1: Last Adaptive	L [Transmitter _in, Transmitter _in] (µH) Setup1: Last Adaptive
1	30.000000	6.378196	1.817564	1.817564	6.400302
2	50.000000	6.398163	0.995023	0.995023	6.422134
3	60.000000	6.408632	0.755501	0.755501	6.400730
4	90.00000	6.341927	0.358898	0.358898	1.342253
5	100.00000	6.343862	0.286646	0.286646	1.331533
6	120.00000	6.360355	0.188060	0.188060	1.365229
7	150.00000	6.364445	0.106292	0.106292	1.387313
8	180.00000	6.379554	0.063594	0.063594	1.350325
9	191.00000	6.364191	0.052773	0.052773	1.340904
10	200.00000	6.349465	0.046385	0.046385	1.359150

11	210.00000	6.368840	0.039894	0.039894	1.362270
12	240.00000	6.369742	0.025961	0.025961	1.369609
13	250.00000	6.342104	0.022648	0.022648	1.351861
14	270.00000	6.372692	0.017413	0.017413	1.384442
15	300.00000	6.355842	0.011961	0.011961	1.355262

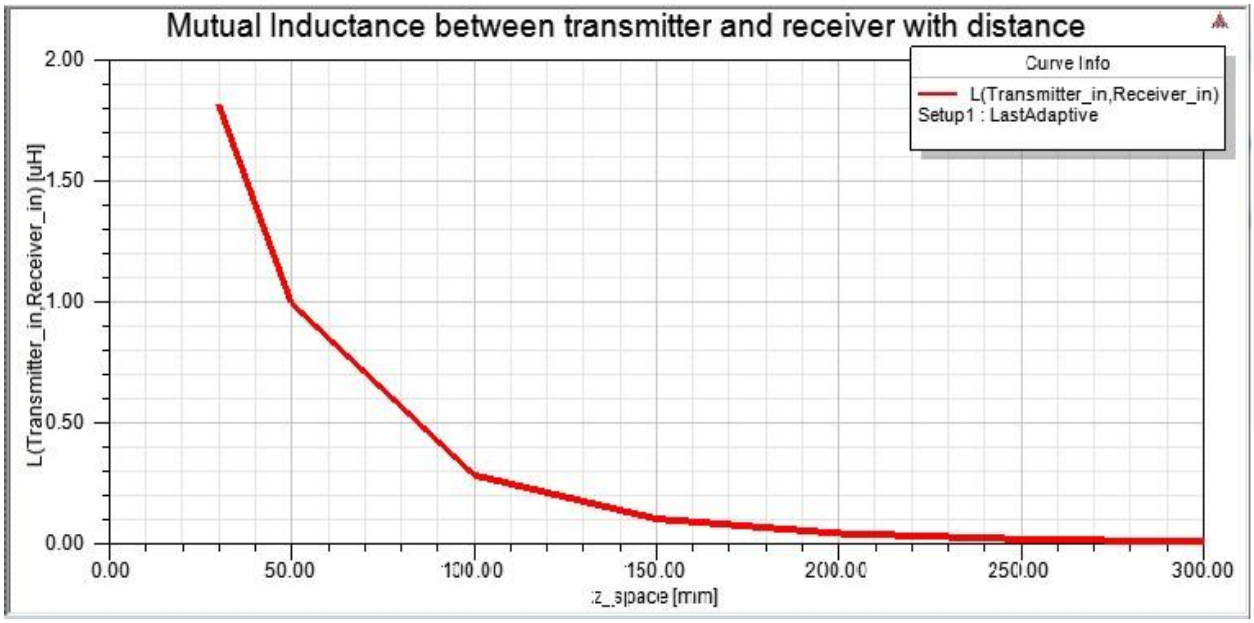

Figure 4-5 Mutual Inductance between transmitting coil and receiving coil

From the figure 4-5 and table 5, it is also noticeable that the amount of mutual inductance between the transmitting coil and the receiving coil slightly changes since each is the sum of its own self-inductance and the mutual inductance of the other coil. As the other coil gets closer due to the direction of the excitation current defined, the value slightly fluctuates because there is still some flux present.

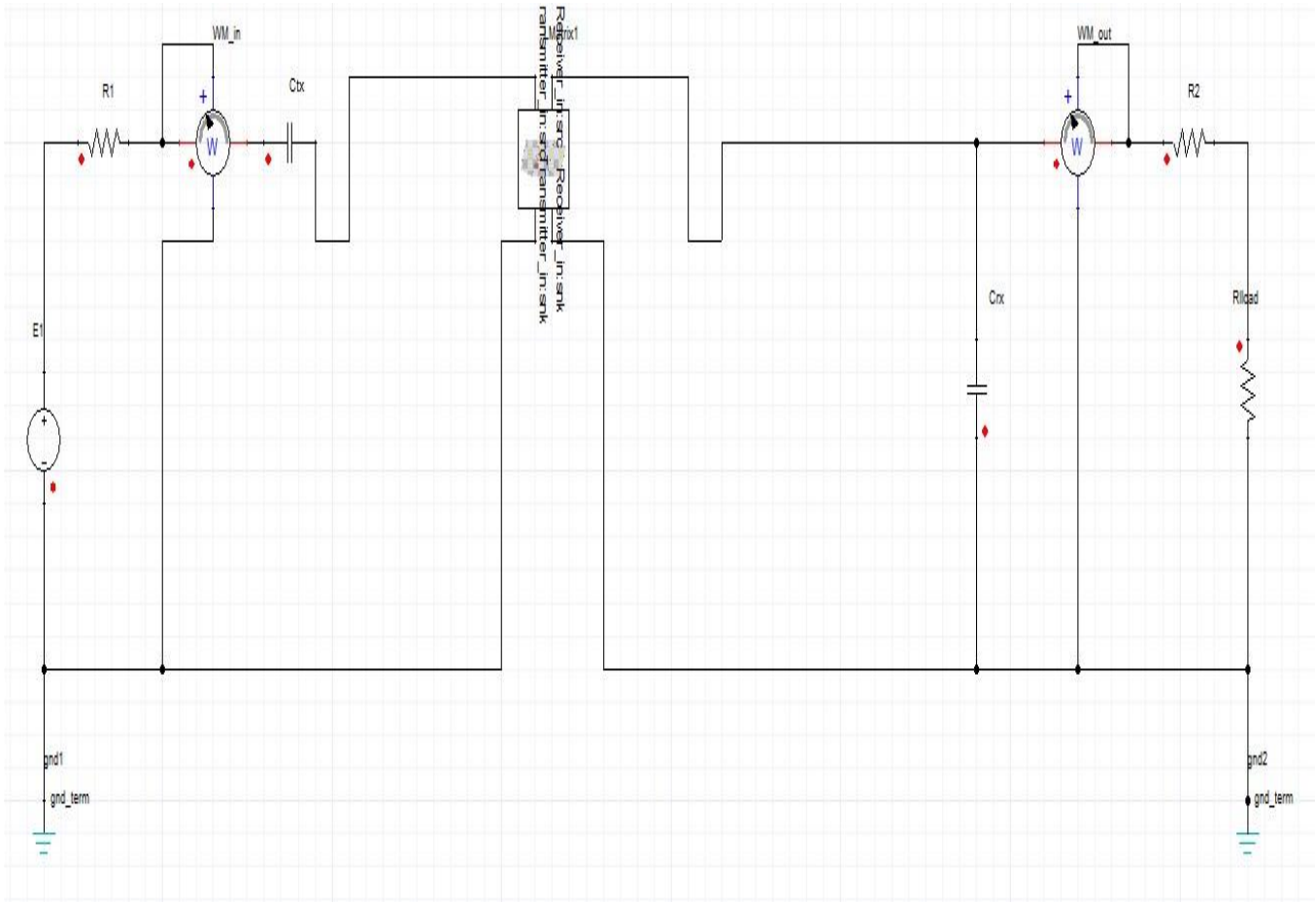

Figure 4-6 Incorporation of the Circuit design with Physical design of Magnetic Resonance Coupling

The design of the system circuit is created in ANSYS Simplorer while the design of the transmitting and the receiving coils is created in ANSYS Maxwell. This Maxwell design held the dynamic inductance information about the coil structure and imported the Simplorer as L parameters. At the transmitting side, the resonance capacitor is connected in series with the inductor to have maximum current flowing through the inductor, hence, maximum power is delivered to the transmitter. At the receiving side, the capacitor was connected in parallel with the inductor to have a maximum voltage drop on the load resistor.

An AC analysis needs to be set up to determine the efficiency of the system. Below I have shown the parameters for the analysis.

Table 6. Parameter values

Parameters	**Value**
Voltage	280V
Frequency	6.5KHz
R_1	9.8μΩ
R_2	9.8μΩ
C_{rx}	20μF
C_{tr}	20μF
R_{Load}	50Ω

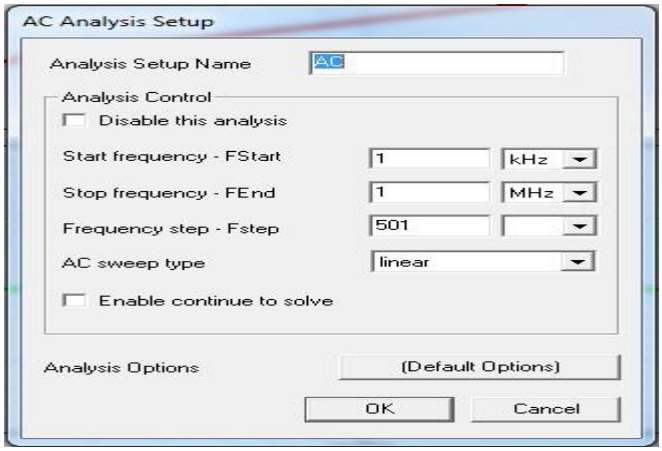

Figure 4-7 Ac Analysis set up Values

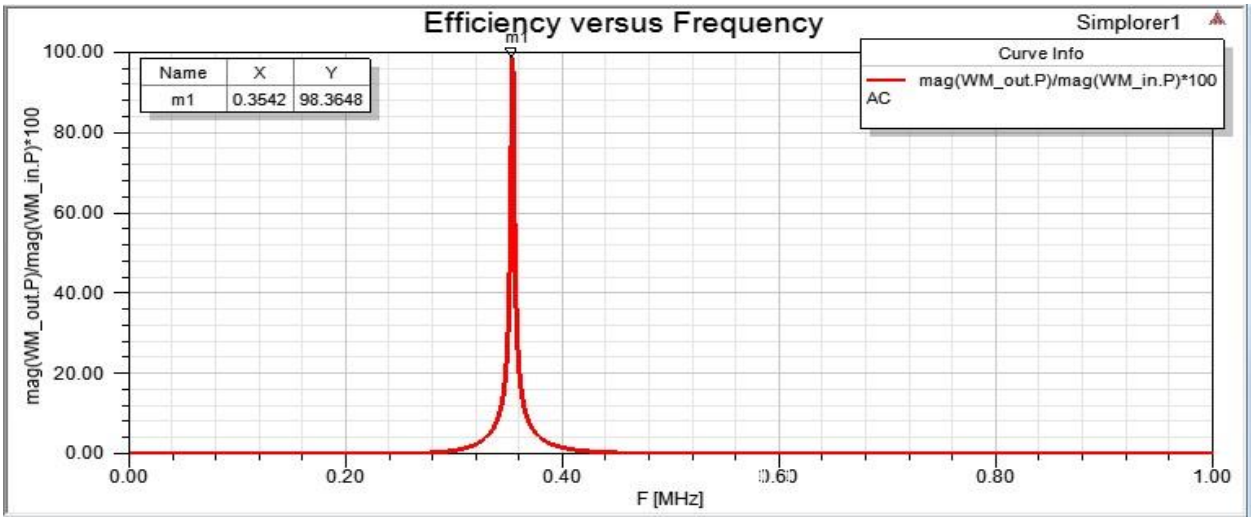

Figure 4-8 Efficiency with Frequency

From figure 4-8, the system's efficiency reaches its peak of about 98.3% at a resonance frequency of 0.35 MHz. At any frequency apart from the resonance frequency, the efficiency reduces. This indicates that the magnetic resonance method is a very efficient way of transferring power wirelessly over a mid-range distance.

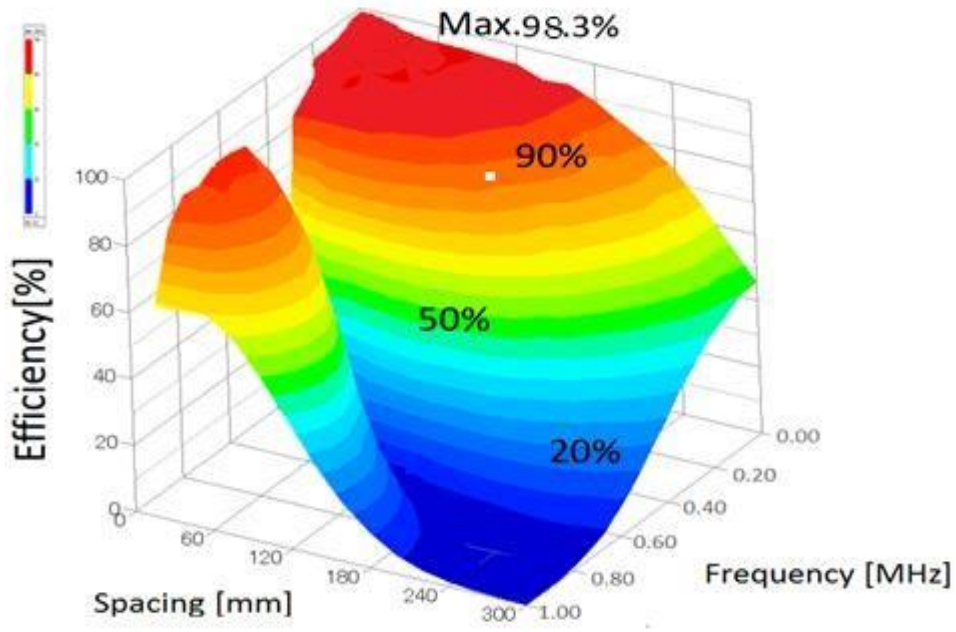

Figure 4-9 3D Rectangular Plot of Efficiency with spacing and frequency

In addition, the 3D rectangular plot helps to verify the efficiency of the system with respect to the spacing between the coils and its operating frequency produced at 98.3%.

The transient analysis is set up to determine the frequency analysis of the system. Below are the values for the setup.

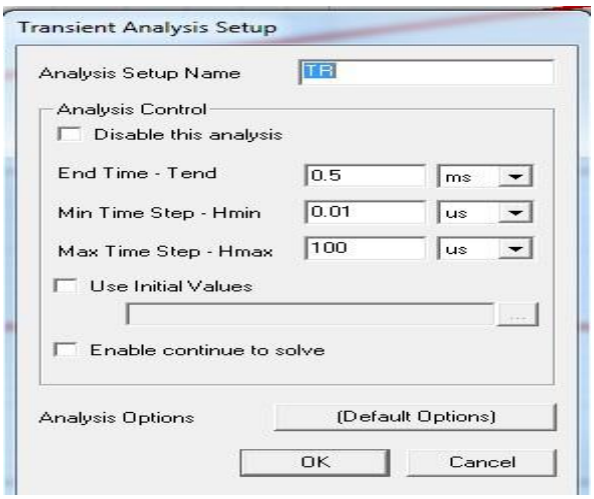

Figure 4-10 Transient Analysis Setup Values

Figure 4-11 Bode plot of efficiency with spacing

Figure 4-12 Bode plot of Input Power with Spacing

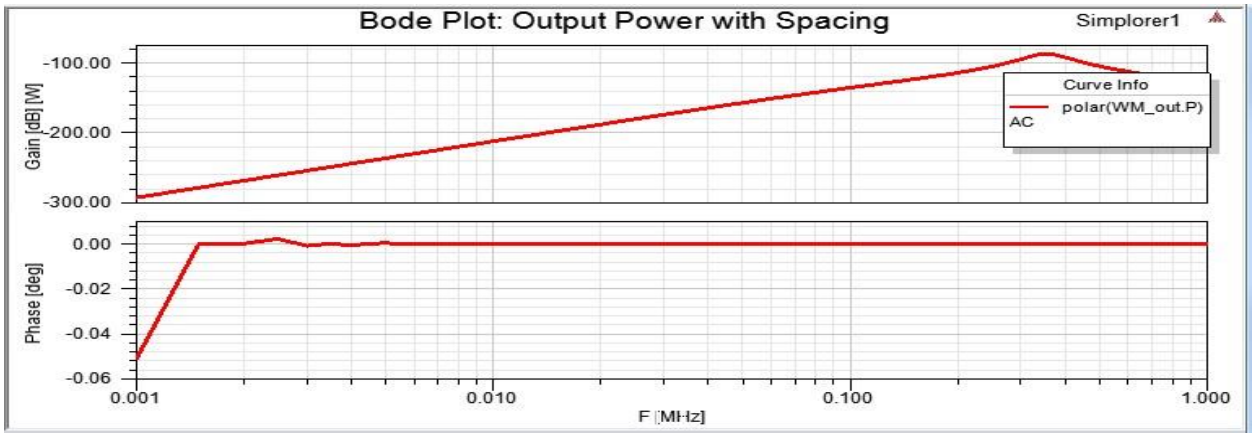

Figure 4-13 Bode plot of Output Power with Spacing

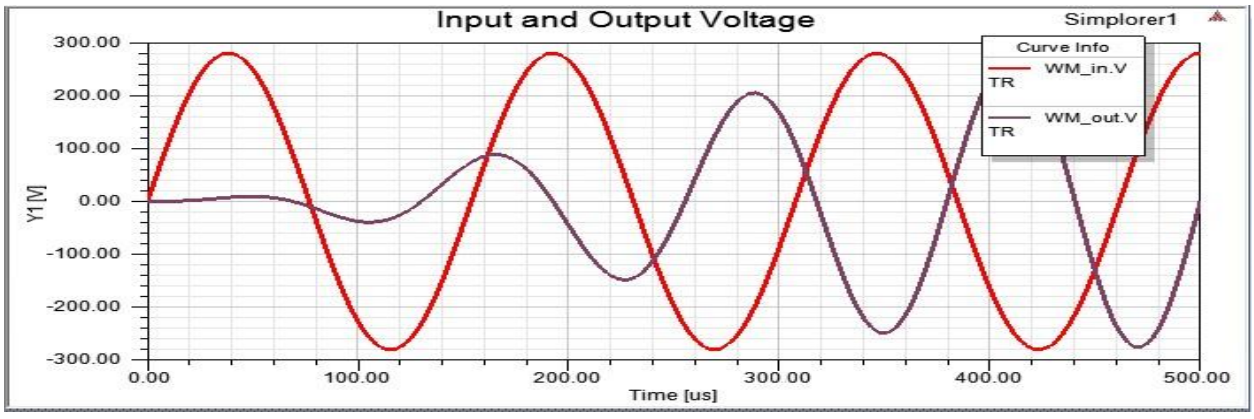

Figure 4-14 Input and output voltage

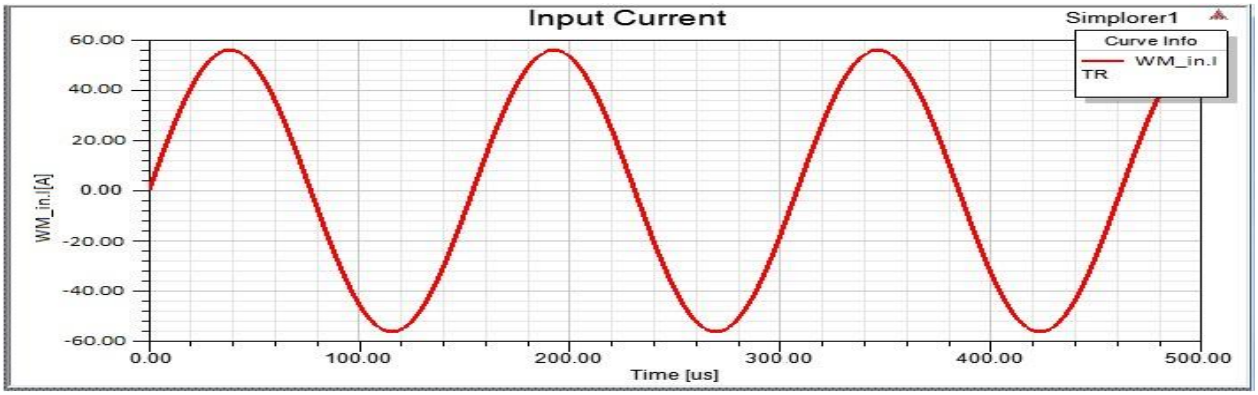

Figure 4-15 Input current

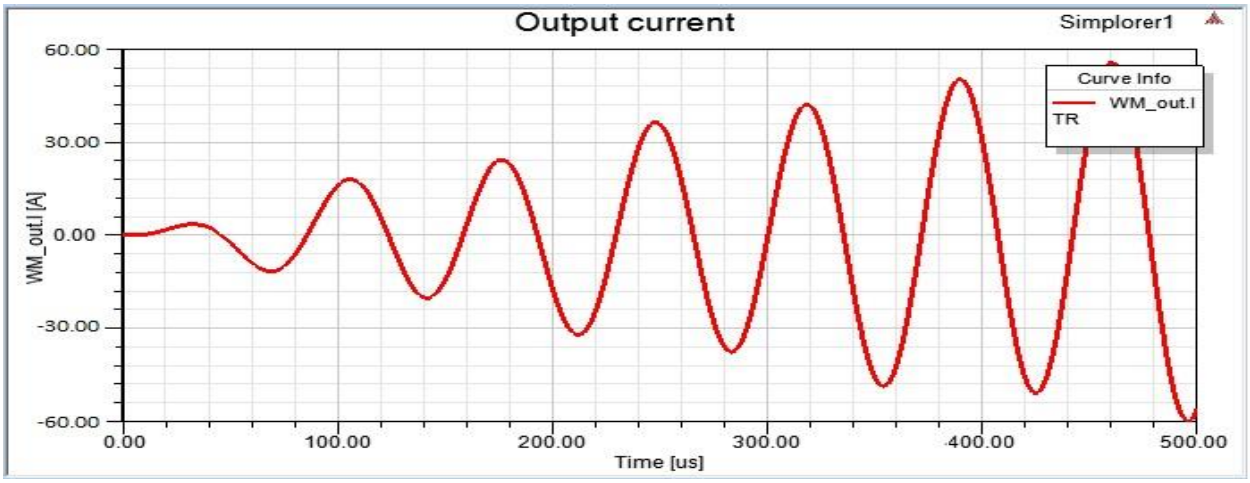

Figure 4-16 Output current

Figures 4-14 to 4-16 show that the input/output voltage and current give a sinusoidal wave. The input current gives 56A (39.9A RMS), the output current gives 52.9A (37.41A RMS), the input voltage is 280 V (198.02V RMS) and output voltage result is 279 V (197.31V RMS).

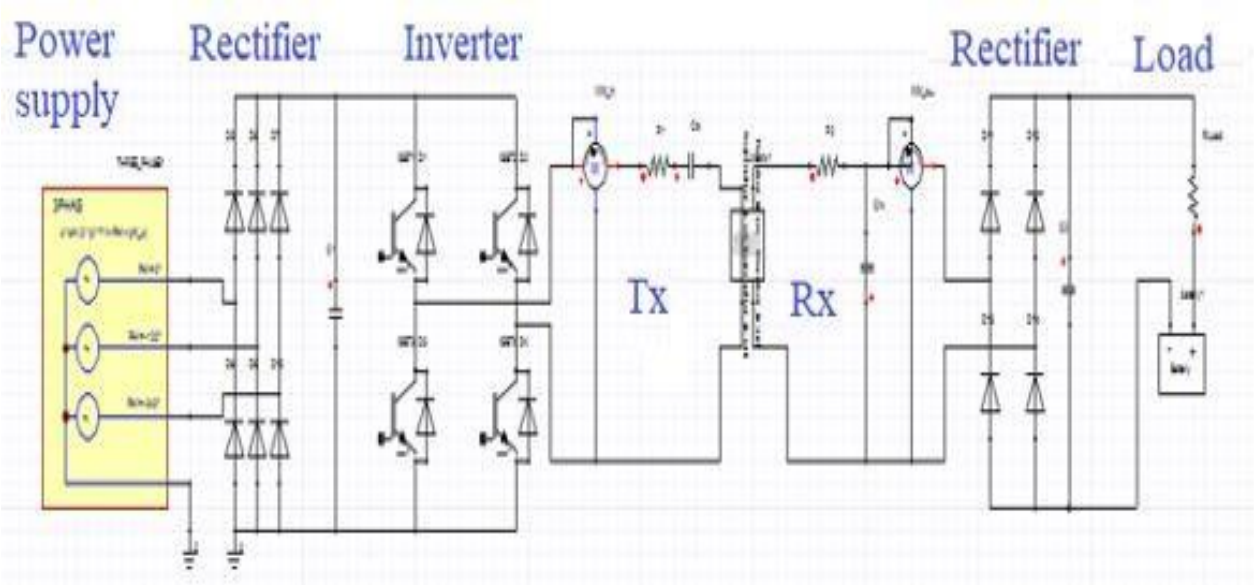

Figure 4-17 Complete magnetic resonance WPT circuit

Table 7 Parameter values for the complete design

Parameters	**Value**
3 phase Voltage	280V
Frequency	10KHz
C_1	900µF
C_2	7µF
R_1	7.1mΩ
R_2	4mΩ
C_{tx}	1.6µF
C_{rx}	4.7µF
R_{Load}	50Ω

Figure 4-17 shows the complete system of a magnetic resonance WPT circuit designed in Maxwell. The circuit consists of a power supply source, rectifier, inverter, transmitting coil, receiving coil, and a load. The power supply, which is an AC source, needs to pass through the rectifier and then be converted back to AC by an inverter because the coils need an AC voltage to operate. The reason why the AC supply passes through the rectifier first is that, the AC voltage from the grid is not suitable for the transmitting and receiving coils. From the formula $Z_c=1/jwc=-jwc$, the

capacitance value might be too small or too big. This then goes into the rectifier to convert it to DC which is needed to charge the load (battery). This system is designed with an output power of 18KW.

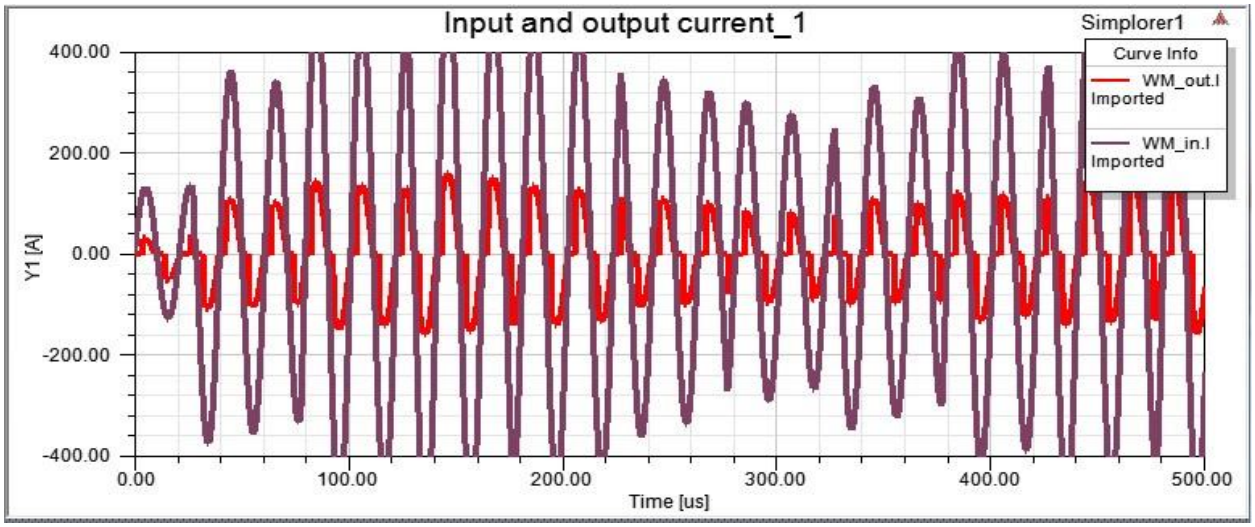

Figure 4-18 Input and output current

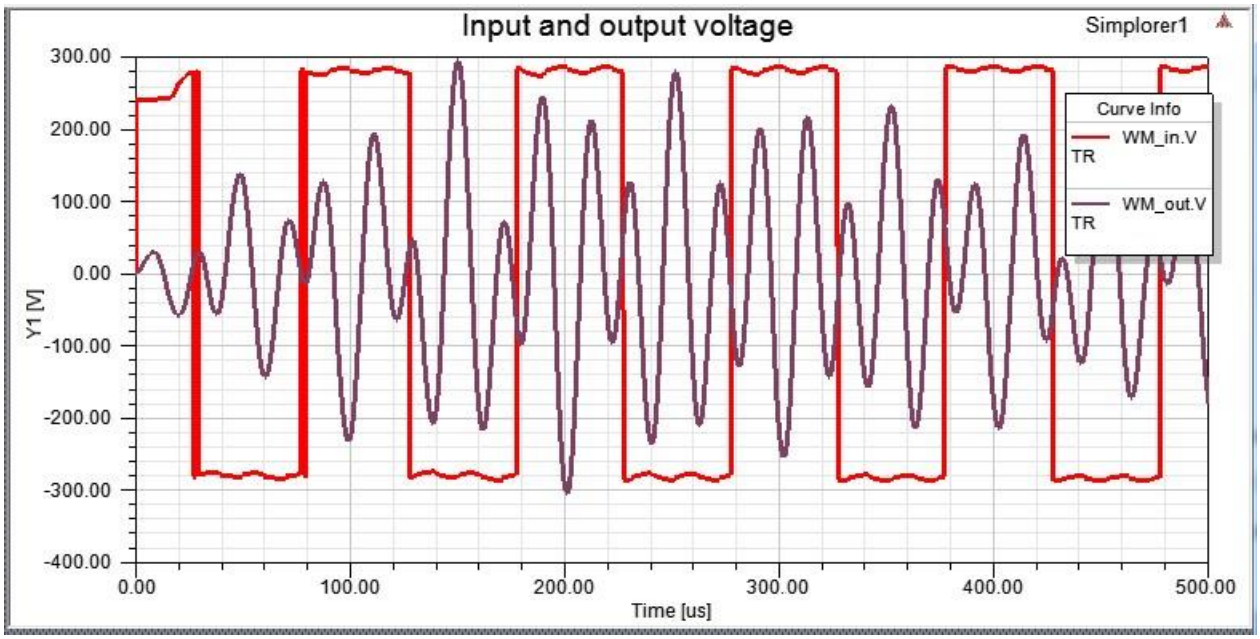

Figure 4-19 Input and output voltage

In figures 4-18 and 4-19, it can be observed that the input current is 390 A (275.9A RMS), the output current is 130 A (91.9A RMS), the input voltage is 280 V (198.02V RMS) and the output voltage is 240V (169.7
RMS).

4.3 Comparing with Magnetic Induction Power Transfer

In magnetic induction wireless power transfer, the current passes through the transmitting coil, which produces a varying magnetic field. This induces a current in the receiving coil which helps to charge the electric vehicle. Its power transfer efficiency depends on the closeness of the two coils.

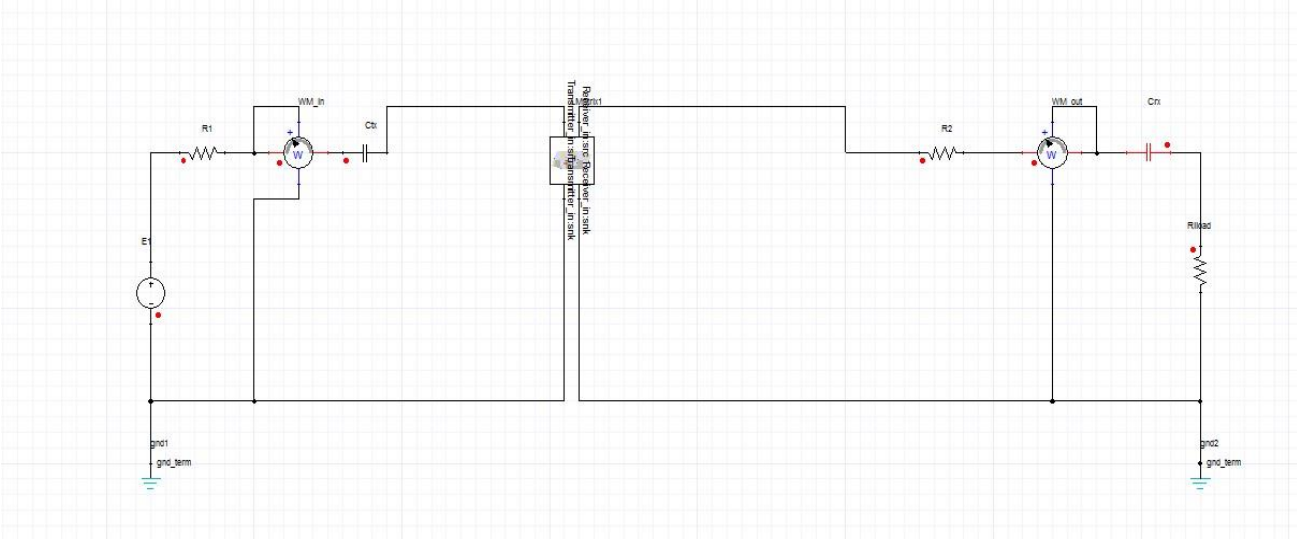

Figure 4-20 Incorporation of the Circuit design with Physical design of Magnetic Induction

Using the same coil design and parameters and keeping the same distance between both coils as in the magnetic resonance method, results show that the efficiency of the inductive coupling method reaches its peak at 60.145%. This confirms that wireless power efficiency is low in the inductive coupling method over large distances.

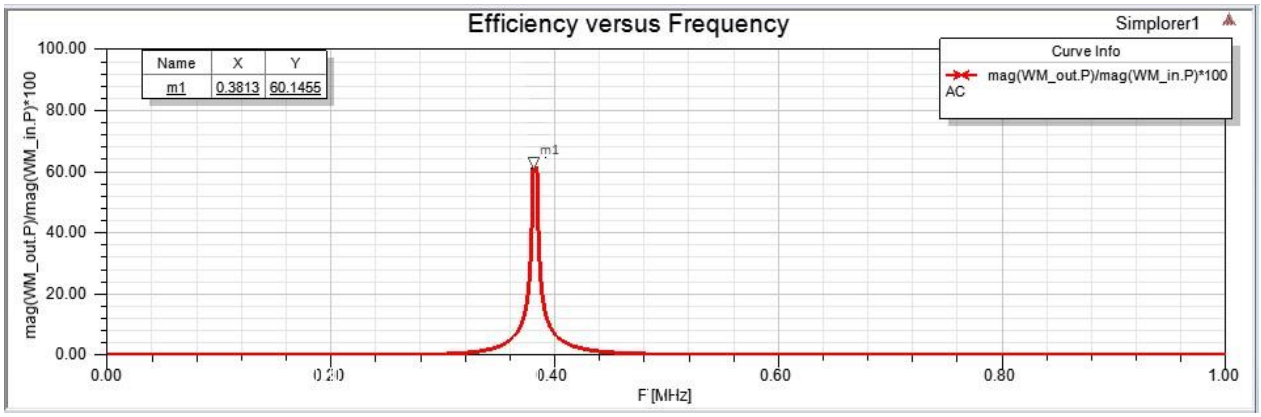

Figure 4-21 Efficiency with Frequency

Figure 4-22 Bode plot of Output Power with Spacing

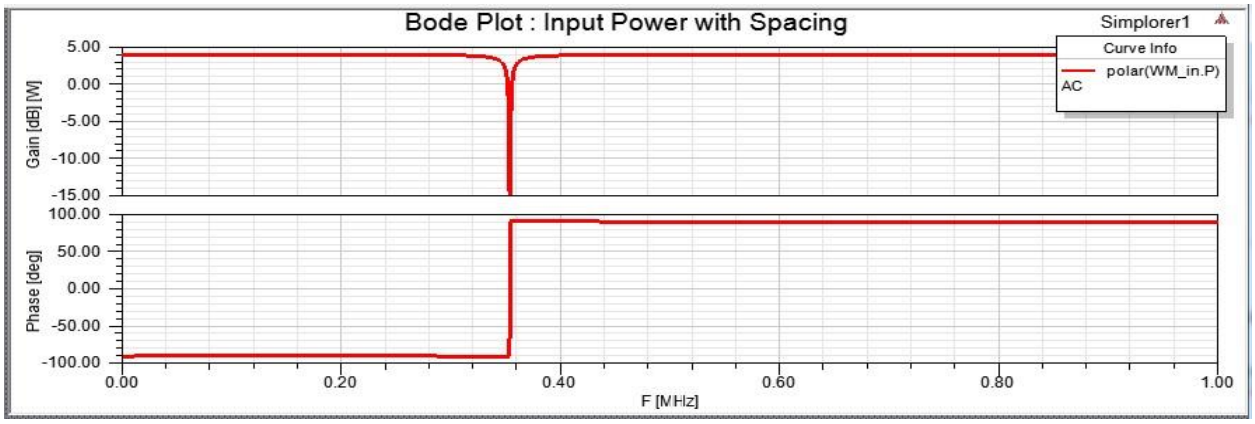

Figure 4-23 Bode plot of Input Power with Spacing

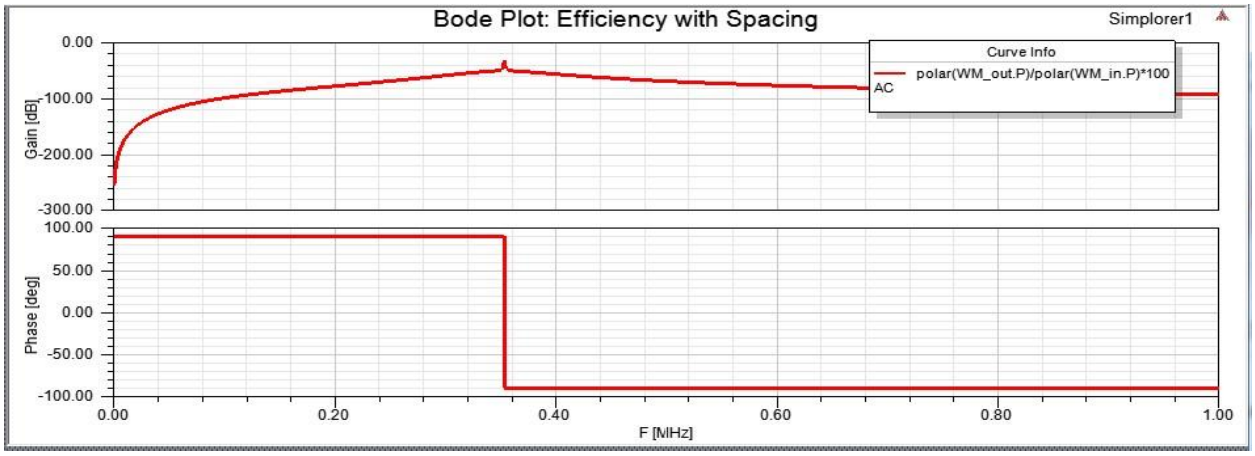

Figure 4-24 Bode plot of Efficiency with Spacing

4.4 Conclusion

This research delved into the effectiveness of the wireless-based resonance charging system through simulation results. The simulation results obtained from ANSYS Maxwell verify the effectiveness of the electromagnetic resonance technique. The energy transfer efficiency depends on the operating frequency. Results show that the energy transfer efficiency of a resonance-based wireless energy transfer system reaches the maximum (98.3%) at the resonant frequency. If the system is set at a frequency other than the resonance frequency, there is an abrupt drop in the energy transfer efficiency. Additionally, the design of a magnetic induction verifies the effectiveness of wireless power transfer with magnetic resonance over large distances as simulation results show that the efficiency of power transfer with the induction method over large distances is about 60%. Therefore, the magnetic resonance wireless charging is a more efficient method for charging the electric vehicle.

CHAPTER FIVE

DESIGN OF A THREE - LEVEL CASCADED PI CONTROLLER WITH MPPT FOR AN ELECTRIC VEHICLE DYNAMIC WIRELESS POWER TRANSFER.

5.1 Abstract

Overcoming the problem of short mileage and long charging time is important in putting the electric vehicle on a full-scale market. A dynamic wireless power system is one of the most effective solutions, as it can supply energy to the electric vehicle while moving. This research work proposes a model which can be implemented in the future for dynamic wireless charging. This research work implements the wireless power transfer considering the closed loop system. A DC to DC converter is designed along with the power conditioning at the receiver end of the arrangement. The wireless power system is designed to supply a load with a power rating of 60W, and a voltage of 12V with a current of 5A. The transmitter and the receiver coils are both working at a resonant frequency of 60Hz. The voltage induced at the receiver end of a wireless transfer system depends on the mutual coupling between the transmitter and the receiver coil, which in turn depends on the separation between the coils and the coil inductance. As the distance between the two coils is getting larger, the voltage at the receiver end of the transmission reduces. To compensate for the variation of the voltage, a three-level PI controller was designed alongside the closed loop of the system. Here, three loops are working inside each other. The outermost loop controls the DC voltage; the intermediate loop controls the voltage to the wireless transformer and the innermost loop controls the current to the wireless transformer. The output of the system is seen to maintain a constant voltage of 12V and a current of 5A while the input voltage is varied from 120V to 80V to 160V to 80V. A fuzzy logic and neuro-fuzzy controller was also designed which proved to be more robust than the PI controller as there was no undershoot in the output voltage. Furthermore, MPPT control was incorporated. The proposed system consists of a solar PV array, boost DC/DC converter, inverter, transmitter coil, a

receiver coil, rectifier, buck converter, and batteries. The MPPT controller is designed to track the highest voltage and current from the PV array required to charge a battery in which the highest power point voltage is seen as 61.5V.

Also, the stability analysis of the closed-loop system of the three-level PI controller is analyzed, and the system is found to be asymptotically stable.

5.2 Introduction

Gasoline engine technology has contributed immensely to the greenhouse effect. To overcome the challenges of pollution and the dwindling world oil reserve, plug-in electric vehicles were proposed. Although the plug-in electric vehicle is currently in high demand, an advancement in technology will be required to remove issues associated with the battery. The drawback of the present battery includes cost, size, weight, slow charging, and low energy density. For instance, the energy density of a lithium-ion battery pack is around 100wh/kg (Madawala, 2008) which is way smaller compared to the gasoline engine. It becomes almost impossible to achieve the range of a gasoline vehicle from a plug-in electric vehicle with the current technology of the battery. The long time required for charging and the various mechanical hassles associated with charging cables are the main challenges of the present plug-in electric vehicle technology, which constrained its widespread distribution.

Wireless power technology was thereby proffered as a solution in eliminating the charging hazards associated with the plug-in electric vehicle and cable related problems too. The idea of dynamic wireless power transfer (DWPT) enables the electric vehicle to charge on the go. This means that an electric vehicle can be charged as it is moving. This increases the driving range while also reducing the need for bulky battery space. This method also reduces the high cost of EV purchase as the size of the battery is reduced significantly. In DWPT, underneath the roads are fixed power tracks which help to transfer power wirelessly as the vehicles move on the road (Illhoe, 2018). In the year

2013, Gumi, South Korea, among the largest city set out two Online Electric vehicle (OLEV) transportation buses to be used in the city (Kelion, 2013).

The figure below shows the OLEV operating in Gumi city in South Korea.

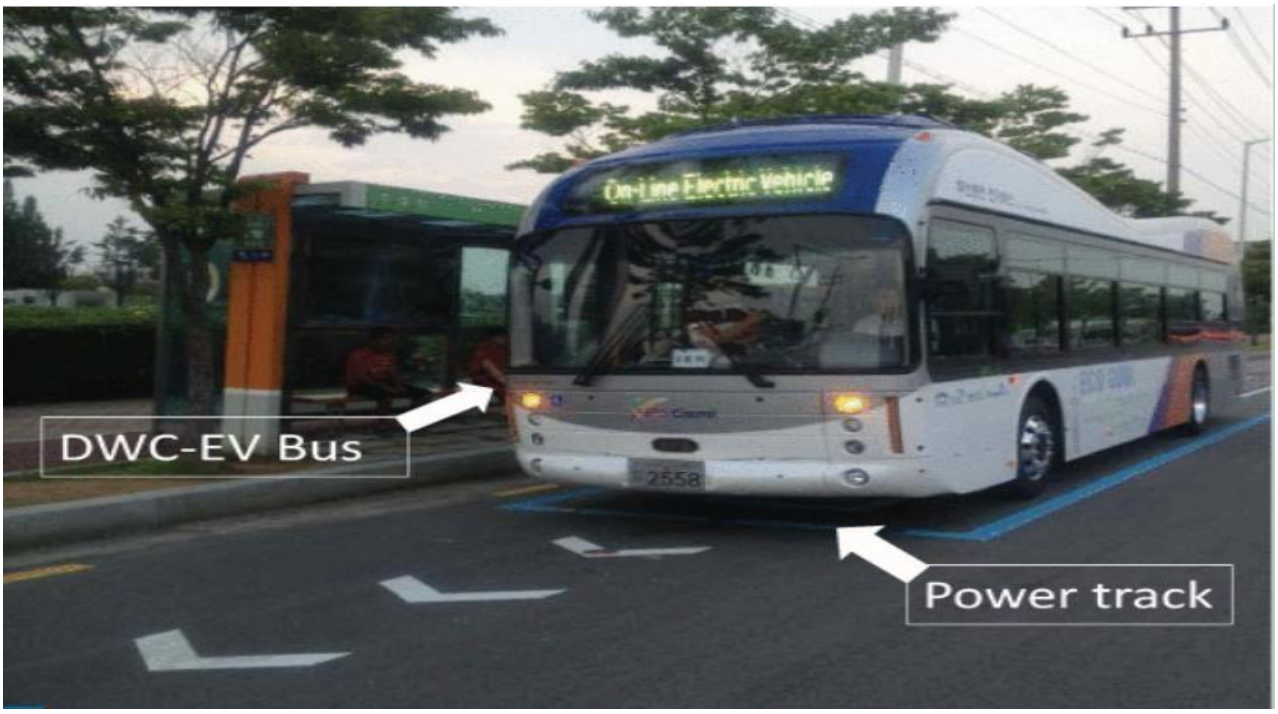

Figure 5-1 Online electric vehicle operating in Gumi, South Korea (Kelion, 2013).

This technique will not only improve the patronage of the electric vehicle but also leads to sustainability in electric vehicle energy. For instance, the idea used in the vehicle-to-grid enhances the distribution of the generated energy which can transcend to another level with wireless power transfer of electric vehicles (Kurs, 2007; Khan, 2013).

As wireless power transmission is a promising technique, researchers have ventured into this technology, and papers have been published on this. Kurs et.al used the phenomenon of self-resonance of strongly coupled coils and proved experimentally the efficiency of non-radiative power transfer at a gap of 16 times the diameter of the coil. Furthermore, an analytical model was developed to validate the result of the experiment for power transfer which is accurate to 95%.

Additionally, wireless transfer using a three-level cascaded MPPT control was designed. MPPT implementation uses an algorithm that normally samples voltages and currents and in turn varying the duty ratio as required. The MPPT controller in this design uses the 'Perturb and observe' method in which voltage is varied by a small amount from the PV array and power is measured. This variation continues until the power stops increasing. This technique is the most popular (Patil, 2018; Haque, 2012).

5.3 Block Diagram and Design

Figure 5-2 below shows the block diagram model of the system. The input is from the AC mains and converts to a direct current with the help of the rectifier. Usually, the AC signal from the wall outlet is unsuitable for the coils because from the formula [Zc= 1/jwc= -jwc], the capacitance might be too small or too big. The voltage output, from the rectifier is converted to the required AC frequency by the inverter circuit switched at a frequency good enough to resonate the transmitting and receiving coils respectively. This is because the coils can only work when AC is applied. The high AC frequency is delivered to the transmitting coil, hence inducing a magnetic field, which is received by the receiving coil through the electromagnetic induction principle. The coil, in turn generates an e.m.f. Next, it passes through the rectifier, and a DC-DC buck converter as the battery requires a DC voltage to operate. A three-level cascaded PI controller helps to control the variation of the voltage induced at the receiver to realize a steady voltage output to the battery.

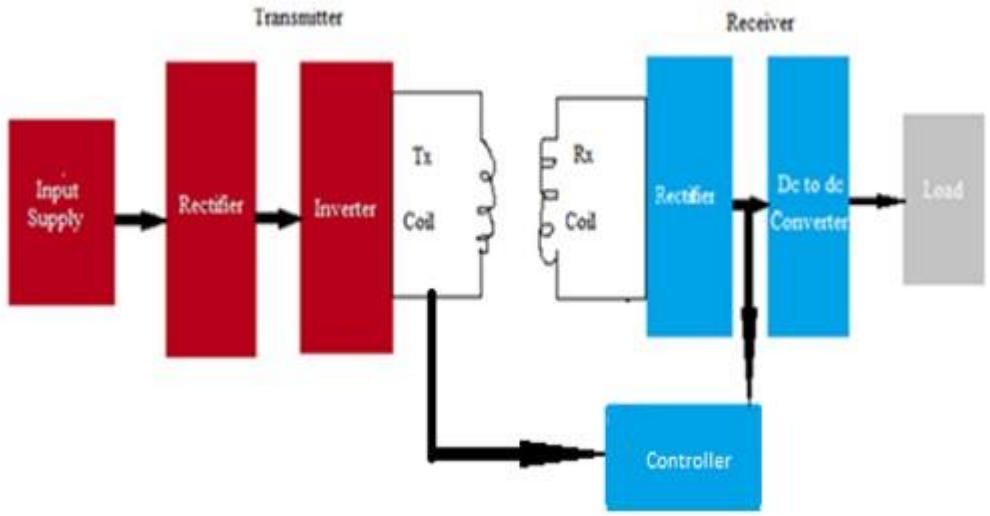

Figure 5-2 Circuit design

5.3.1 Rectifier

The proposed design uses a full wave rectifier. The rectifier circuit is built using the diode and the filter capacitor.

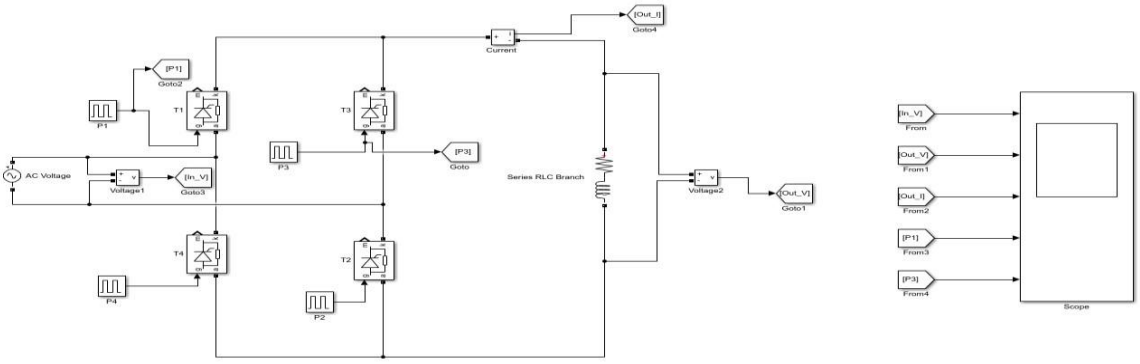

Figure 5-3 Simulink rectifier design

The design of this system powers a load at 12 V, 2.6 A. The sinusoidal input with a peak voltage value of 120 V goes into the rectifier circuit to obtain an output voltage of 76v dc.

$V_{DC}= (2V_p)/\pi$ =76 V since V_p=120 V

$Voltage\ ripple = \frac{I_{dc}}{F.C} = \frac{V_{dc}}{R.L.C}$. The capacitance of the capacitor C=28 µf.

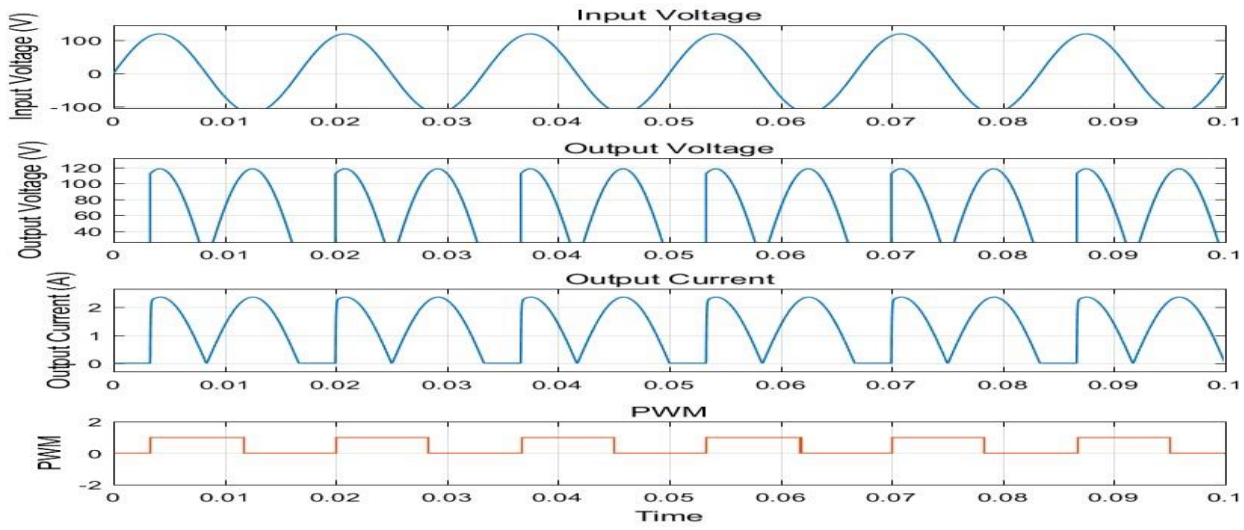

Figure 5-4 Simulink rectifier result

5.3.2 Inverter

The output of the rectifier feeds into the inverter. The element making up the inverter is the MOSFET, and the pulse generation circuit. The Simulink model design of the inverter is in figure 5-4 below. Note that the pulse generator of the inverter produces switching pulses, which feeds into the inverter input; hence, the inverter generates a square wave, which feeds into the transmitting end of the coil.

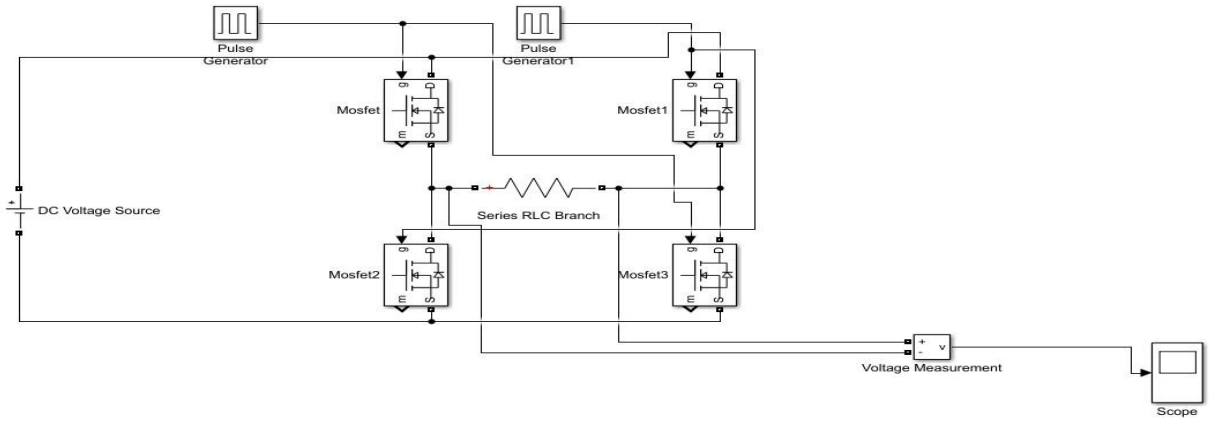

Figure 5-5 Simulink inverter circuit

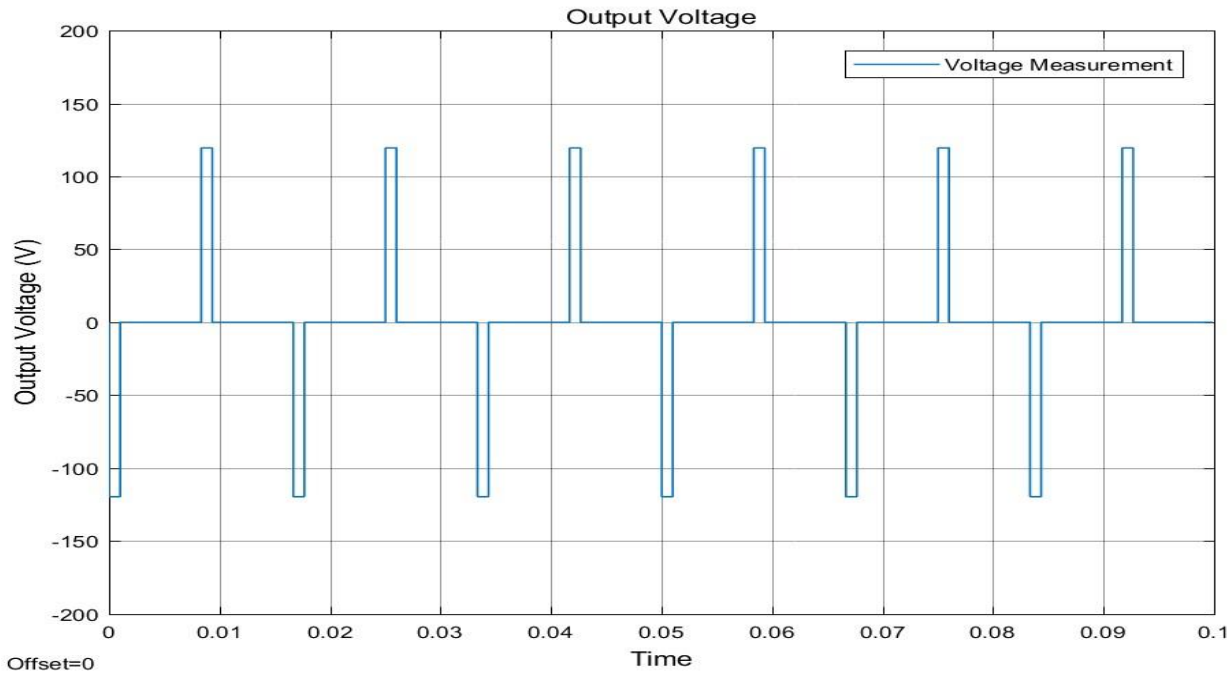

Figure 5-6 Simulink inverter result

5.3.3 Transmitter Coil

The output of the inverter goes into the transmitter coil whose operating frequency is 60 Hz. The calculation of the inductance of the coil is by using the wheelers long coil formula (Kim, 2016).

$$L = \frac{r^2.N^2}{9r+10l} \text{.....5.1}$$

Where l= air core length, r= the radius of the coil in inches. A length of 9.5 cm is assumed for this research work, the thickness of the 4 mm, and a diameter of 8.5 cm. From the above parameters given the inductance of the L=19.1 µH, and a capacitance of C=0.3µF is assumed.

5.3.4 Receiver Coil

The design of the receiver coil works at the same resonance frequency as the transmitter coil. A flat spiral spring winding with inner diameter r (Di) = 1.15 cm, thickness (w) =1 mm, spacing between the coils (s) = 0.54 mm, no. of turns N = 45 is assumed for the receiver coil.

The calculation of the coil's inductance is by using the formula below (Kim, 2016)

$$\frac{N^2 \times A^2}{30 \times A - 11 \times D} \ldots\ldots\ldots\ldots\ldots\ldots 5.2$$

$$\frac{D_i + N(w+s)}{2} \ldots\ldots\ldots\ldots\ldots\ldots 5.3$$

The coil has an inductance of approximately 94.5µH and capacitance of 0.02µF. The mutual inductance between the primary and the secondary coil is given as $\sqrt[k]{L_1 L_2}$. The coupling coefficient k varies between the value of 0.2 to 0.5. The value of k used in the calculation of the mutual inductance between the two coils is 0.2, hence a mutual inductance of 12µH is derived from the expression above.

5.3.5 Buck Converter

The main elements of the buck converter circuit include the diode, inductor, capacitor, a pulse generating circuit, and the MOSFET switches.

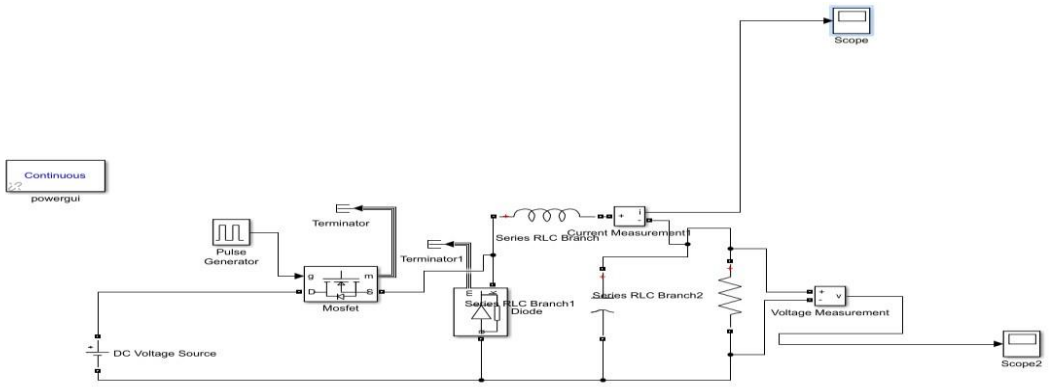

Figure 5-7 Simulink buck design.

The output of the buck converter is given as:

$V_{out} = D.V_{in}$, where D=duty cycle, assuming 16 % duty cycle with V_{in}=76v, V_{out}=12 V. Output current I_o, $I_{out} = \frac{V_{out}}{R}$. Assuming R=4.5 Ω, I_{out}=2.6 A.

The inductance of the buck converter is given by,

$$L = \frac{V.D}{F_{sw}.DI_L} \ldots\ldots\ldots\ldots\ldots\ldots 5.4$$

Here V= 76V, F_{sw}=switching frequency= 60Hz, DI_L=4% of the output current =0.104A, L=4.8mH. L=5mH is chosen.

$$C = \frac{DI_L}{8F_{sw}.DV_{out}} \text{……...…5.5}$$

Assuming 4 % voltage ripple = 0.8 V, C=2 µF.

5.3.6 Proportional Integral (PI) Controller.

This work shows a self-tuning technique for designing the pi controller. The controller helped to achieve a constant voltage output from the chopper for the various input range of voltage.

Dc(s)= $K_p + {}^{K}{}_{s}{}^{I} + K_{Ds}$…….5.6

U(t)= $K_p e(t) + K_I \int_{t0}^{t} e(t)\,dt + K_D \frac{d}{dt} e(t)$……5.7

K_p is the system's gain. This affects the speed of the system by either increasing or decreasing it.

K_I is the integral feedback which tracks the previous values to limit steady state error.

K_D is the derivative feedback to the system which helps limit overshoot, hence, enhances stability. It is important to note that the magnetic resonance system designed only needs pi because the system does not require much speed.

The method used to tune the PI controller is the Trial and Error method. In this method, the Ki is set to zero while the Kp value is increased until the system oscillates. The value at which Kp oscillates is 10. At this oscillating point, Ki is varied until the system stops to oscillate and reaches a steady state of Ki =1200.

5.3.7 Simulation Results and Analysis

The open loop and closed loop simulation results for the proposed wireless power transfer system is obtained. The simulation of the system is carried out in the MATLAB Simulink software.

An alternating current input of 120v is fed into the rectifier circuit and an output voltage of 75v is obtained with a ripple voltage varying between 74v-75v. Figure 46 below shows the ripple in the output voltage of the rectifier. This output voltage is fed into the inverter whose switch is operated at a frequency of 60Hz, which corresponds to the resonance frequency of the coil. The block diagram of the open loop system for the WPT system is shown in figure 5-8 below.

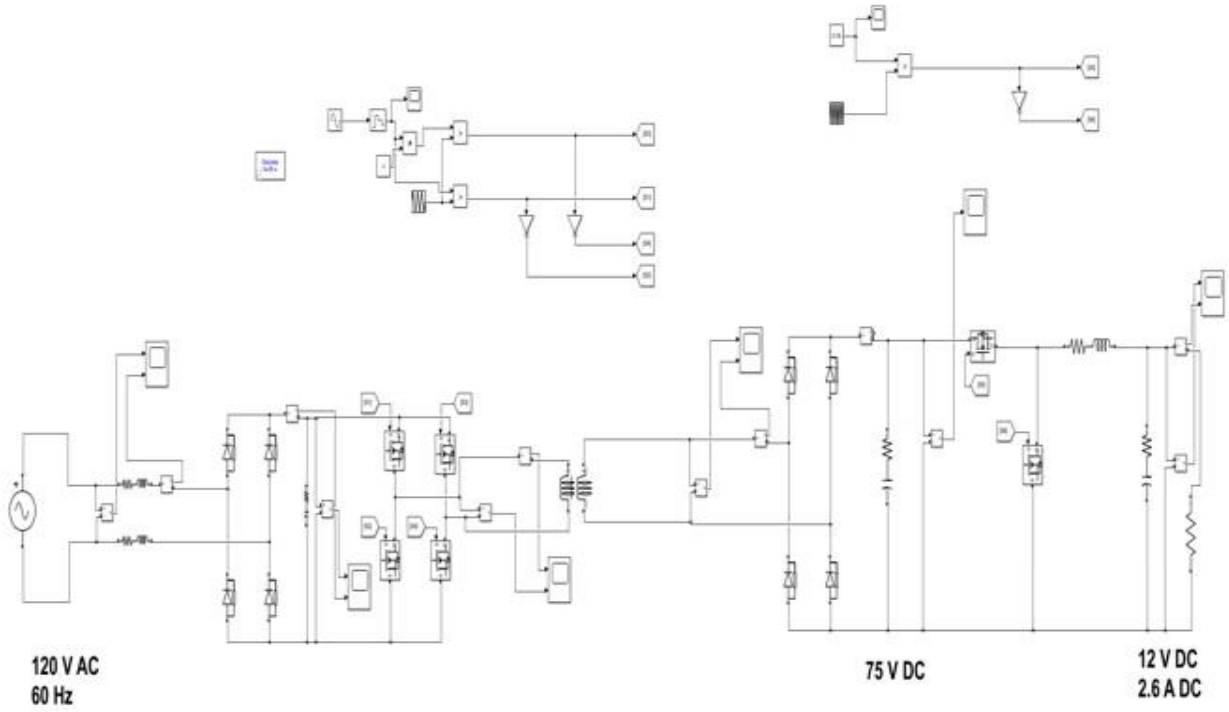

Figure 5-8 Open loop for WPT Simulink diagram

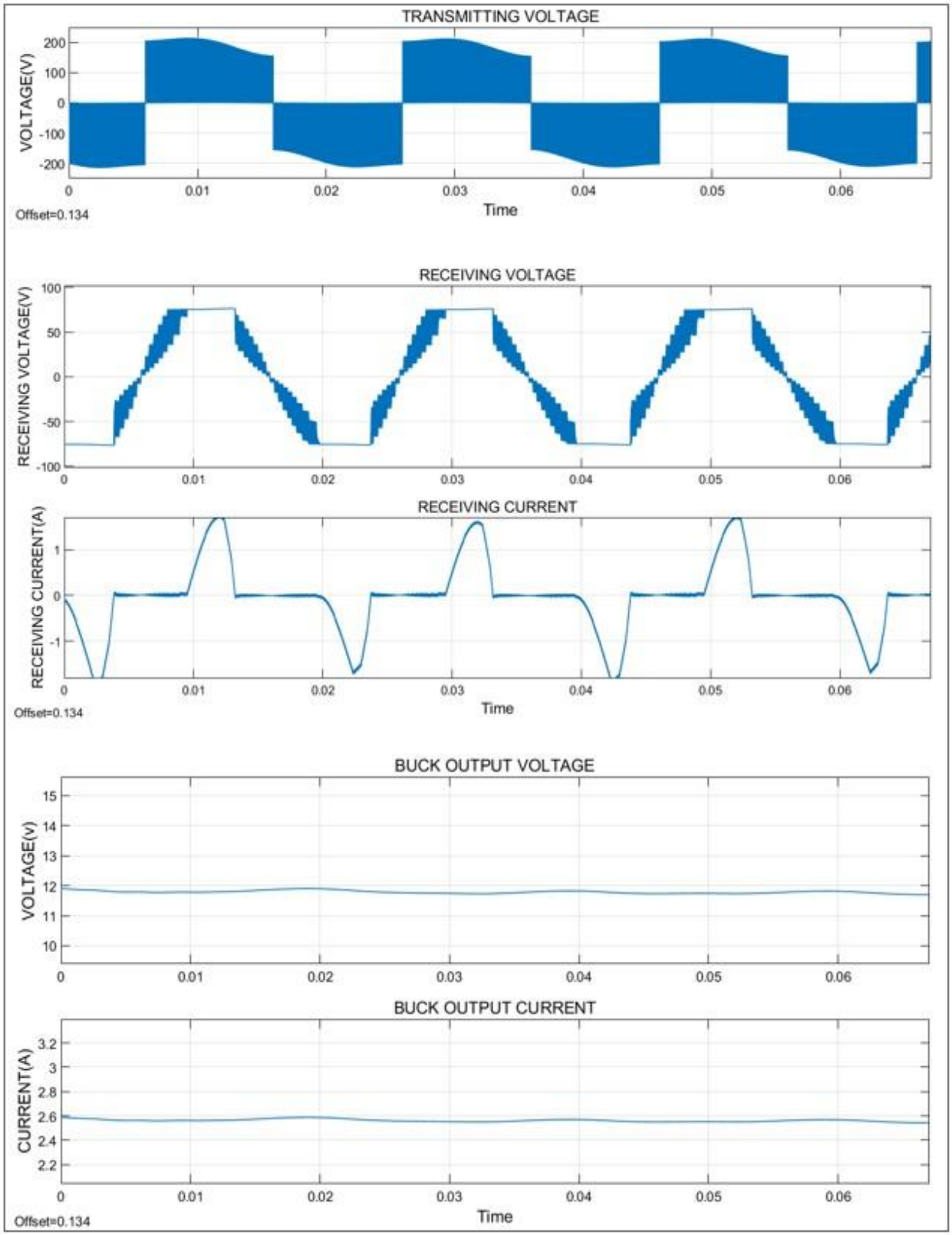

Figure 5-9 Open loop simulation results

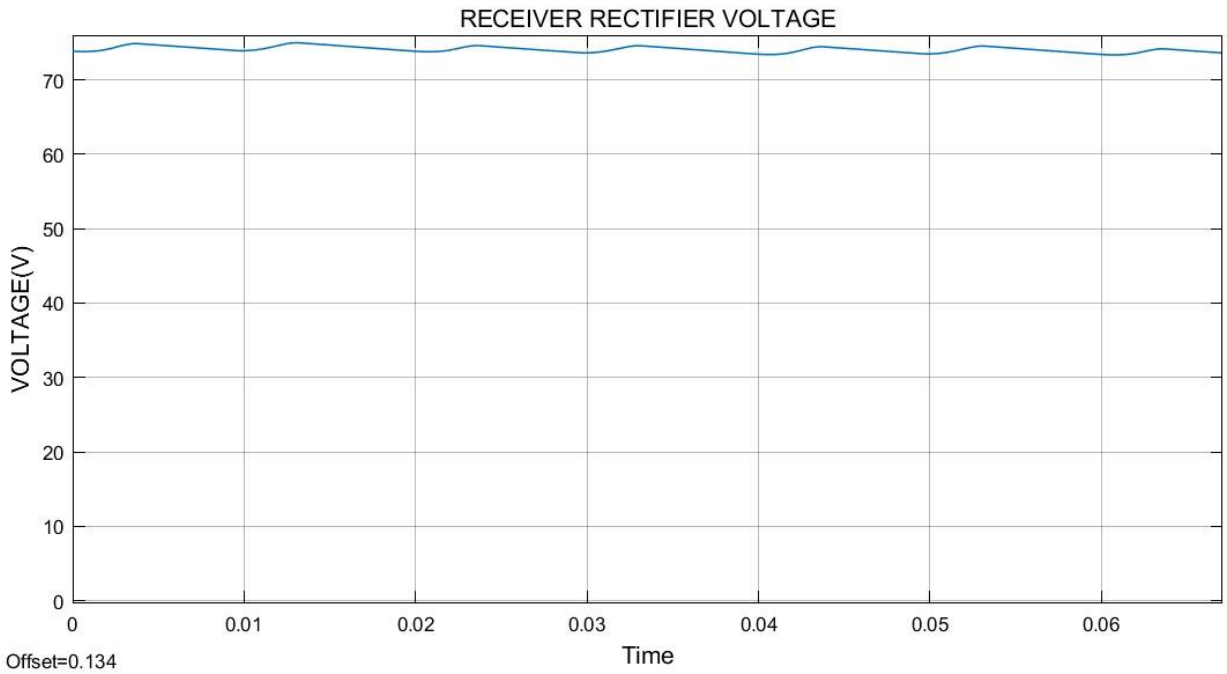

Figure 5-10 Output of the diode rectifier (receiver side)

The open loop simulation results of the various stages are shown below, where a transmitting voltage of 200 V and a receiving voltage of 76 V is observed. These two signals have a frequency of 60 Hz. The receiver side rectifier output is obtained as 76 V which is fed as input into the buck converter stage. The output from the buck converter was found to be 11.9V and the output current of 2.59 A is obtained. Voltage and the current output of the buck converter are shown in figure 5-11 below.

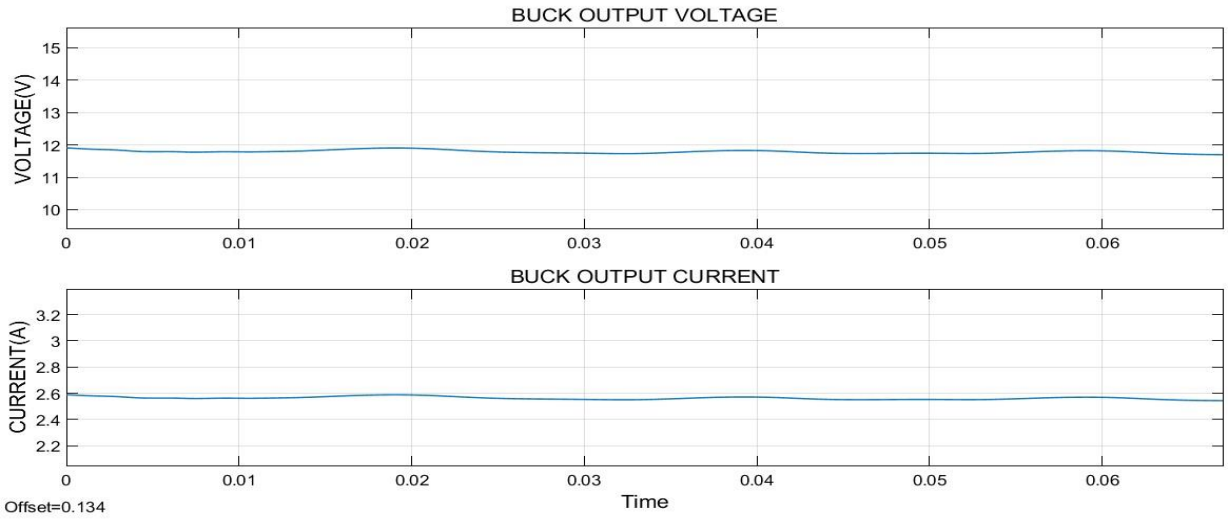

Figure 5-11 DC-DC buck converter output voltage and current

The effect of variation in the input side of the buck converter is then carried out to understand the effect of the controller at the receiver end. While changing the input voltage from 120 V-80 V, this results in an output voltage variation of 6 V to 17 V and output current variation of 1.2 A-3.9 A. The input into the buck converter is assumed to be varying as the spacing that exists between both coils are varied. The figure below shows the simulation result for varying input.

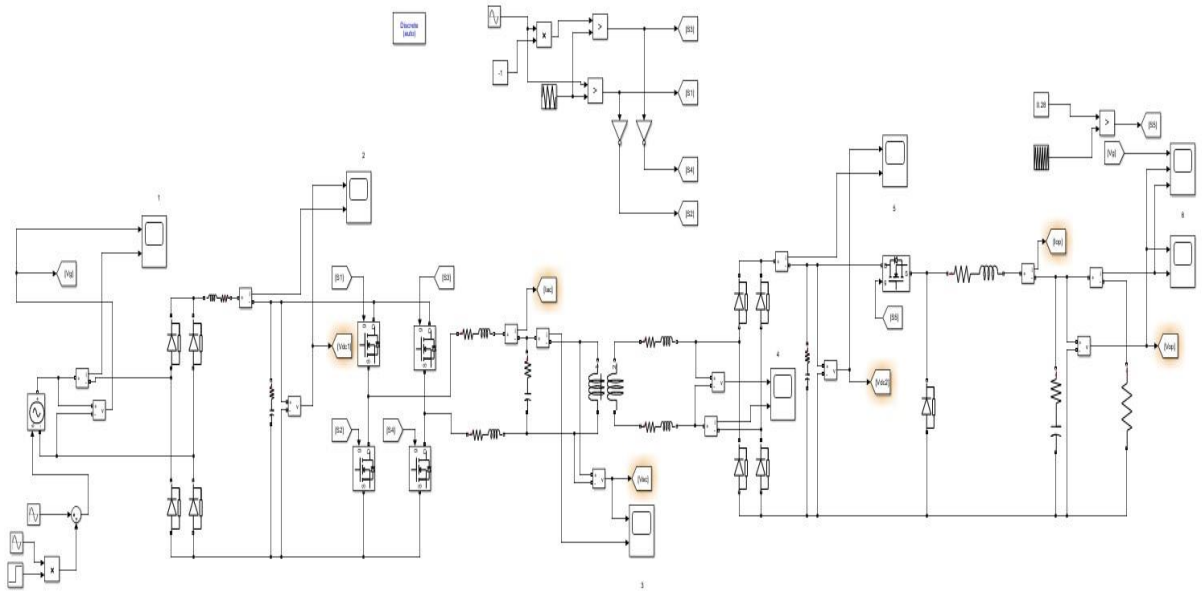

Figure 5-12 Open loop circuit

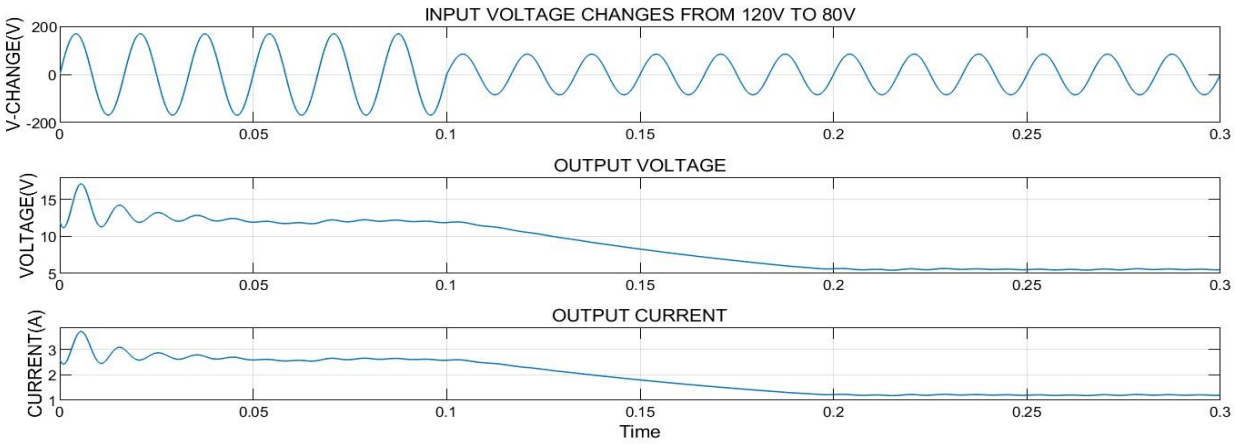

Figure 5-13 Open loop simulation result for change in input

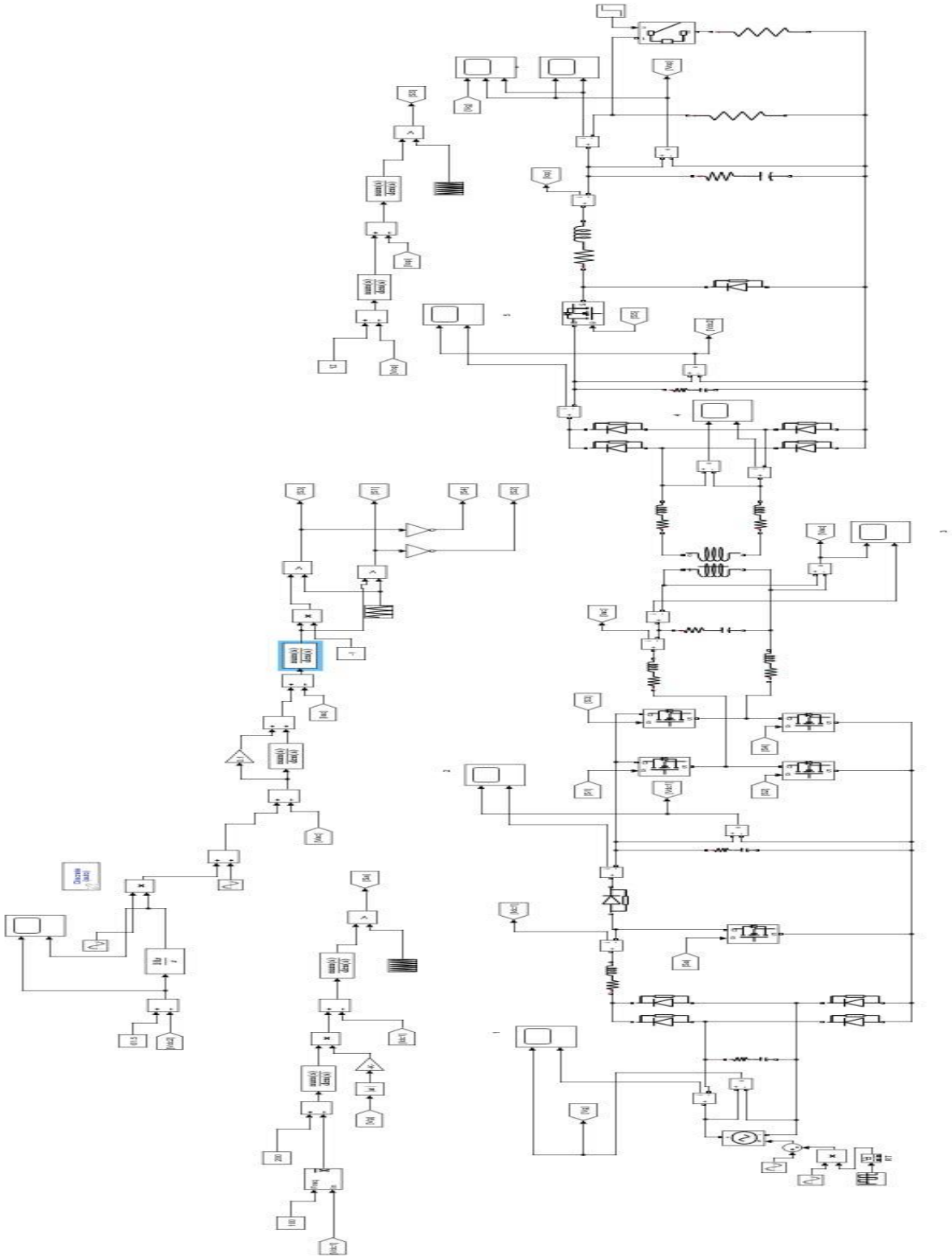

Figure 5-14 Closed loop circuit for 3-level cascade

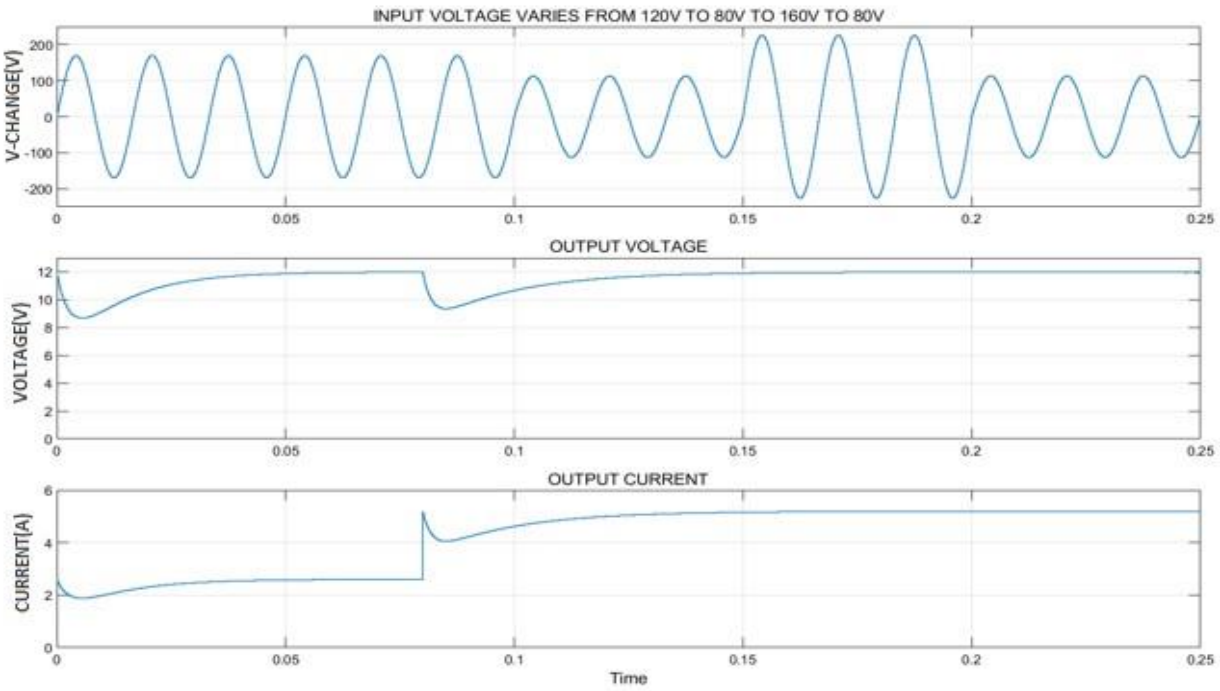

Figure 5-15 Closed loop 3-level cascade simulation result

In figure 5-14, the outermost loop controls the DC voltage. The intermediate loop controls the input voltage to the transmitter coil and the innermost loop controls the receiver current.

It can be seen from figure 5-15 that the proportional integral controller generates a constant voltage of 12V and constant current of 5A when the input voltages vary from 120 V to 80 V to 160 V to 80 V. Hence, the stability of the output power is established.

5.3.8 Comparison with Fuzzy Logic Controller

FLC offers a kind of algorithm which transforms the English-like control technique which depends on human reasoning into an automated control technique (Gupta, 1980). Different experiments show that the FLC produces better results compared to the ones gotten from conventional control techniques. Fuzzy logic control is closely related to conventional defined arithmetical control and man-based action taken (Gupta, 1980). In FLC, an input is transformed into various members of its related membership functions which is dependent on their value (Zadeh,

1974). The input goes through some human-based rules to produce an output. The output of an FLC is deduced based on fuzzification of the input and output by means of its related MFs. In 1965, fuzzy logic was developed by Prof. L. A. Zadeh from the University of California, Berkeley (Jin, 2000). Dr. E. H. Mamdani, a professor from London University, implemented fuzzy logic in a real application to control an automated engine using steam in 1974; up until then, FLC was unpopular (Jin, 2000). For the proposed wireless power transfer system, there are 1 input, 1 output and 7 membership functions each for both input and output. The input is the voltage error and output are the current reference.

If error is low, the output is kept low, if error is high, the output is high.

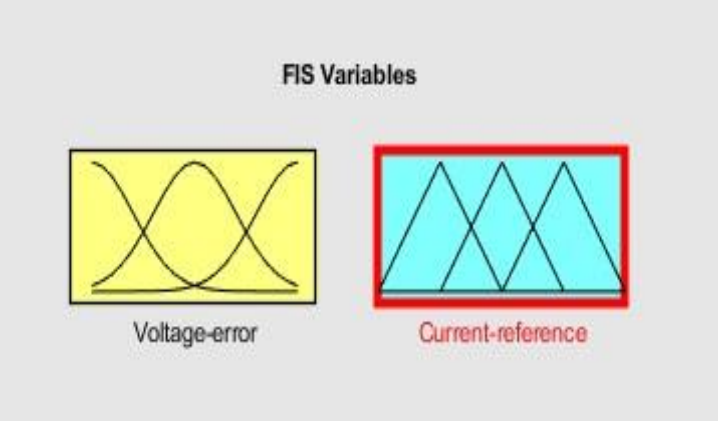

Figure 5-16 Fuzzy Inference System Variables

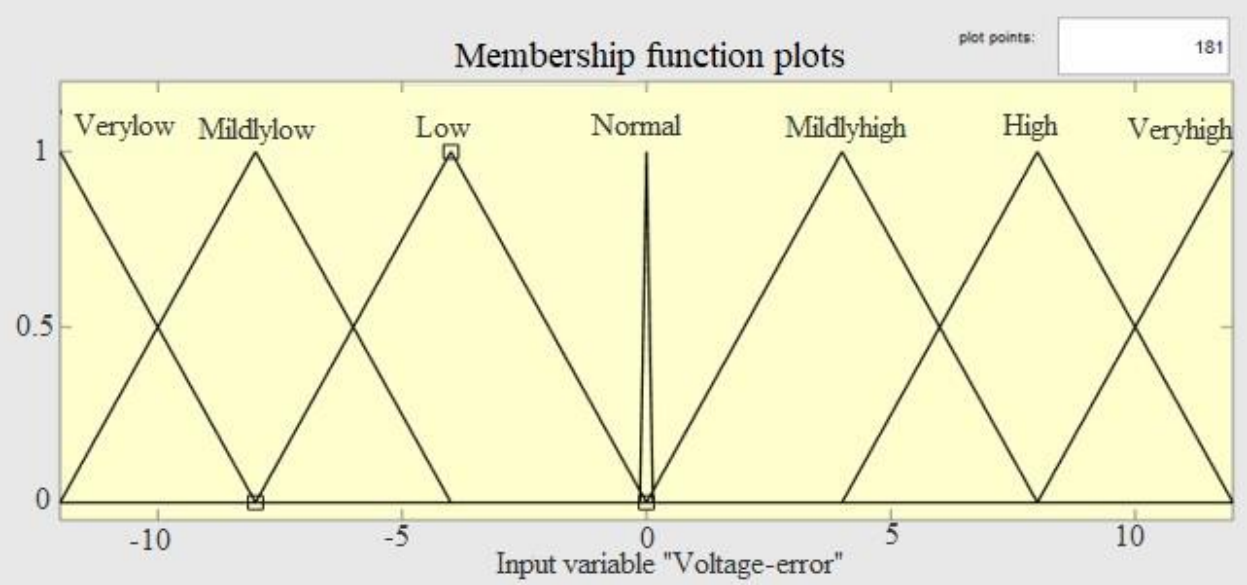

Figure 5-17 Input variable and its membership functions

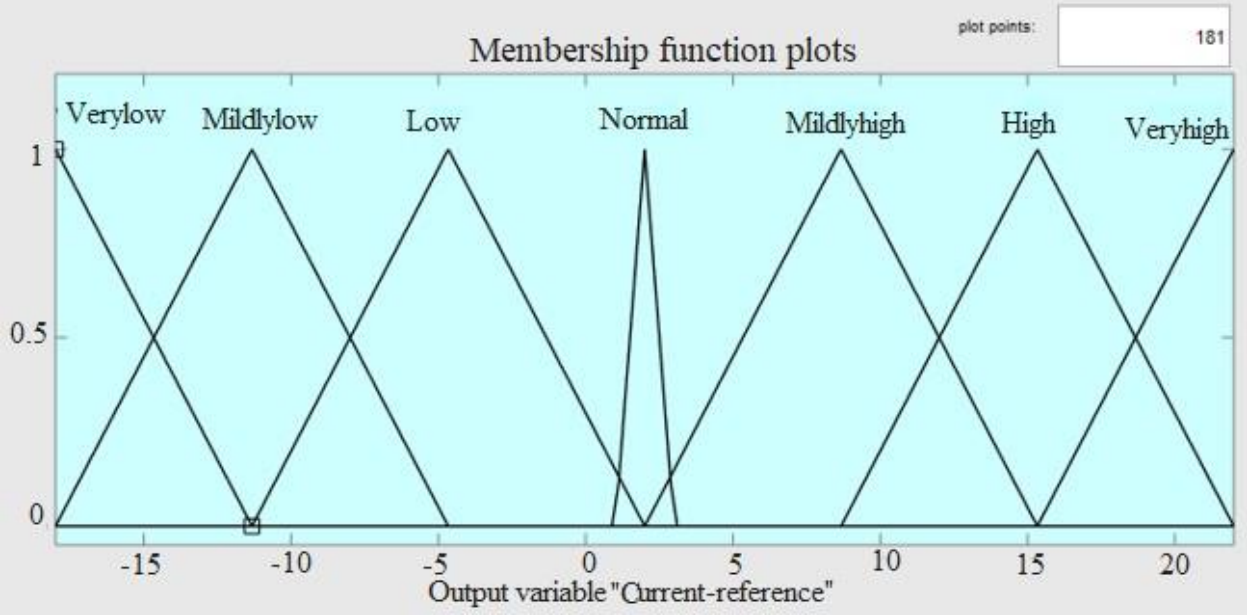

Figure 5-18 Output variable and its membership functions

There are three main steps required to implement fuzzy logic technique: Fuzzification- changes the crisp input data into the MFs; Fuzzy inference process- combines the MFs with the control rules

to give the output understood by fuzzy and defuzzification– uses various strategies to derive each related output, then places it in a tabular form. The defuzzification technique used here is the centroid method.

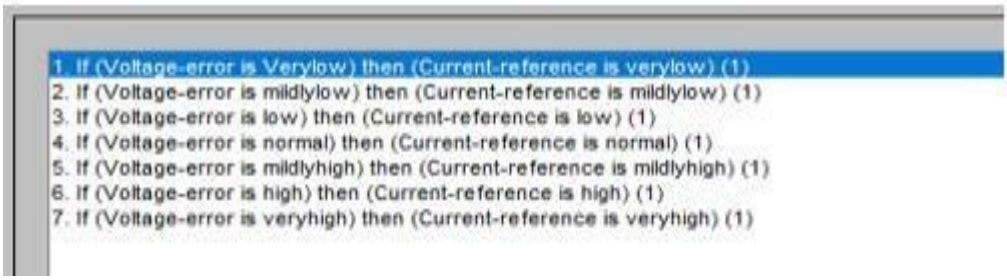

Figure 5-19 Fuzzy logic control rules

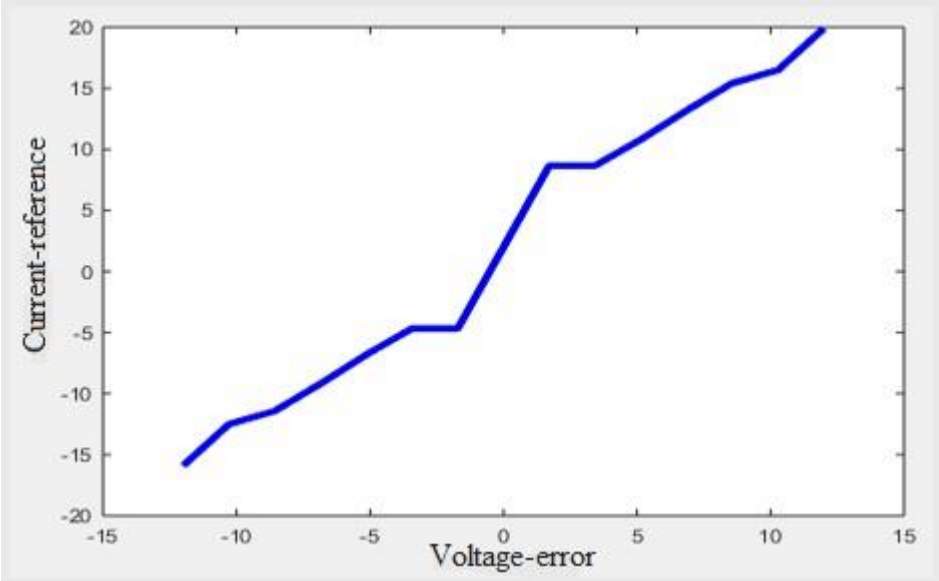

Figure 5-20 Fuzzy surface viewer

Figure 5-20 shows that when voltage error is low, the output current is low and vice versa. Hence, the implementation of fuzzy logic gives desirable characteristics to reject the low disturbance.

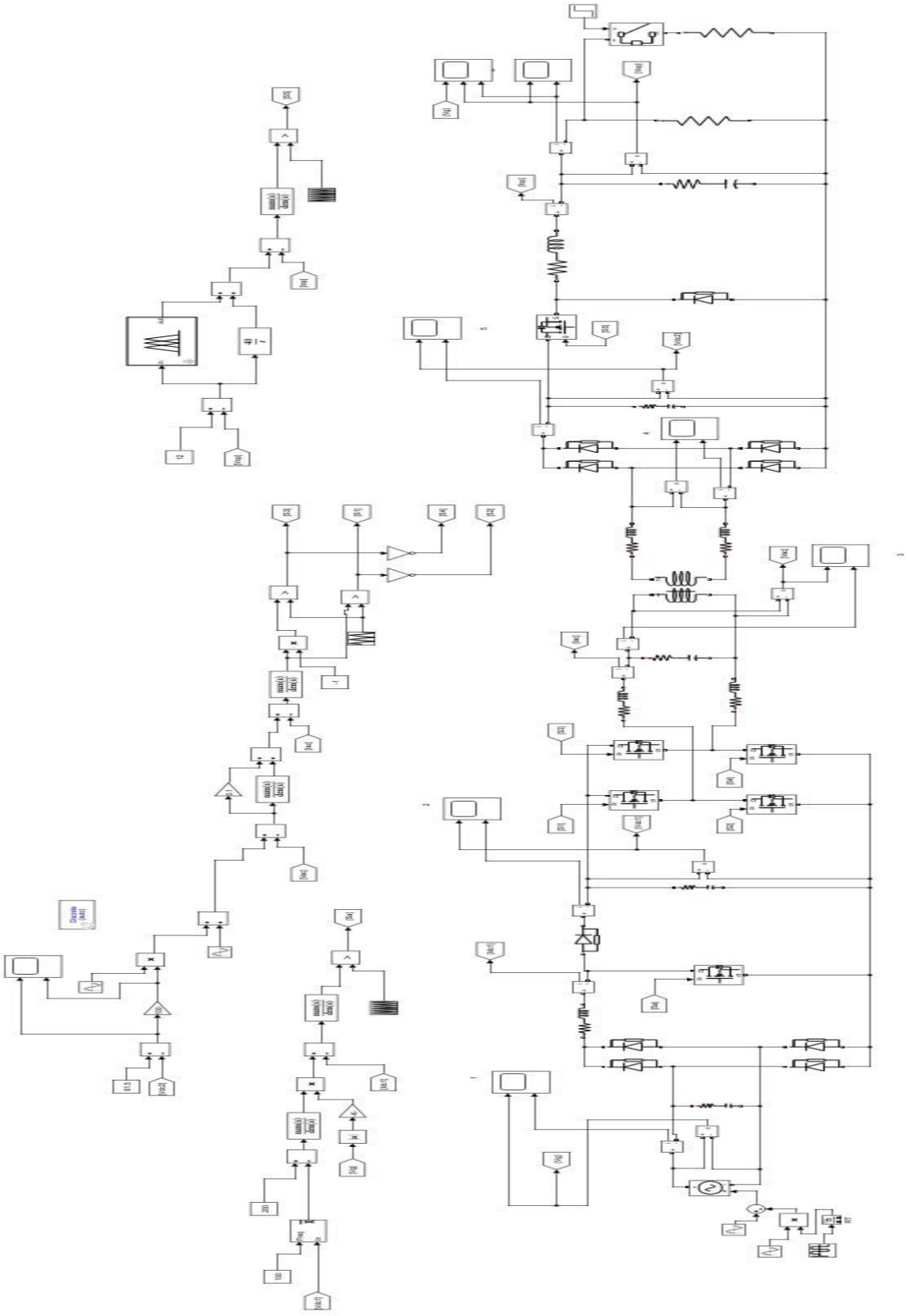

Figure 5-21 Fuzzy logic Controller design

The input to the fuzzy logic is the voltage error and the output is the current reference. Here, the output (current reference) is changed based on the error. If the error is low, the output is kept low and if the error is high, the output is kept high.

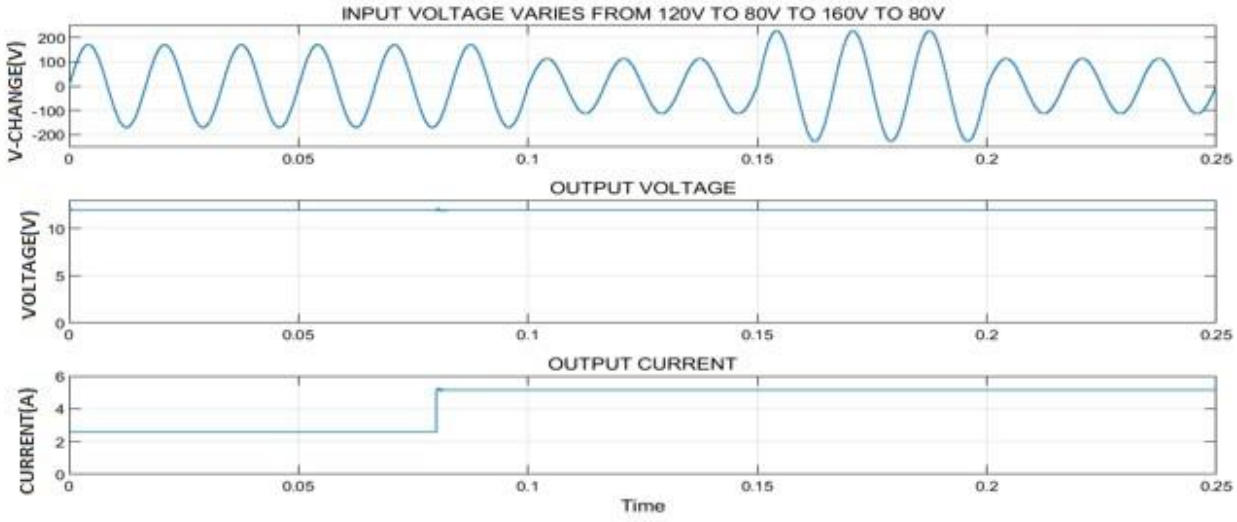

Figure 5-22 Fuzzy logic controller simulation result

From figure 5-20, at T=0.08 Sec an additional load resistance of 2.6 Ohm resistor is connected in parallel across the output, this mimics the sudden load change in a real-life application. It is easily observed that the conventional control (PI) fails to achieve a constant voltage when the load current increases as it drops at a certain level before reaching the rated value of 12 V. This voltage dip is totally undesirable in real life applications as the performance of the load will deteriorate or in some cases, failure may occur. With the FLC, a constant output voltage of 12 V is maintained as the load current increases without a voltage dip. The fuzzy logic controller helps to reduce the output impedance of the buck converter and hence the voltage dip due to the load addition is negligible. Therefore, this shows the robustness of the system.

5.3.9 Comparison with a Neuro-Fuzzy Controller

A neuro-fuzzy system is a kind of fuzzy system which utilizes a learning algorithm that is deduced from neural network to control its parameters i.e. its sets and rules. This system can be observed as

a 3-layer feedforward neural network. The input shows the first layer, the rules of the fuzzy shows the hidden layer, and the output shows the third layer (Jang, 1993). The proposed neuro fuzzy system is designed by mapping an input and an output with seven MFs each to the rules.

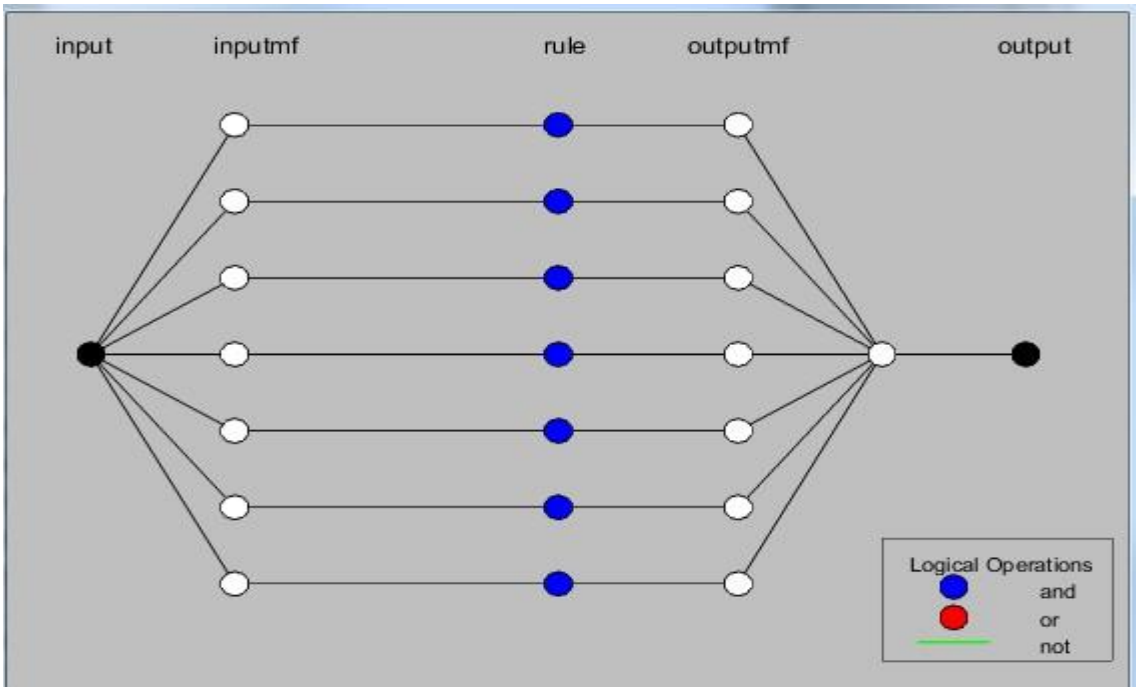

Figure 5-23 Neuro-fuzzy structure

Then, input/output data is loaded for training. Afterwards, the FIS model is trained by an adaptive neural fuzzy inference system (ANFIS) to match with the data used for training by adjusting the MF with respect to the error condition. This modification enables the fuzzy system to learn from the data that has been modelled. The adjustment is done with the aid of an optimization method which is either hybrid or back propagation algorithm. For this system, hybrid algorithm is used, and the number of epochs is 10. The

ANFIS was first introduced in 1993 by Jang (Jang, 1993).

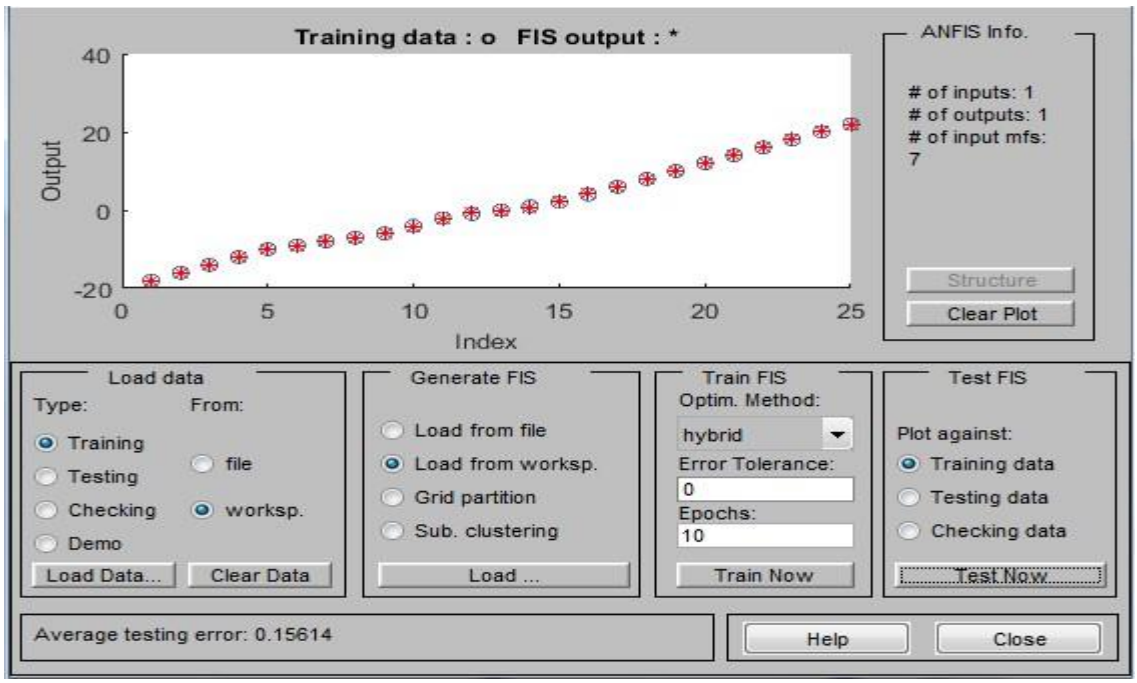

Figure 5-24 Neuro-fuzzy training diagram

Normally, for better operation of the system, the input/output data for training must completely represent the features of the trained FIS data (Jang, 1993). Neuro-fuzzy is more accurate because it uses a neural network to train the fuzzy. The model used for this research work is the Sugeno model and the defuzzification method used is the wtaver. Figure 5-24 shows that the average testing error is 0.15614 which indicates that the fuzzy system has learned well from the data modelled.

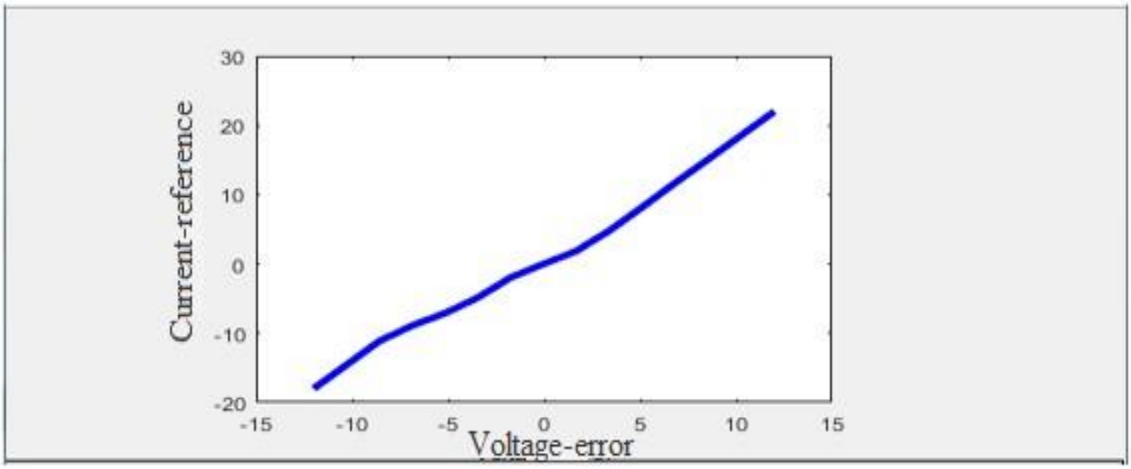

Figure 5-25 Neuro-fuzzy surface viewer

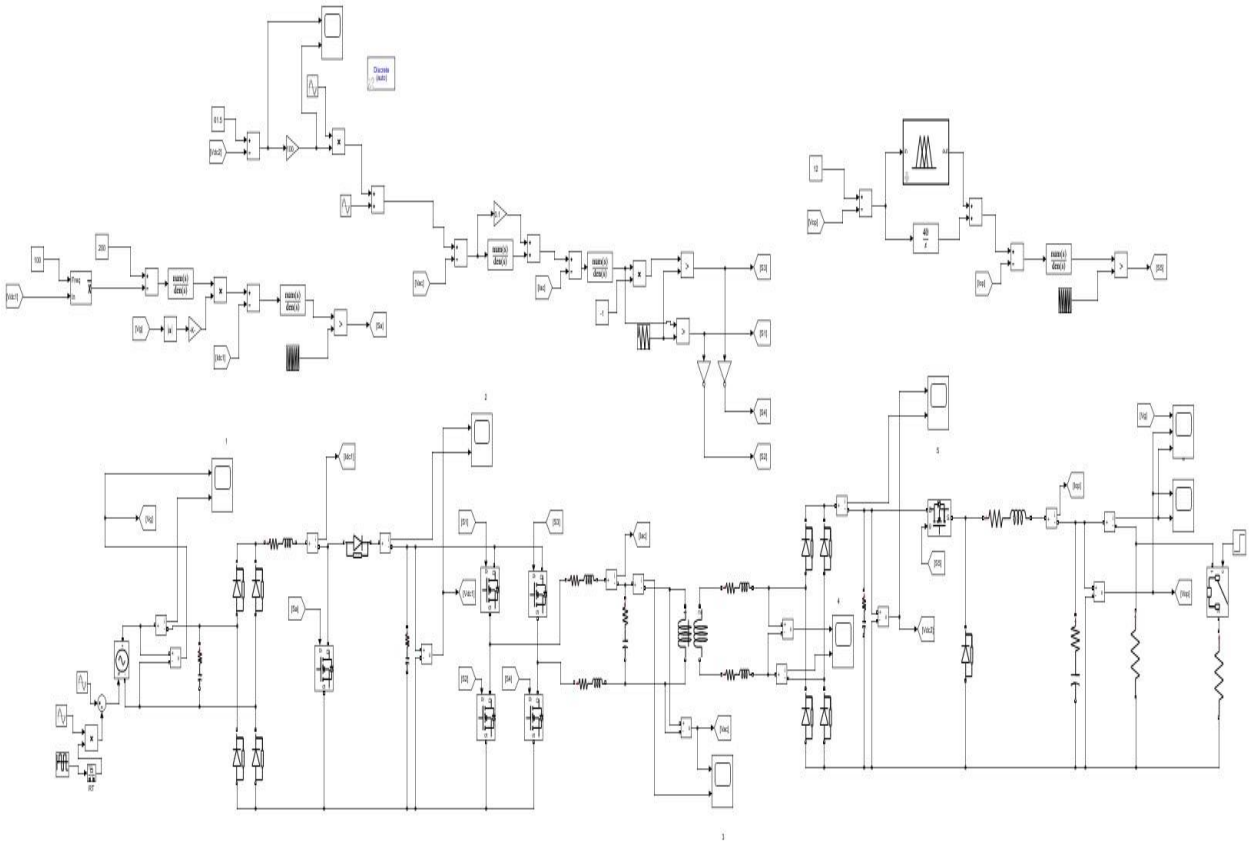

Figure 5-26 Neuro-fuzzy Controller design

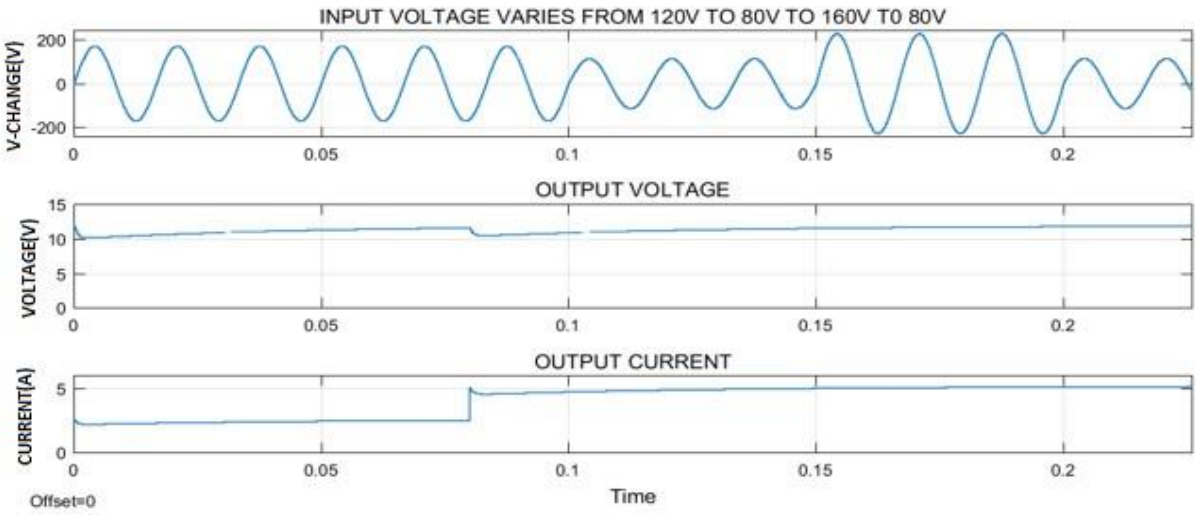

Figure 5-27 Neuro-fuzzy simulation design

Figure 5-25 shows that at 0.08 Sec, where a load of 2.6 Ohm resistor is connected in parallel across the output to depict sudden load change in a real-life scenario; the undershoot is negligible. The output voltage is 12 V and output current is 5 A which is desired.

5.3.10 Comparison with a Single-Level PI Controller

In figure 5-28, a single-level PI controller is designed in which the PI controls the input voltage to the receiver. Figure 5-28 shows the simulation results in Simulink where a change in input voltage from 120 V to 80 V to 160 V to 80 V to 160 V results in an unstable voltage value of 15 V and the current value of 3 A. Therefore, the single-level PI controller is not desirable compared to the other control methods used in this research work.

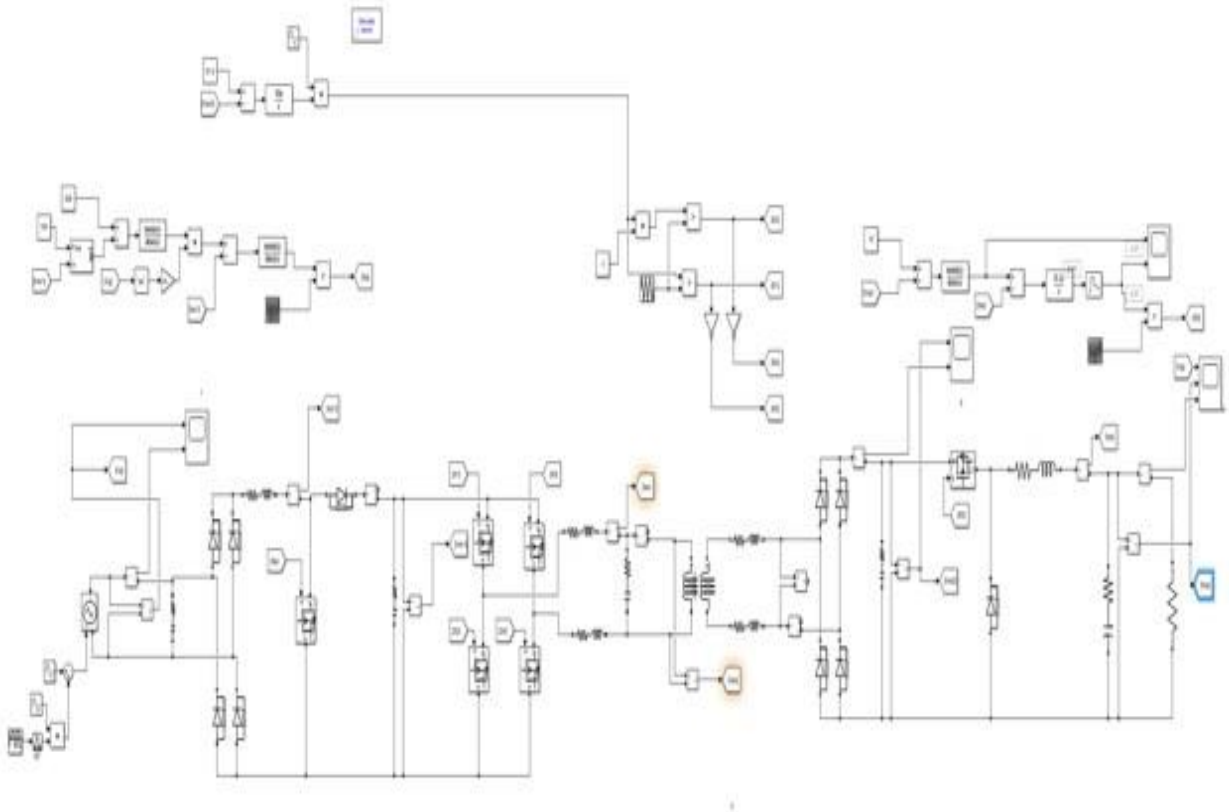

Figure 5-28 Closed loop circuit for 1-level

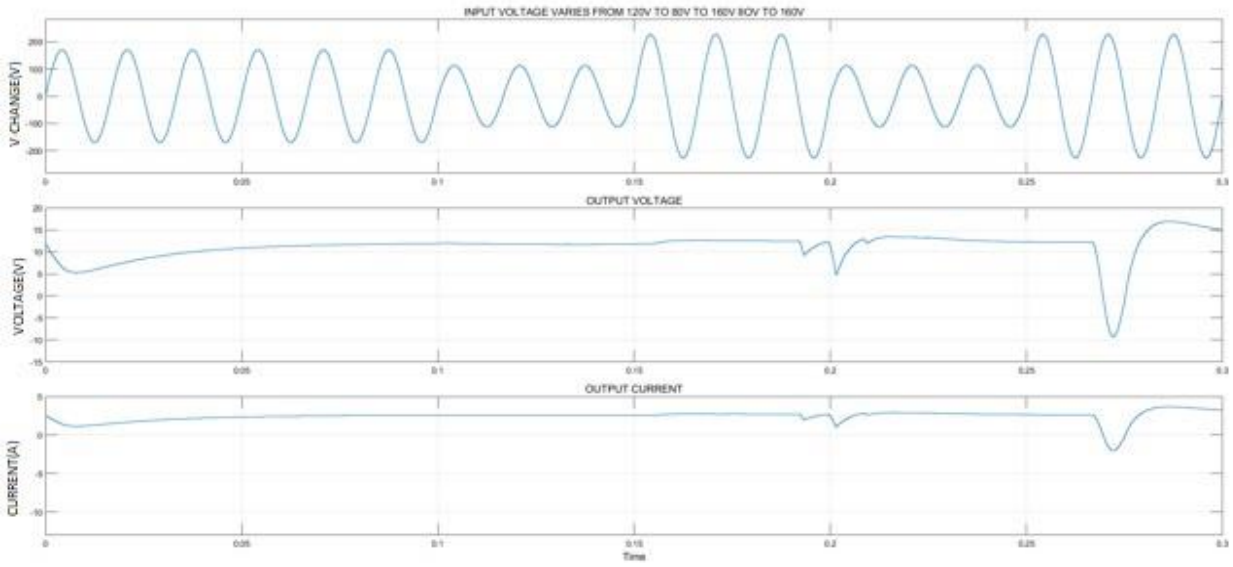

Figure 5-29 Closed loop 1- level simulation result

5.4 Summary of the Different Control Methods Used

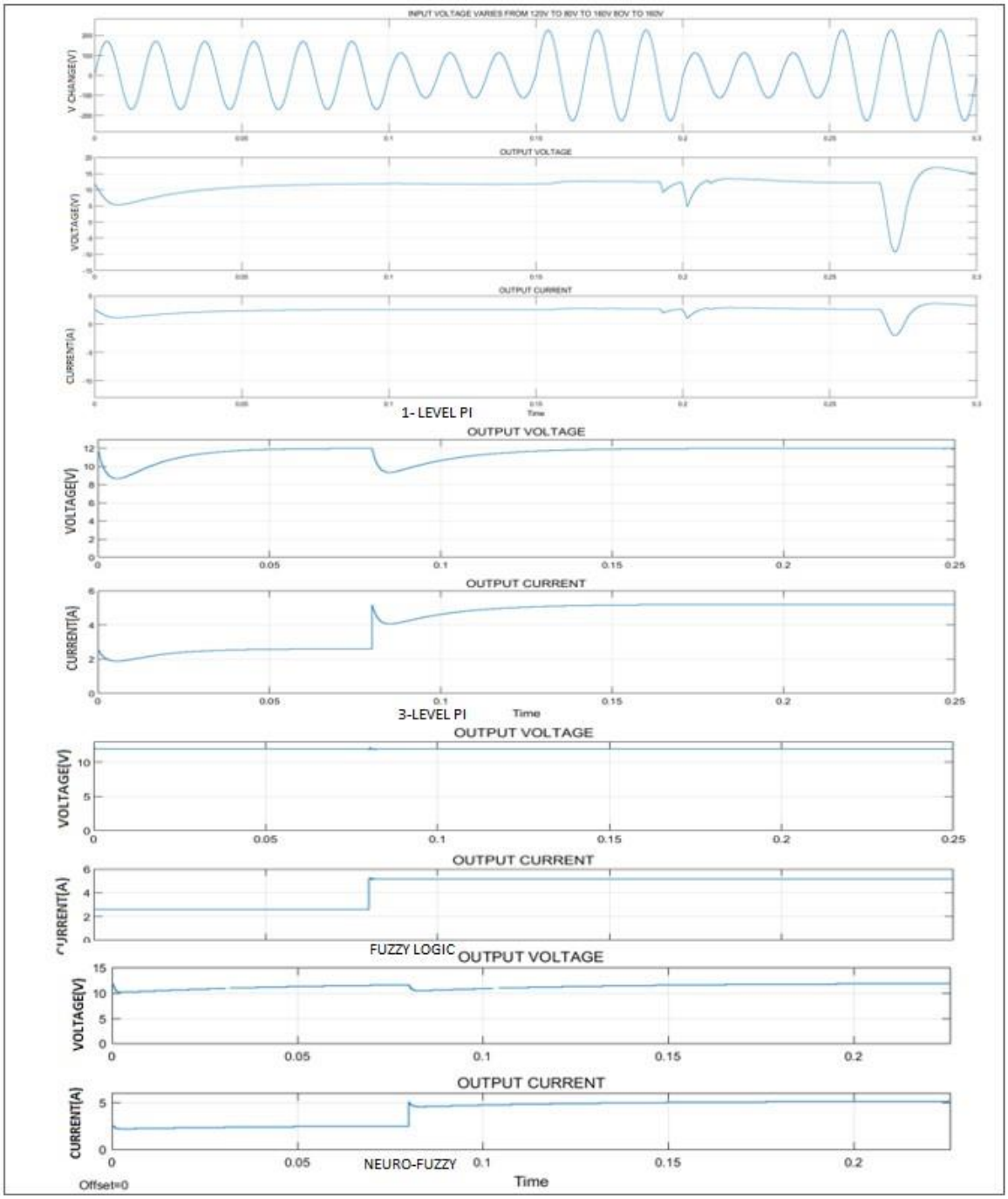

Figure 5-30 Summary results of all the different controllers used

Figure 5-30 shows that the fuzzy controller and the neuro-fuzzy controller are more robust and stable than the 3-level and 1-level PI controller.

5.5 Modelling of Wireless Power Transfer Using Three-Level Cascaded PI Controller with MPPT

The design of the model is in MATLAB/Simulink. For MPPT to work well, there must be a variable power sink, so a solar PV array was included. MPPT helps to track the maximum voltage and current from the PV array. Since the PV panels are DC devices, the voltage from the PV panel passes through the boost converter (DC-DC converter) to boost the voltage of the PV panel to 240 V. This is because for MPPT to work properly, the source impedance must be equal to the load impedance. This results into the drop of half of the source voltage across the source impedance, thereby delivering half of the voltage to the load. Therefore, to satisfy this condition, and still have 120V delivered to the rectifier, the source voltage must increase to 240 V, hence, the need for the boost converter. The inverter helps to convert the DC voltage back to AC voltage as the transmitter and receiver coils need AC supply. The AC voltage from the receiving coil passes through the rectifier and then passes through the buck converter to step down the voltage to that needed to charge the load (battery).

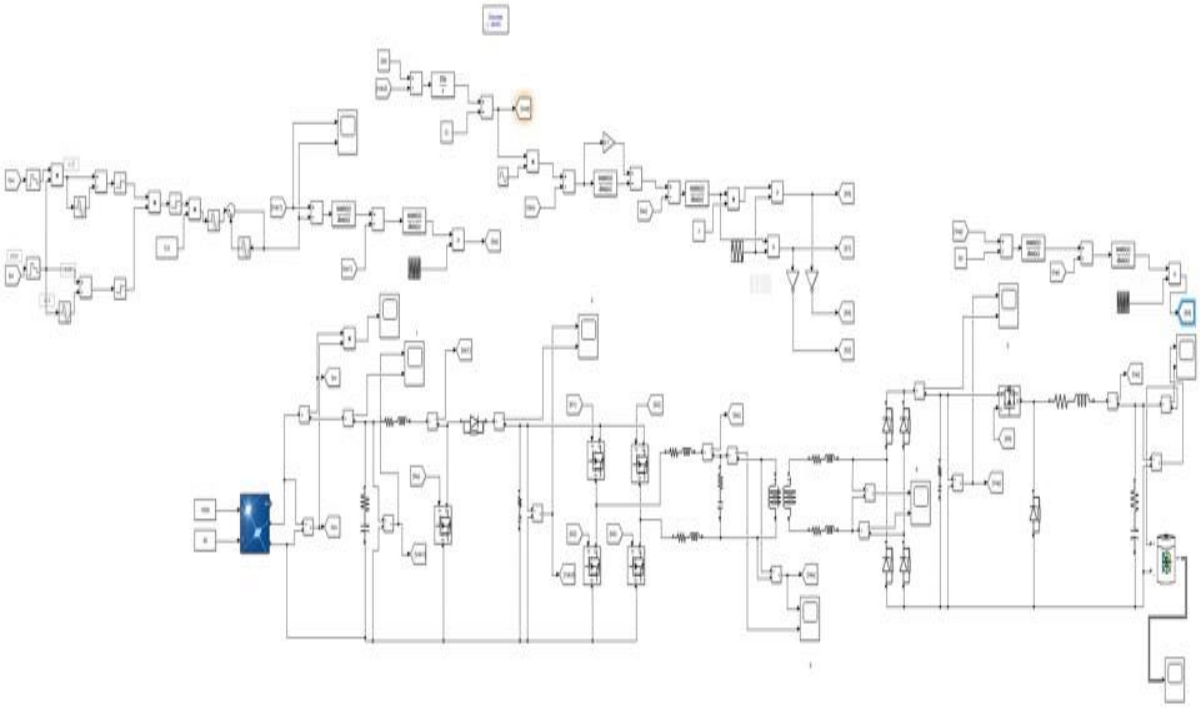

Figure 5-31 Complete design of the MPPT controlled WPT

PV Module Characteristics

Table 8 below shows the PV module requirements used for this simulation.

Table 8: Data requirements of the PV module used

Maximum power (P_{MPP})	30.5(W)
Voltage at P_{MPP} (V_{MPP})	61.5 (V)
Current at P_{MPP} (I_{MPP})	0.496 (A)
Short circuit current (I_{SC})	0.6 (A)
Open circuit Voltage (V_{OC})	71 (V)

Figures 5-32 and 5-33 show the V-I and P-V characteristics of the PV module are reached for a constant temperature of 25^0C, 40^0C and at 1000 W/m2 irradiance.

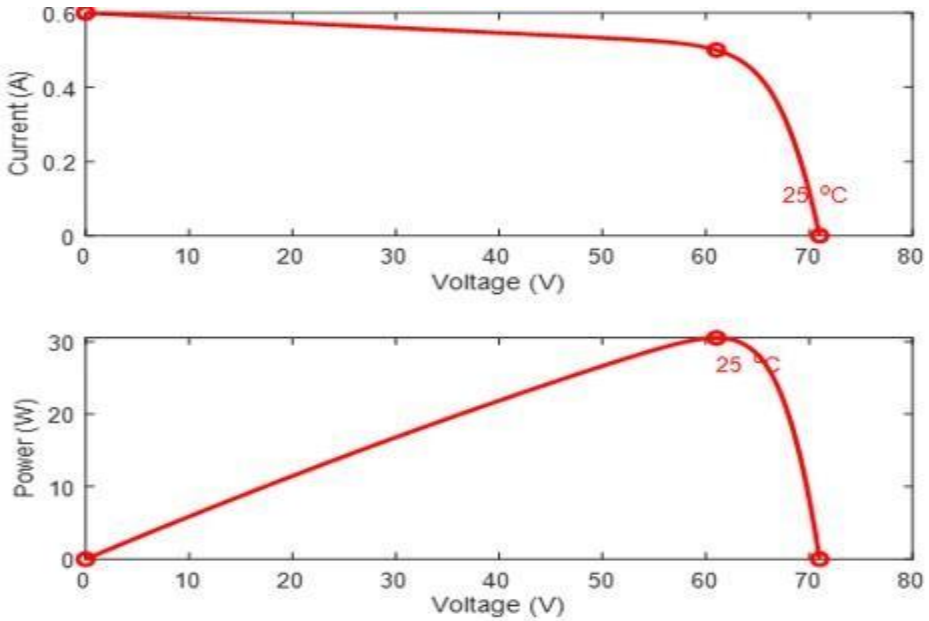

Figure 5-32 V-I and P-I characteristics at 25^0C

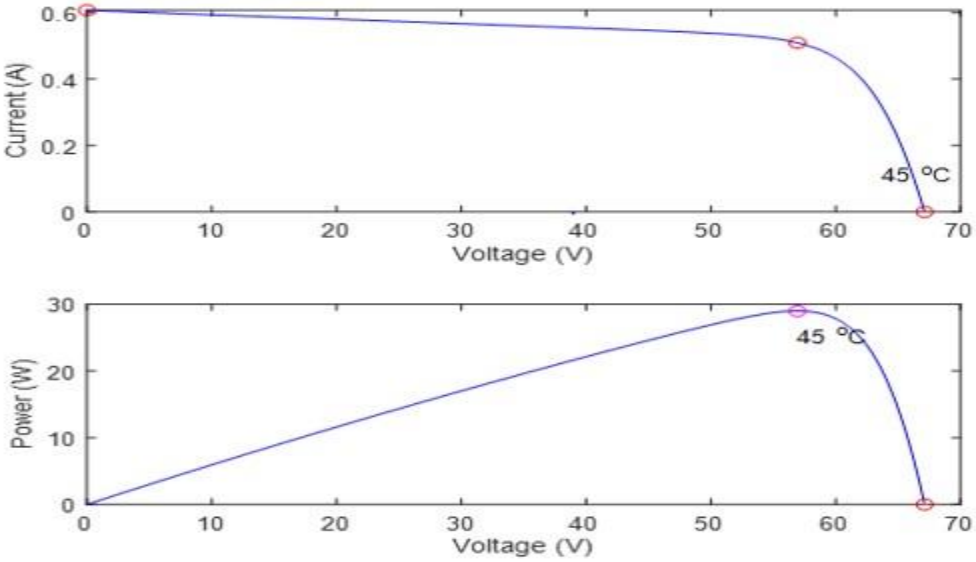

Figure 5-33 V-I and P-I characteristics at 40^0C

5.6 Simulation Results and Analysis

Simulations are done in MATLAB/Simulink at an irradiance of 1000 W/m2 and temperature of (25^0C, 40^0C). The result in figures 5-34 and 5-35 show that the voltage is 61.5 V, current is 0.496A, and output power of the PV array is 30.5 W. The voltage and current to the transmitter coil are regulated by the second level voltage-current controller.

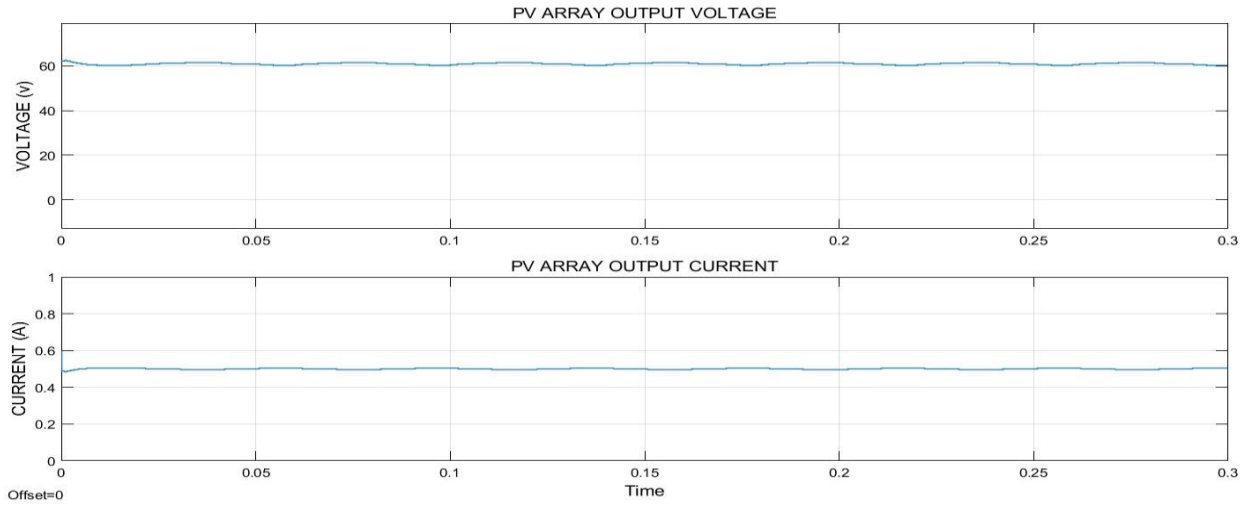

Figure 5-34 PV array output voltage and current

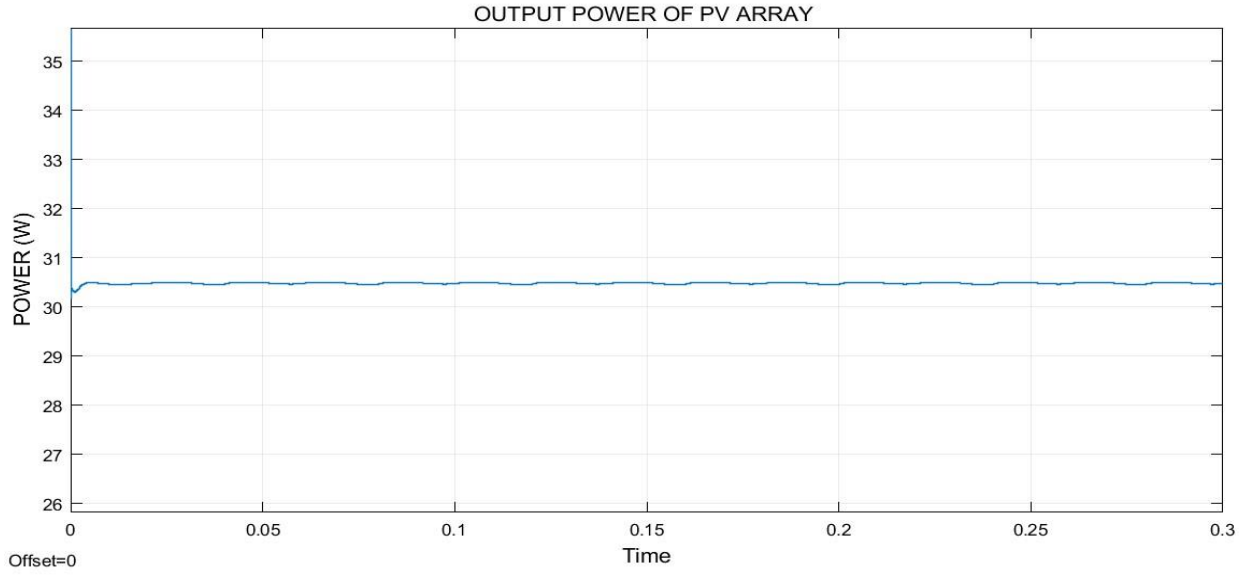

Figure 5-35 PV array output power

In figure 5-36, the output of the boost converter voltage and current regulated by the outermost loop of the three-level controller.

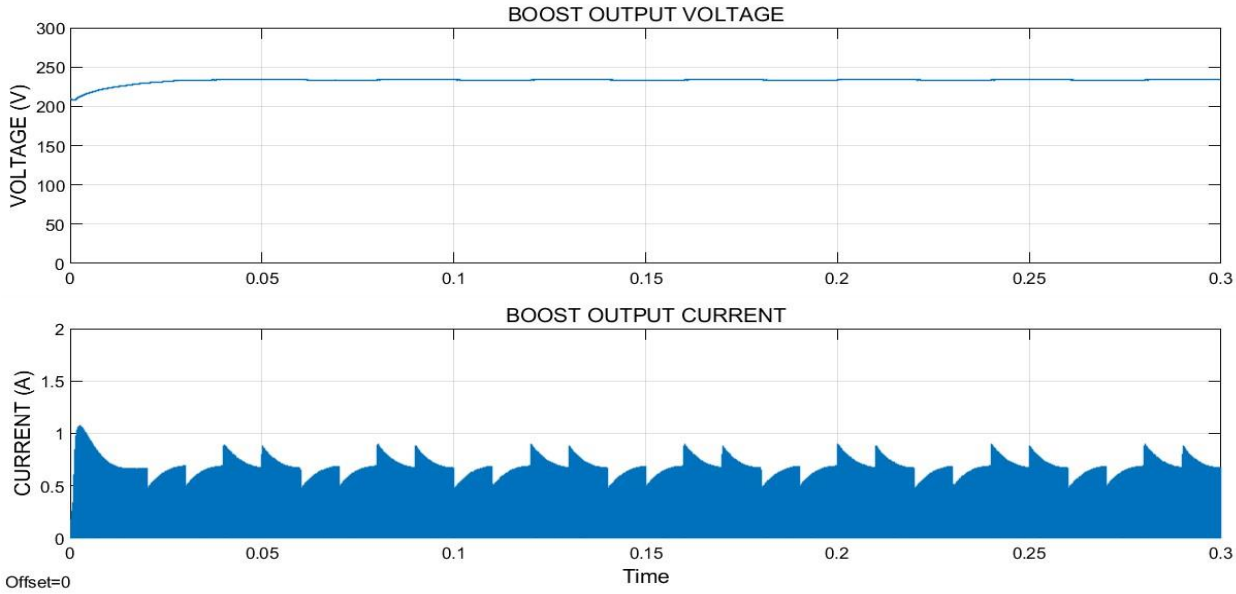

Figure 5-36 Boost output voltage and current

In figure 5-37, the voltage and current from the pure sinusoidal excitation of the transmitter coil at 500 Hz is maintained by the intermediate loop of the three-level controllers.

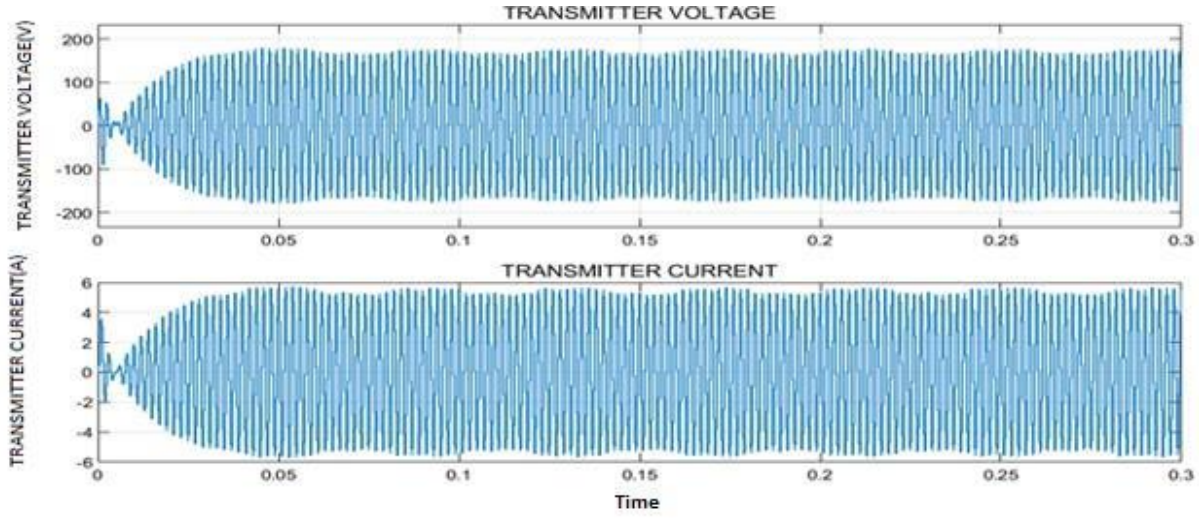

Figure 5-37 Transmitter voltage and current

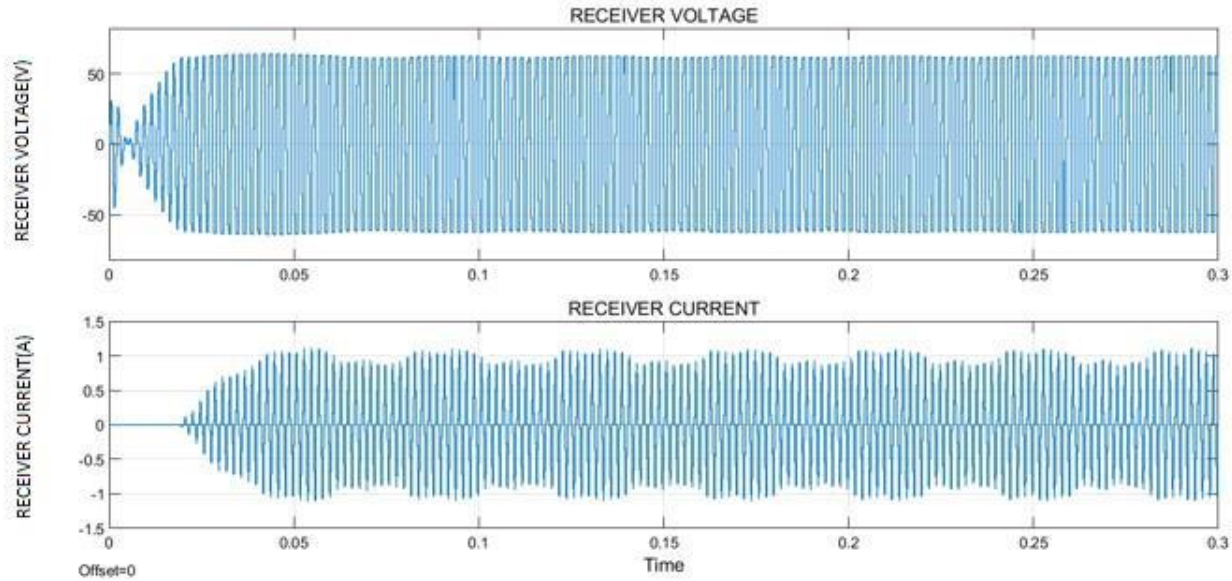

Figure 5-38 Receiver voltage and current

In figure 5-39, the receiver-rectified side is regulated by innermost loop of the three-level controllers.

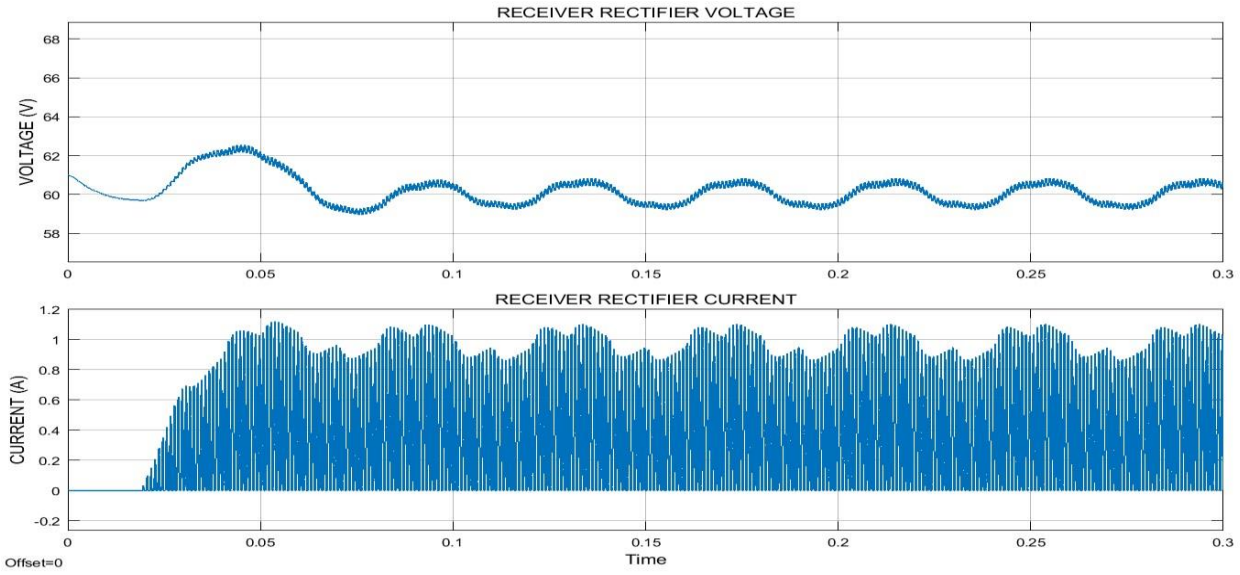

Figure 5-39 Receiver rectifier voltage and current

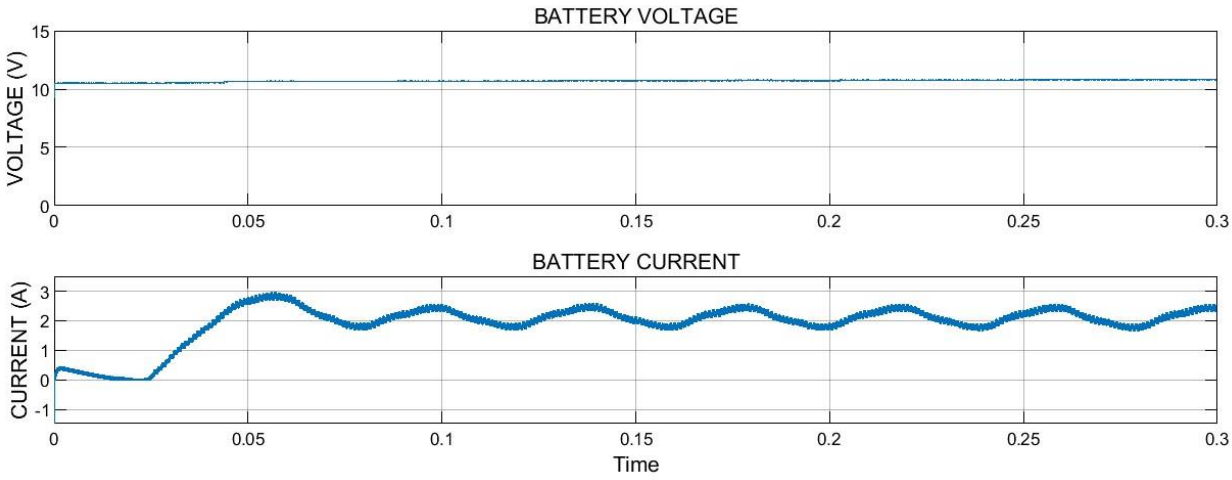

Figure 5-40 Battery voltage and current

In figure 5-41, the initial state of charge is 40%, battery current is negative for charging and battery voltage is 11.9 V

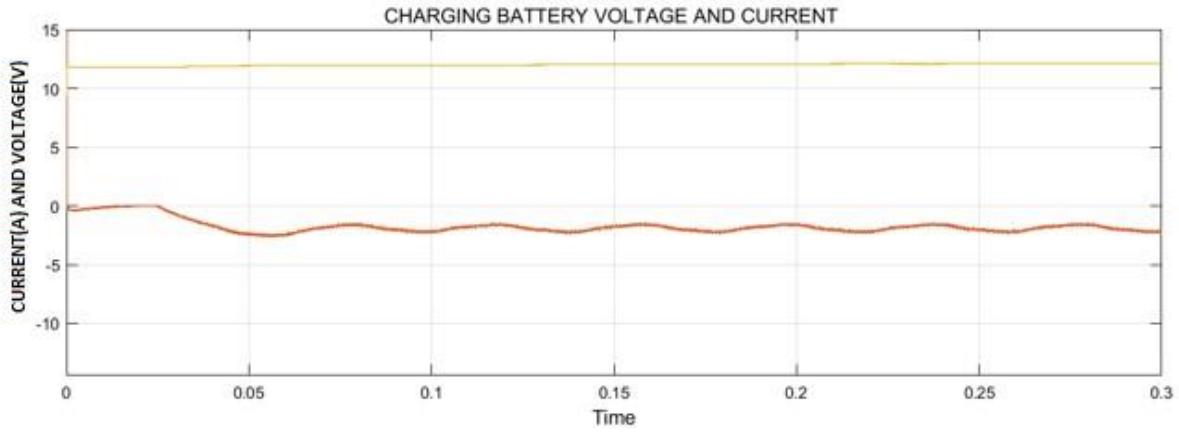

Figure 5-41 Charging Battery voltage and current

Figure 5-42 shows that the maximum power point voltage is 61.5 V. This is the peculiar behavior of Perturb and Observe based MPPT algorithm. They do not settle at the maximum power point, but rather bounce around it.

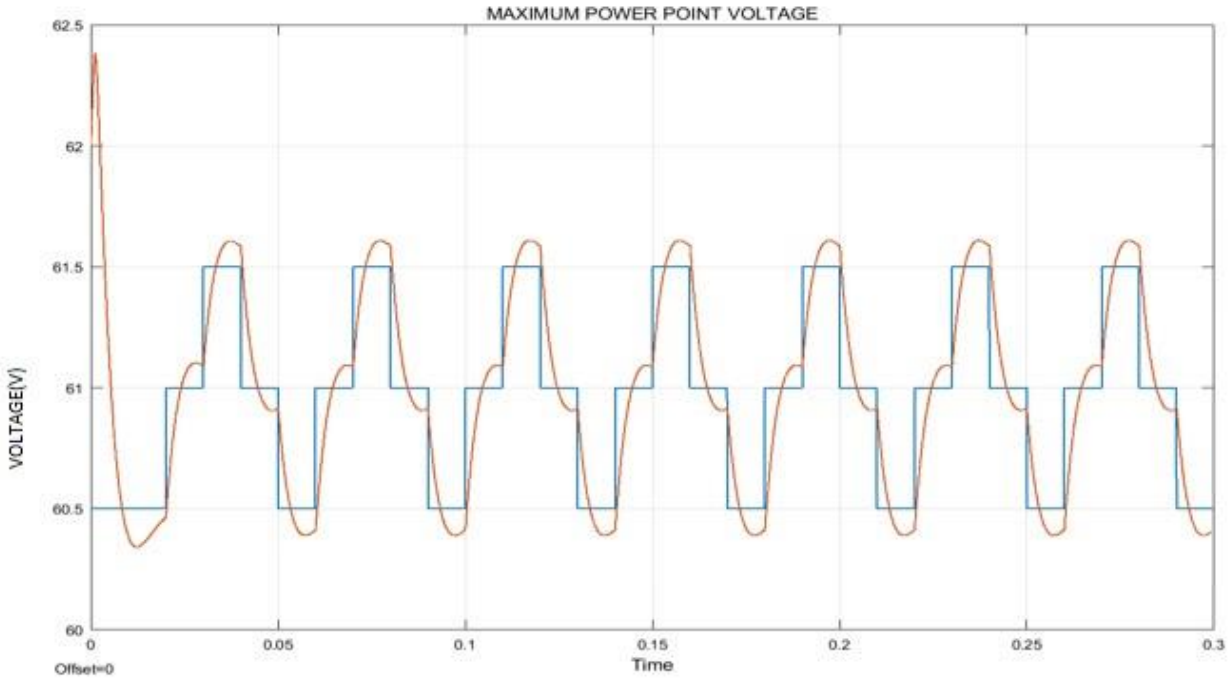

Figure 5-42 Maximum power point voltage

5.7 Stability Analysis

For the stability analysis of the closed loop system used in Figure 5-43, a buck converter modeled in Simulink is considered.

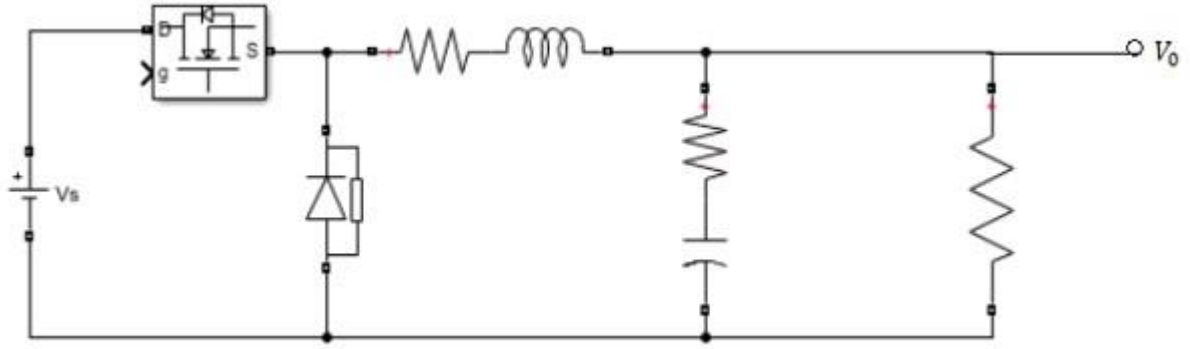

Figure 5-43 DC-DC buck converter model

With respect to the buck converter model above, from the MOSFET, the switch (S) closes during the ON state; hence, energy flows from the source voltage (vs) to the inductor (L). Here, the current that passes through the inductor goes up at a steady state, which charges the inductor.

Figure 5-44 shows the linearized form of the buck converter to be able to apply the control theory. The control signal used here is the duty cycle and load current on the output voltage.

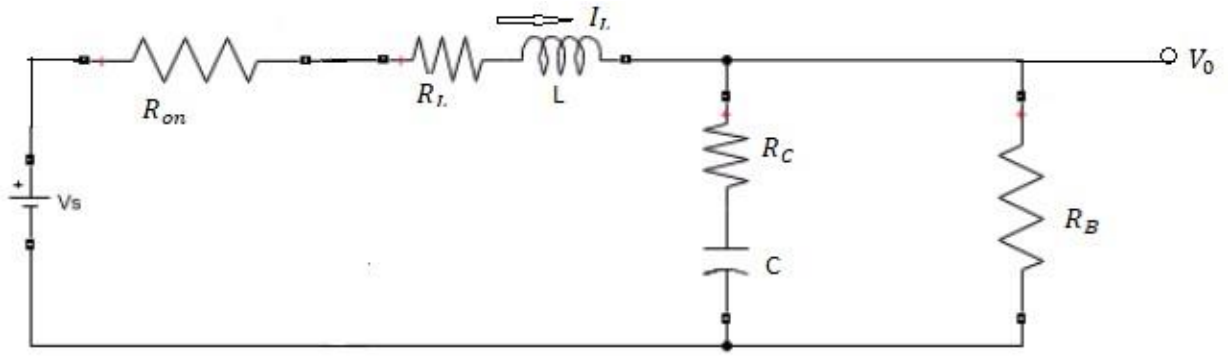

Figure 5-44 Linearized DC-DC buck converter model

Applying Kirchhoff's law in the above figure in its ON state i.e. when S is closed (Sumsurooa, 2018)

$$-V_s + R_{on}I_L + L\frac{di_l}{dt} + R_L.I_L + V_0 = 0 \text{.....5.1}$$

$$L\frac{di_l}{dt} = V_s - R_{on}I_L - R_L.I_L - V_0 \text{.....5.2}$$

$$I_C = I_L - I_R \text{.....5.3}$$

$$I_C = I_L - \frac{V_0}{R_B} \text{.....5.4}$$

Where

$$V_0 = V_C + I_c.R_c \text{.....5.5}$$

$$\frac{V_0 - V_c}{R_c} = I_C \text{.....5.6}$$

Combining equation 5.4 and 5.6,

$$\frac{V_0 - V_c}{R_c} = I_L - \frac{V_0}{R_B} \text{.....5.7}$$

$$V_0(R_B + R_C) = R_B(V_C + I_L.R_c) \text{.....5.8}$$

$$V_0 = \frac{R_B(V_C + I_L.R_c)}{R_B + R_c} \text{.....5.9}$$

Putting equation 5.9 in 5.6

$$I_C = \frac{\frac{R_B(V_C + I_L.R_c)}{R_B + R_c} - V_C}{R_c} \text{.....5.10}$$

$$I_C = I_L \frac{R_B}{R_B + R_c} - \frac{V_C}{R_B + R_c} \text{.....5.11}$$

Then,

$$C\frac{dv}{dt} = I_L \frac{R_B}{R_B + R_c} - \frac{V_C}{R_B + R_c} \text{.....5.12}$$

Hence,

$$L\frac{di_L}{dt} = V_s - \left(R_{on} + \frac{R_B.R_c}{R_B + R_c} + R_L\right).I_L - V_C \frac{R_B}{R_B + R_c} \text{..5.13}$$

Then the State Space equation matrices is as follows,

$$\begin{bmatrix} L \\ C \end{bmatrix} \begin{bmatrix} \frac{di_L}{dt} \\ \frac{dv_C}{dt} \end{bmatrix} = \begin{bmatrix} -\left(R_{on} + \frac{R_B.R_c}{R_B + R_c} + R_L\right) & -\frac{R_B}{R_B + R_c} \\ \frac{R_B}{R_B + R_c} & -\frac{1}{R_B + R_c} \end{bmatrix} \begin{bmatrix} i_L \\ V_C \end{bmatrix} + \begin{bmatrix} 1 \\ 0 \end{bmatrix}.V_s$$

$$\begin{bmatrix} V_0 \\ I_R \end{bmatrix} = \begin{bmatrix} \frac{R_B.R_c}{R_B + R_c} & \frac{R_B}{R_B + R_c} \\ \frac{R_c}{R_B + R_c} & \frac{1}{R_B + R_c} \end{bmatrix} \begin{bmatrix} i_L \\ V_C \end{bmatrix} + \begin{bmatrix} 0 \\ 0 \end{bmatrix}.V_s$$

We know that the general state space equation is $\dot{x} = AX + Bu$

$$\text{y} = CX + D$$

Therefore

$$A = \begin{bmatrix} -\frac{1}{L}\left(R_{on} + \frac{R_B.R_c}{R_B + R_c} + R_L\right) & -\frac{1}{L}.\frac{R_B}{R_B + R_c} \\ \frac{1}{C}.\frac{R_B}{R_B + R_c} & -\frac{1}{C}.\frac{1}{R_B + R_c} \end{bmatrix}$$

$$B = \begin{bmatrix} 1 \\ 0 \end{bmatrix}$$

$$C = \begin{bmatrix} \frac{R_B.R_c}{R_B + R_c} & \frac{R_B}{R_B + R_c} \\ \frac{R_c}{R_B + R_c} & \frac{1}{R_B + R_c} \end{bmatrix}$$

$$D = \begin{bmatrix} 0 \\ 0 \end{bmatrix}$$

$$\dot{x_1} = \frac{di_L}{dt};\ \dot{x_2} = \frac{dv_C}{dt} \quad \text{.....5.14}$$

And,

$R_L = 0.025\ , L = 2e^{-3}H, C = 1.5e^{-3}F, R_c = 0.001, R_B = 4.6, R_{on} = 1e^{-3}$

Substituting values in A, $\begin{bmatrix} \dot{x_1} \\ \dot{x_2} \end{bmatrix} = \begin{bmatrix} -13.499 & -499.89 \\ 666.52 & -144.89 \end{bmatrix} \begin{bmatrix} x_1 \\ x_2 \end{bmatrix} + \begin{bmatrix} 1 \\ 0 \end{bmatrix} . V_s$

From equation 5.14

$$x_1 = i_L$$

$$x_2 = v_C$$

Substituting values in C, $y = \begin{bmatrix} 0.00099 & 0.999 \\ 0.00083 & 0.083 \end{bmatrix} \begin{bmatrix} x_1 \\ x_2 \end{bmatrix}$

Therefore, the system matrices can be gives as

$$\begin{bmatrix} \dot{x_1} \\ \dot{x_2} \end{bmatrix} = \begin{bmatrix} -13.499 & -499.89 \\ 666.52 & -144.89 \end{bmatrix} \begin{bmatrix} x_1 \\ x_2 \end{bmatrix} + \begin{bmatrix} 1 \\ 0 \end{bmatrix} . V_s \text{.....5.15}$$

From

$$y = \begin{bmatrix} 0.0099 & 0.999 \\ 0.00022 & 0.217 \end{bmatrix} \begin{bmatrix} x_1 \\ x_2 \end{bmatrix} \text{.....5.16}$$

Finding Lyapunov of the system matrix in equation 5.15, $f|V(x_1, x_2) - V(x_1, x_2)|$

Assuming a value for $V_x = {x_1}^2 + {x_2}^2$

Substituting equation 5.5.16,

$$= f\left|-13.499{x_1}^2 - 499.89{x_2}^2 + 666.52{x_1}^2 - 144.89{x_2}^2 - {x_1}^2 + {x_2}^2\right|$$

$$=182.22{x_1}^2 + 13496x_1x_2 + 249890.012{x_2}^2 + 444248.9{x_1}^2 + 193144.16x_1x_2 +$$

$$20993.1121{x_2}^2 - {x_1}^2 + {x_2}^2$$

$$=444431.12{x_1}^2 + 270883.124{x_2}^2 + 13496x_1x_2 - {x_1}^2 + {x_2}^2$$

For,

$x = \leq 0$,

Then. $f|V(x_1, x_2) - V(x_1, x_2)| \leq 0$, Therefore, the system is asymptotically stable

5.8 Conclusion

The work shows how a wireless power system over a short range of dynamic distance implemented a proportional integral, fuzzy logic, neuro-fuzzy controller. The three-level cascaded PI controller for dynamic wireless power transfer is designed to power a load of 12 V and 5 A. The simulation of the circuit is in the MATLAB Simulink software with an output voltage of 12 V and 5 A. This simulation is compared to a single PI level controller and its effectiveness is validated. The voltage transmitted in a wireless power transfer depends on the distance between two coils. A closed loop circuit using the proportional integral controller implemented at the receiving end of the wireless power transfer to eliminate the variation of voltage is due to varied spacing existing between both coils. The values of Kp and Ki are selected using the trial and error method until a constant load voltage and current is maintained for varied spacing between the transmitting and receiving coil. The variation in distance is achieved by varying the coupling coefficient between the coils, which in turn changes the mutual inductance of the coils. A fuzzy logic and a neuro-fuzzy controller was also designed which proved to be more robust than the PI controller as there was no undershoot in the output voltage. Additionally, the design of the MPPT controller tracks the highest voltage and current from the PV array required to charge a battery in which the highest power point voltage is 61.5V. The stability analysis of the closed-loop system of a three-level PI controller for an electric vehicle dynamic wireless power transfer in figure 52 is analyzed and the system was found to be asymptotically stable.

CHAPTER SIX

CONCLUSION

6.1 Conclusion

In chapter one, the history of wireless power transfer was discussed alongside various methods that can be employed. Each of the techniques were discussed in which their advantages and disadvantages were highlighted. Its application was also included using an electric vehicle as a case study. The most efficient technique was emphasized which also included its advantages.

In chapter two, the work of many researchers that have carried out studies that are related to wireless power transfer is discussed which is termed as the literature review.

In chapter three, magnetic resonance wireless electric vehicle charging was discussed. The main compensation structures of this technique were also highlighted. The different resonant circuit was mentioned and the circuit model for this method with its equation was derived. Simulation results were carried out showing the effects of parameters such as an inductor, capacitor, load and coupling coefficient on efficiency. The challenges related to magnetic resonance coupling were emphasized.

In chapter four, the method used to carry out this research was discussed in detail. The design of the entire circuit model and the physical model was done using ANSYS Simplorer and Maxwell respectively. Simulation results indicate the effectiveness of the magnetic resonance wireless electric vehicle charging over large distances and the efficiency was seen to be 98.3%. The magnetic inductive method was also discussed using the same design and parameters as the magnetic resonance, and simulation results show that efficiency is 60.3%. This further confirmed the effectiveness of the magnetic resonance method.

In chapter five, a closed loop circuit using a three-level cascaded PI controller was implemented in this wireless charging of electric vehicles to eliminate the variation of voltage because of varied spacing existing between both coils, hence, delivering a constant voltage and constant current to the load. The effectiveness

of this control method was verified with simulations and comparison with a single PI controller. A fuzzy logic and a neuro-fuzzy controller were also designed which proved to be more robust than the PI controller as there was no undershoot in the output voltage. Furthermore, a wireless power transfer with three - level cascaded MPPT control was designed. The proposed system consisted of a solar PV array, boost DC/DC converter, inverter, transmitter coil, a receiver coil, rectifier, buck converter, and batteries. The MPPT controller was designed to track the highest voltage and current from the PV array required to charge a battery in which the highest power point voltage is seen to be 61.5 V. Additionally, the stability analysis of the closed-loop system of a three-level cascaded PI controller for an electric vehicle dynamic wireless power transfer in figure 52 was analyzed and the system was found to be asymptotically stable.

6.2 Future work

The magnetic resonance wireless power transfer system designed in chapter 4 should be enhanced by doing further magneto static and experimental analysis.

In chapter 5.5 where I used the adaptive neuro-fuzzy inference (ANFIS) model to train the system's data, it is observed that the number and type of MFs affect the ANFIS model. To this effect, the root means square error and the number of epochs is used to choose the suitable model. Hence, future work should review the type of MFs, number of MFs, epochs, inputs, rules and the training data for the improvement of the ANFIS model for the implementation of a more efficient dynamic wireless power transfer system.

For future work, the neuro-fuzzy controller should be designed in such a way that the input and output data for training completely represents the features of the trained FIS data.

REFERENCES

Telsa, N.; Marincic, A. S., " Nikola Tesla and the wireless transmission of energy," *IEEE Trans. Power App. Syst.,* vol. PAS-101, no. 10, pp. 4064–4068, Oct.1982.

Hui, S. Y., " Planar wireless charging technology for portable electronic products and Qi.," *IEEE Trans. Power App. Syst.,* vol.101, no. 6, pp. 1290–1301, June 2013.

Ahn, D.; Hong, S., " Wireless power transmission with self-regulated output voltage for biomedical implant," *IEEE Trans. Ind. Electron,* vol.61, no. 5, pp. 2225–2235, May 2014.

IHI Corporation, "Making electric vehicles easier to use,"*www.ihi.co.jp/en,* vol. 46, no. 1, 2013.

Lu, X.; Niyato, D.; Wang, P.; Kim D.I., "Wireless charger networking for mobile devices: fundamentals, standards, and applications", *IEEE Wireless Communications*, 2015.

Kurs, A.; Karalis, A.; Moffatt, R.; Joannopoulos, D.; Fisher, P.; Soljacic, M., "Wireless Power Transfer via Strongly Coupled Magnetic Resonances, " *Science*, vol. 317, no. 5834, pp. 83- 86, Jul. 2007.

Habib, S.; Haque, A., “Impulsive noise mitigation in wireless communication systems using EMD technique”. *In 2012 7th International Conference on Electrical and Computer Engineering*, pp. 291-294, December 2012.

Jeong, I.S.; Jung, B.I.; You, D.S.; Choi, H.S., "Analysis of S-Parameters in magnetic resonance WPT using superconducting coils," *IEEE Transactions on Applied Superconductivity,* vol. 26, no. 3, April 2016.

Haque, A.; Sumaiya, S., “An overview on the formation and processing of nitrogen-vacancy photonic

centers in diamond by ion implantation". *Journal of Manufacturing and Materials Processing*, 1(1), 6, 2017.

Choi, Y.; Kwak, B.; Mgungbok, A.,"4KW Magnetic resonance wireless power transfer system," *Gwanju, Korea*, 2014.

Beh, T.C.; Imura, T.; Kato, M.; Hori, Y., "Basic study of improving efficiency of wireless power transfer via magnetic resonance coupling based on impedance matching," *IEEE International Symposium,* pp. 2011-2016, July 2010.

Sample, A.P.; Meyer, D. A.; Smith, J. R., "Analysis, experimental results and range adaptation of magnetically coupled resonators for wireless power transfer." *IEEE Transaction on Industrial Electronics*, vol.58, no. 2, pp. 544-554, 2011.

Wang, Q.; Li, H.," Research on the wireless power transmission system based on coupled magnetic resonances,"*International Conference Electronics Communication Control, Ningbo, China*, pp. 2255-2258, Sept. 2011.

Xue-hui, L.; Wang, He.; Zhang, Y.S., "Analysis on the Efficiency of Magnetic Resonance Coupling Wireless Charging for Electric Vehicles," Procedure *on IEEE Conference Cyber Technology Automated Control Intelligent System. Nanjing,* pp. 191-194, May 2013.

Karalis, A.; Joannopoulos, J.D.; Soljai, M.," Efficient wireless non- radiative mid-range energy transfer." *Annual Physics Conference, N.Y*, pp. 34-48, Jan. 2008.

Sample, A.P.; Meyer, D. A.; Smith, J. R., " Analysis, experimental results and range adaptation of magnetically coupled resonators for wireless power transfer." *IEEE Transactions on Industrial Electronics*, vol.58, no. 2, pp. 544-554, 2011.

Hasanzadeh, S.; Vaez-Zadeh, S.; Hassanpour, A.I., "Optimization of a contactless power transfer system for electric vehicles," *IEEE Transactions on Vehicular Technology*, 2012.

Kurs, A.; Karalis, A.; Moffatt, R.; Joannopoulos, J. D.; Fisher, P.; Soljacic, M., "Wireless power transfer via strongly coupled magnetic resonances, " *Science*, vol. 317, no.5834, pp. 83- 86, Jul. 2007.

Illhoe, H.; Young, J.J.; Young, D.K.; Min, S.L., System optimization for a dynamic wireless charging electric vehicles operating in a multiple-road environment," *IEEE Transactions on Intelligent Transport Systems*, vol 19, n0. 6, June 2018.

Kelion, L.; *South Korean Road Wirelessly Recharges OLEV Buses*, [Online]. Available: http://www.bbc.com/news/technology23603751

Musavi, F.; Edington, M.; Eberle, W.; "Wireless power transfer: a survey of EV battery charging technologies. " *IEEE Energy Congress and Expo., Raleigh*, pp. 1804-1810, Sept. 2012.

Cheon, S.; Kim, Y. H..; Kang, S. Y.; Lee, M. L.; Lee, J. M.; Zyung, T. "Circuit-model-based analysis of a wireless energy-transfer system via coupled magnetic resonances," *IEEE Trans. Ind. Electron., Vol*. 58, no. 7, pp. 2906-2914**,** Jul. 2011.

Wireless Power Consortium. *http://www.wirelesspowerconsortium.com/* (available 2014).

Shital, R; Khutwad, Gaur, S., "Wireless charging system for electric vehicle, "*International Conference on Signal Processing, Communication, Power and Embedded System (SCOPES*), 2016

Covic, G. A.; Boys, G.T.," Modern trends in inductive power transfer for transportation applications," *IEEE Journal of Emerging and Selected Topics in Power Electronics*, vol. 1, no. 1, March 2013.

Haque, A.; Narayan, J., “Electron field emission from Q-carbon”, *Diamond and Related Materials*, 86, 71-78, 2018.

Wu, G. A.; Covic, J. T.; Boys, D. J.; Robertson P., "A series-tuned inductive-power-transfer pickup with a controllable AC-voltage output." *IEEE Transactions on Power Electronics*, vol. 26, no. 1, pp. 98109, Jan. 2011.

Siqi, L.; Chunting, C.M., "*Wireless Power Transfer for Electric Vehicle Applications," IEEE Journal of Emerging and Selected Topics in Power Electronics,* vol. 3, no. 1, March 2015.

Vilathgamuwa, D.M.; Sampath, J.P.K, "Power Systems." *Springer Science and Business Media Singapore*, 2015.

Mahbub, A. R.; Haque, A.; Ghosh, K.,” Fabrication and Magnetic Characterization of CFO/NiO and CFO/NiS Heterostructures”. *Journal of Superconductivity and Novel Magnetism*, 1-8, 2019.

Swain, K.; Neath, M. J.; Madawala, U. K.; Thrima, D. J "A dynamic multivariable state-space model for bidirectional inductive power transfer systems." *IEEE Trans. Power Electron.* vol. 27, no. 11, Nov. 2012.

C.S. Wang, O. H. Stielau and G. A. Covic. "Design considerations for a contactless electric vehicle battery charger." *IEEE Transaction Industrial Electronics*, vol. 52, no. 5, pp. 1308-1314, Oct. 2005.

Kawasaki, S.; Kobayashi, Y.; Yoshida, S.; "High-power, high efficiency microwave circuits and modules for wireless power transfer based on Green-Eco technology." *Proceedings of IEEE Radio and Wireless Symposium,* 2013.

Shinohara, N.; Kubo, Y.; Tonomura, H.," Wireless charging for electric vehicle with microwaves" 3rd

International Electric Drives Production Conference (EDPC), 2013.

Hossain, M.S.; Barua, A., "Charging electric vehicles via microwave energy transmission and analysis of advanced energy storage system." *Rajshahi University of Engineering & Technology*, 2012.

Rozario, D.; Azeez, N.A.; Williamson, S.S., "Analysis and Design of Coupling Capacitors for Contactless Capacitive Power Transfer Systems in Proc." *IEEE Transportation Electrification Conference and Expo USA*, 2016.

Haque, A., Abdullah-Al Mamun, M.; Taufique, M. F. N.; Karnati, P.; Ghosh, K., " Temperature dependent electrical transport properties of high carrier mobility reduced graphene oxide thin film devices'. *IEEE Transactions on Semiconductor Manufacturing*, 31(4), 535-544, 2018.

You, Y.S.; Yi, K.H.; "*Capacitive* Coupling Wireless Power Transfer with Glass dielectric layers for Electric Vehicles." *IEEE International Conference on Consumer Electronics, Berlin,* 2016

Vincent, D.; Sang, P.H.; Williamson, S.S.; "Feasibility study of hybrid inductive and capacitive wireless power transfer for future transportation," *IEEE Transportation Electrification Conference and Expo (ITEC)*, 2017.

Liu, C.; Hu, A.P.; Nair, N.K.C., "Modelling and analysis of a capacitively coupled contactless power transfer system, "IET Power Electron., vol. 4, pp. 808 –815, 2011.

Haque, A.; Abdullah-Al Mamun, M.; Taufique, M. F. N.; Karnati, P.; Ghosh, K., "Temperature dependent electrical transport properties of high carrier mobility reduced graphene oxide thin film devices". *IEEE Transactions on Semiconductor Manufacturing*, 31(4), 535-544, 2018.

Lu, F.; Zhang, H.; Hofmann, H.; Mi, C., "Charging Application," *IEEE Transactions on Power Electron.*"

vol. 31, no. 12, pp. 8541-8551, 2016.

Qiu, C.; Chau, K.T.; Ching, T.W.; Liu, C., "Overview of Wireless Power Transfer for Electric Vehicle Charging." Pp. 17-20. November 2014.

Tan, L.; Li, J.; Fu, C.; Huang, X., "Modeling and analysis of a 3kw wireless charging system for electric vehicle, "*IEEE PELS Workshop on Emerging Technologies*, *Wireless Power Transfer*, May 2017.

Ravikiran, V.; Keshri, R.K.; Chen, M.C.; Hsieh, H.C.; Liu, Y.C.; Chiu, H.J., "High-efficiency wireless power transfer system for electric vehicle applications," *IEEE Transactions on Circuits and Systems—Ii: Express Briefs*, vol. 64, no. 8, August 2017.

Chung, Y. D.; Lee, C. Y.; Kang, H.; Park, Y.G., "Design considerations of superconducting wireless power transfer for electric vehicle at different inserted resonators," *IEEE Transactions on Applied Superconductivity*, vol. 26, no. 4, June 2016.

Hata, K.; Imura, T.; Hori, Y., "efficiency maximization of wireless power transfer based on simultaneous estimation of primary voltage and mutual inductance using secondary-side information," *IECON 42nd Annual Conference of the IEEE Industrial Electronics Society*, 2016.

Ravikiran, V.; Keshiri, R.K., "Comparative evaluation of S-S and P-S topologies for wireless charging of electrical vehicles, "*IEEE Industrial Electronics Society Annual Conference*, pp. 5324-5329, Nov. 2017.

Liao, C.; Li, J.; Li, S., "Design of LCC impedance matching circuit for wireless power transfer system under rectifier load, "*CPSS Transactions on Power Electronics and Applications*, vol.2, no.3, Sept. 2017.

Klaus, B.; Barth, D.; Sillmann, B.; Leifried, T., "Design and implementation of a transmission system for high-performance contactless electric vehicle charging, "*IEEE Transportation Electrification Conference and Expo*, pp. 39-44, June 2017.

Tran, D.H; Vu, V.B.; Choi, W., "Design of a high-efficiency wireless power transfer system with intermediate coils for the on-board chargers of electric vehicles, "*IEEE Transactions on Power Electronics*, vol. 33 pp. 175-187, Feb. 2018.

Mahmud, M.H.; Elmahmoud, W.; Barzegaran, M.R.; Brake, N., "Efficient wireless power charging of electric vehicle by modifying the magnetic characteristics of the transmitting medium, "*IEEE Transactions on Magnetics*, vol. 53 no. 6, June 2017.

Yeo, T.D.; Kwon, D.; Khang, S.T.; Yu, J. W., "Design of maximum efficiency tracking control scheme for closed-loop wireless power charging system employing series resonant tank, "*IEEE Transactions on Power Electronics*, vol. 32, no. 1, January 2017.

Zhang, Y.; Zhao, Z.; Jiang, Y., "Modeling and analysis of wireless power transfer system with constant-voltage source and constant-current load, "*IEEE Energy Conversion Congress and Exposition*, pp. 975-979, Oct. 2017.

Kim, H.; Song, C.; Kim, D.H.; Jung, D.H., "Coil design and measurements of automotive magnetic resonant wireless charging system for high-efficiency and low magnetic field leakage, "*IEEE Transactions on Microwave Theory and Techniques*, vol. 64, no. 2, February 2016.

Haque, A., & Narayan, J., “Stability of electron field emission in Q-carbon”. *MRS Communications*, 8(3), 1343-1351, 2018.

Kim, H.; Song, C.; Kim, D.H.; Jung, D.H., Kim, I.M.; Kim, Y.; Kim, J.; Ahn, S.; Kim, J., "Coil design and

measurements of automotive magnetic resonant wireless charging system for high-efficiency and low magnetic field leakage," *IEEE Transactions on Microwave Theory and Techniques*, no. 2, 2016.

Zhang, X.; Yuan, Z.; Yang, Q.; Li, Y.; Zhu, J., "Coil Design and Efficiency Analysis for Dynamic Wireless Charging System for Electric Vehicles, "*IEEE Transactions on Magnetics,* vol. 52, no. 7, February 2016.

Cho, Y.; Yuan, Z.; Kim, J.J.; Kim, Y. D.H.; Lee, S., "Thin PCB-Type Metamaterials for Improved Efficiency and Reduced EMF Leakage in Wireless Power Transfer Systems, "*IEEE Transactions on Microwave Theory and Techniques,* vol. 64, no. 2, February 2016.

Dolara, A.; Leva, S.; Longo, M.; Castelli-Dezza, F.; Mauri, M., "Coil Design and Magnetic Shielding of a Resonant Wireless Power Transfer System for Electric Vehicle Battery Charging," *6th International Conference on Renewable Energy and Research and Applications*, Nov.5-8 2017.

Campi, T.; Cruciani, S.; Maradei, F.; Feliziani, M., "Conducted Emission of Wireless Power Transfer Charging System in Electric Vehicle," *IEEE International Symposium on Electromagnetic Compatibility & Signal/Power Integrity*, Oct.2017.

Cui, H.; Zhong, W.; Li, H.; He, F.; Chen, M.; Xu, "A Study on the Shielding for Wireless Charging Systems of Electric Vehicles, "*IEEE Applied Power Electronics Conference and Exposition,* April 19, 2018.

Campi, T.; Cruciani, S.; Feliziani, M.; Maradei, F., "Magnetic Field Generated by a 22 kW-85 kHz Wireless Power Transfer System for an EV, "*IEEE AEIT International Annual Conference*, pp. 1-6, Sept. 2017.

Wang, Q.; Li, W.; Kang, J.; Wang, Y., "Electromagnetic Safety of Magnetic Resonant Wireless Charging System in Electric Vehicles, "*IEEE PELS Workshop on Emerging Technologies: Wireless Power Transfer,* pp. 1-4, May 2017.

Wang, Q.; Li, W.; Kang, J.; Wang, Y., "Magnetic Field Distribution in a WPT System for Electric Vehicle Charging, "*2016 Progress in Electromagnetic Research Symposium (PIERS)*, pp. 5165, August 2016.

Mandip, J.S.; Joey H., "Wireless Power Transmission Using Magnetic Resonance." *Cornell College PHY 312*, December 2011

Hui, W.X.; He, Z.; Shun, L.Y., "Analysis on the Efficiency of Magnetic Resonance Coupling Wireless Charging for Electric Vehicles, "*IEEE International Conference on Cyber Technology in Automation Control and Intelligent Systems*, May 26-29, 2013

Bahareh, B.; Bruce, D. C.; Nader B.; Alan, B.M., "Dielectric properties of 3D-printed materials for anatomy specific 3D-printed MRI coils, "*Journal of Magnetic Resonance*, 2018

Ching, Y.; Zhong, L.; Chen, M.; Hsieh, H.; Liu, Y.; Chiu, H., "High Efficiency Wireless Power Transfer System for Electric Vehicle Applications". *IEEE Transactions on Circuits and Systems,* vol. 64, no.8, 2017.

Zhang, W.; Mi, C., "Compensation Topologies of High-Power Wireless Power Transfer Systems," *IEEE Transactions Vehicle Technology*, vol. 65, no. 6, 2016: 4768-4778.

Gao, Y.; Ginart, A.; Farley, K.B.; Tse, Z.T.H., "Misalignment Effect on Efficiency of Wireless Power Transfer for Electric Vehicles, "*2016 IEEE Applied Power Electronics Conference and Exposition (APEC)*, 2016.

Etacheri, V.; Marom, R.; Elazari, R.; Salitra, G.; Aurbach, D., "Challenges in the development of advanced Li-ion batteries: a review. Energy Environ, *"Science,* 4:3243–3262, 2011.

Madawala, U.K.; Schweizer, P.; Haerri, V.V., "Living and mobility—a novel multipurpose in-house grid

interface with plug in hybrid blue angle, "*IEEE international conference on sustainable energy technologies*, 2008.

Kurs, A.; Karalis, A.; Moffatt, R.; Joannopoulos, J.D.; Fisher, P.; Soljacic, M., "Wireless power transfer via strongly coupled magnetic resonances", *Science*, vol.317, no.5834, pp. 83-86, 2007.

Khan, M.; Arifin, M.; Haque, A.; Al-Masood, N., "Stability analysis of power system with the penetration of photovoltaic based generation". *Int. J. Energy Power Engr*., 2, 84-89, 2013.

https://en.wikipedia.org/wiki/Maximum_power_point_tracking#Perturb_and_observe

Patil, D.; Miller, J.M.; Fahim, B.; Balsara, P.T., "Wireless Power Transfer for Vehicular Applications: Overview and Challenges", *IEEE Transactions on Transportation Electrification*, vol. 4, no.1, March 2018.

Haque, A.; Rahman, M. A., "Study of a solar PV-powered mini-grid pumped hydroelectric storage & its comparison with battery storage". *In 2012 7th International Conference on Electrical and Computer Engineering*, pp. 626-629, December 2012.

Gupta, M.M.; Tsukamoto, Y., "Fuzzy logic controllers a perspective," *Proc. Joint Automatic Control Conf.*, San Francisco, pp. FAlO-C, Aug. 1980.

Zadeh, L.A., "Fuzzy sets," *International Journal Information Control*, 8:338-353, 1980.

Mamdani, E. H.; Assilion, S., "An experiment in linguistic synthesis with a fuzzy logic controller," *Intl J. Man-Machine Stud*, 7:1-13, 1974.

Sumsurooah, S.; Odiavic, M.; Bozhko, S.; Boroyevich, D., "Robust stability analysis of a dc-dc buck converter under multiple parameter uncertainties", *IEEE Transactions on Power Electronics*, vol. 33, pp. 5426-5441, June 2018.

Jin, Y., "Fuzzy modeling of high-dimensional systems: Complexity reduction and interpretability

improvement", *IEEE Transactions on Fuzzy Systems*, 8(2), 212-221, 2000.

Jang, S.R., "ANFIS: Adaptive-Network-Based Fuzzy Inference System," *IEEE Trans. Systems, Man, and Cybernetics*, vol. 23, no. 3, pp. 665-684, May/June 1993.